A Design for Controllability Methodology for PEM Fuel Cells including the effect of Material Surface Defects on the Dynamic System Performance

By

Víctor Fontalvo Morales

A dissertation submitted in partial fulfilment of the requirements for the degree of
Doctor of Philosophy

Mechanical Engineering Department
Universidad del Norte
Barranquilla - Colombia

Major Professors:
Dr. Humberto Gómez
Dr. Marco Sanjuan
Committee Members:
Dr. George Nelson
Dr. Antonio Bula
Dr. Abel Hernandez
Dr. Juan Tibaquirá

July 2019

Declaration of Authorship

I, Víctor Fontalvo Morales, declare that this thesis titled, 'A Design for Controllability Methodology for PEM Fuel Cells including the effect of Material Surface Defects on the Dynamic System Performance' and the work presented in it is my own. I confirm that this work submitted for assessment is my own and is expressed in my own words. Any uses made within it of the works of other authors in any form (e.g., ideas, equations, figures, text, tables, programs) are properly acknowledged at any point of their use. A list of the references employed is included.

- This work was done wholly or mainly while in candidature for a research degree at this University.
- Where any part of this thesis has previously been submitted for a degree or any other qualification at this University or any other institution, this has been clearly stated.
- Where I have consulted the published work of others, this is always clearly attributed.
- Where I have quoted from the work of others, the source is always given. With the exception of such quotations, this thesis is entirely my own work.
- I have acknowledged all main sources of help.

Signed: Víctor Fontalvo Morales

Date: July 2019

Abstract

Electric power has become indispensable for the development of society. Our quality of life is entirely dependent on the availability of electric energy in the industrial, commercial, and residential sectors. Most of this energy is currently obtained from non-renewable sources (oil, natural gas, and coal mainly). Unfortunately, the continuous combustion of these fuels has severely impacted the environment due to the continuous emissions of greenhouse gases. Therefore, the need to explore alternative energy sources in a wide array of applications is essential for the sustainability of our way of life. Hydrogen is one of the promising fuels of the future, which would allow a transition to a cleaner generation matrix. Although hydrogen is mostly obtained from reforming of natural gas, different pathways from renewable resources are developed and being researched. Therefore, the study of devices operating with hydrogen contributes to the construction of a sustainable future. Fuel cells are one of the most effective ways to transform hydrogen into electrical power. By definition, a fuel cell is an electrochemical device capable of producing electrical energy from a fuel and an oxidant. For Proton Exchange Membrane (PEM) fuel cells the fuel is hydrogen, which is supplied to the anode, and the oxidant agent is oxygen (or air) supplied to the cathode. In this research, a methodology is developed for the selection of fuel cells materials, considering how their properties influence the cell dynamic response. To achieve this, a test bench was designed and constructed to characterize the PEM fuel cells dynamic response, and laboratory tests were developed to perform defect characterization. Different membrane assemblies were tested to analyze the impact of their properties on the cell settling time, and therefore, determine its effect on the controllability of the system.

Acknowledgements

First of all, I want to thank God because without Him and His infinite blessings, nothing would be possible.

I also want to thank my parents who with their effort and support, initially made it possible for me to become an engineer, and then to embark on this trip called doctorate.

Most notably, I want to thank my beloved Mayra for her patience, and tolerance through the process of preparing this dissertation; thanks for believing in me.

I want to thank in an extraordinary way the professors Humberto Gómez and Marco Sanjuan for their guidance, support, and patience throughout the development of this research, without their tremendous experience and advice, the development of this research would not have been possible.

Also, I want to thank Dr. George Nelson for his kind welcome at the University of Alabama in Huntsville and provide me with resources required to complete this research, as well as for his comments and observations regarding this document. I additionally want to express my gratitude to Hernando Gonzales and Prehit Patel for their help and guidance throughout my stay in the United States. Likewise, I want to thank Fulbright, and the Government of the United States for the resources granted, which made my livelihood possible during this time.

Finally, I want to thank my friends, who gave me their support during the fulfillment of this dissertation.

The authors want to thank COLCIENCIAS and Fondo Nacional de financiamiento para la Ciencia, la tecnología y la innovación Francisco José de Caldas for their support in the project identified with the code 1215-669-46500 which supported this research.

Contents

List of Figures

List of Tables

Abbreviations

AFC	**A**lkaline **F**uel **C**ell
BET	**B**raunauer-**E**mmett-**T**eller
BOM	**B**ill **O**f **M**aterials
CE	**C**oncurrent **E**ngineering
DAQ	**D**ata **A**c**Q**uisition
DFC	**D**esign **F**or **C**ontrollability
DFX	**D**esign **F**or **X**
DMFC	**D**irect **M**ethanol **F**uel **C**ell
DOE	**D**esign **O**f **E**xperiments
FOPDT	**F**irst **O**rder **P**lus **D**ead **T**ime
GDL	**G**as **D**iffusion **L**ayer
MCFC	**M**olten **C**arbonate **F**uel **C**ell
MEA	**M**embrane **E**lectrode **A**ssembly
MFC	**M**ass **F**low **C**ontroller
MIMO	**M**ultiple **I**nput **M**ultiple **O**utput
MPPT	**M**aximum **P**ower **P**oint **T**racking
PAFC	**P**hosphoric **A**cid **F**uel **C**ell
PCB	**P**rinted **C**ircuit **B**oard
PEMFC	**P**roton **E**xchange **M**embrane **F**uel **C**ell
PID	**P**roportional **I**ntegral **D**erivative
PWM	**P**ulse **W**idth **M**odulation
SOFC	**S**olid **O**xide **F**uel **C**ell
XRD	**X**-**R**ay **D**iffraction

Physical Constants

Faraday constant	F	=	96 485.332 89(59) $C \cdot mol^{-1}$
Ideal gas constant	R_u	=	8.314 $kPa \cdot m^3 \cdot kg^{-1} \cdot K^{-1}$
Standard atmosphere	atm	=	101 325 Pa

Symbols

A_{fc}	fuel cell area	m^2
c_j	molar concentration of specie j	$mol \cdot m^{-3}$
D	diffusion coefficient	
I	current	A
m	mass	kg
$\dot{m}$	mass flow rate	$kg \cdot s^{-1}$
M	molar mass	$kg \cdot kmol^{-1}$
n_d	electro-osmotic drag coefficient	
N	molar flow per unit area	$kmol \cdot s^{-1} \cdot m^{-2}$
n_{fc}	number of fuel cells in the stack	
p	pressure	Pa
s	liquid saturation	
t	time	s
T	temperature	K
V	volume	m^3

Greek Letters

α_{H_2O}	conductivity correction coefficient	
γ	volumetric condensation coefficient	
δ	diffusion layer thickness	
ε	medium porosity	
λ	water content	
ρ	mass density	$kg \cdot m^{-3}$

ϕ	relative humidity	
ω	absolute humidity	$kg_v \cdot kg_a^{-1}$

Superscripts

a	anode
c	cathode
$cool$	cooling
ch	channels
GDL	gas diffusion layer
gen	generation
pur	purge
$reac$	reaction
$surr$	surroundings

Subscripts

a	dry air
c	contact
fc	fuel cell
g	gas
H_2	hydrogen
H_2O	water
i	input
ion	ionic
l	liquid
ma	moist air
N_2	nitrogen
o	output
ohm	ohmic
O_2	oxygen
sat	saturation
th	theoretical

v	water vapor

To my family

Chapter 1

Introduction

Electric power has become indispensable for the development of society. Our quality of life is entirely dependent on the availability of electric energy in the industrial, commercial, and residential sectors. Most of this energy is currently obtained from non-renewable sources (oil, natural gas, and coal mainly). Unfortunately, the continuous combustion of these fuels has severely impacted the environment due to the continuous emissions of greenhouse gases. Therefore, the need to explore alternative energy sources in a wide array of applications is essential for the sustainability of our way of life.

Hydrogen is one of the promising fuels of the future, which would allow a transition to a cleaner generation matrix. Although hydrogen is mostly obtained from reforming of natural gas, different pathways from renewable resources are developed and being researched. Therefore, the study of devices operating with hydrogen contributes to the construction of a sustainable future.

Fuel cells are one of the most effective ways to transform hydrogen into electrical power. By definition, a fuel cell is an electrochemical device capable of producing electrical energy from a fuel and an oxidant. For Proton Exchange Membrane (PEM) fuel cells the fuel is hydrogen, which is supplied to the anode, and the oxidant agent is oxygen (or air) supplied to the cathode.

While it is true that the basic principle of the operation of fuel cells dates back more than a century ago, there are still many challenges to be addressed both in terms of the materials used in the cell and in the control strategies implemented in order to guarantee its efficient operation. Although these two topics are studied

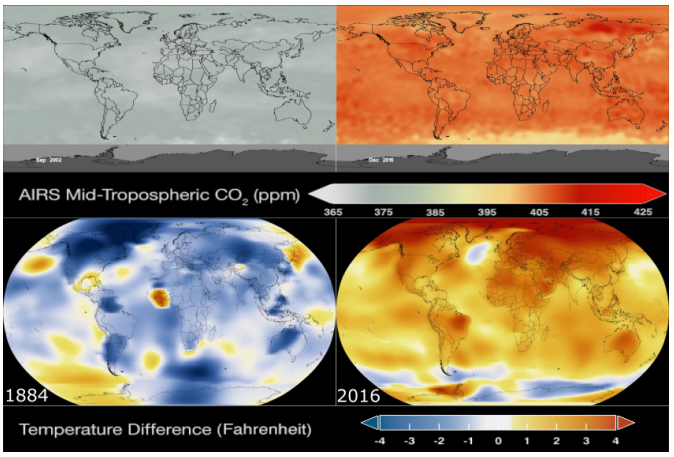

FIGURE 1.1: Distribution of CO_2 concentration at altitudes 1.9 - 8 miles (above) and global temperature variation (below). NASA [2016]

separately, the materials selected for key cell components and their defects affect the performance, controllability, and response time of the cell's control system.

1.1 Problem Statement

The average global temperature, according to NASA [2016] reports, has increased 0.87°C with respect to the average temperature of the years 1951 - 1980, with substantial increases in CO_2 levels in the atmosphere as can be seen in Figure 1.1. One of the main contributors of these CO_2 emissions are the power generation systems.

About 81% of the energy sources used by humanity in 2014 were obtained from coal, natural gas, and oil. The trend is worrying, from 1973 to 2014, humanity has doubled its fossil fuel dependency (see Figure 1.2 from International Energy Agency [2016]) from 6101 Mtoe to 13699 Mtoe in four decades.

Electricity consumption in the last four decades has increased about four times, representing 18.1% of total world energy consumption in 2014 compared to 9.4% in 1973 (see Figure 1.3). This means that it is necessary to improve the technologies for the generation and storage of electrical energy, especially those that have a sustainable operation and whose negative impact on the environment is the lowest possible. Fuel cells are a strong alternative for the generation of electrical energy with virtually no harmful emissions. However, they are not as popular due to their high costs, durability, and slow dynamic response.

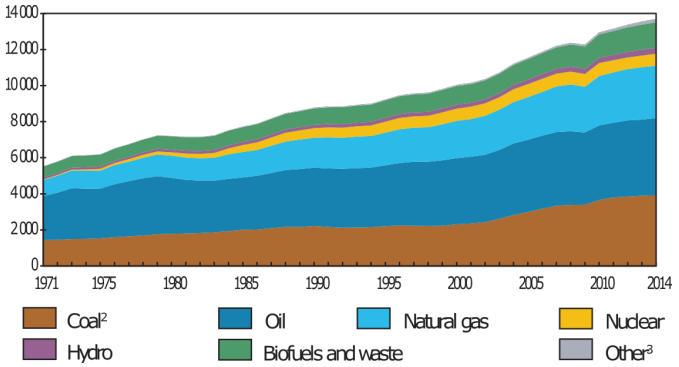

FIGURE 1.2: World energy sources from 1971 to 2014 (International Energy Agency [2016])

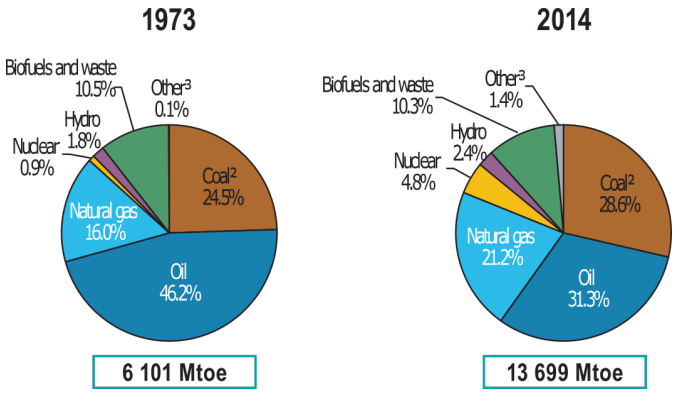

FIGURE 1.3: World Energy Consumption (International Energy Agency [2016])

This research aims to investigate how can the dynamic performance of a fuel cell system be improved in the design stage by selecting appropriated materials that balance performance and controllability without increasing the control system complexity.

Many research works are currently being carried out both in the areas of materials and control systems, however, most of them are not articulated. The review carried out will show that no greater effort has been placed in investigating how the properties of the materials are impacting the dynamic response of the fuel cells.

1.2 Research and Objectives

The main objective of this research is **to design and evaluate a design-for-controllability methodology (including a material selection method) for PEM fuel cells, which considers the effect of electrode surface defects**

in the system dynamic performance. In order to achieve this main objective, the following specific objectives must be completed:

1. develop a system of indicators (or metrics) to jointly evaluate the performance of the fuel cell and its control system.
2. characterize and model the impact of the properties of the constituent materials of the PEMFC in their performance and controllability.
3. characterize and model the impact of channel geometry and moisture-modifying devices on PEMFC performance and controllability.
4. characterize the impact of the surface defects of the constituent materials on the performance and controllability of the PEMFCs.
5. design a methodology for the selection of materials in the cell which integrates economic, performance, and controllability criteria.

1.3 Research originality

This research has the following contributions:

1. a parametric electrochemical model for PEM fuel cell which considers material properties.
2. a characterization of the effect of material properties on the system dynamic response and its controllability characterization.
3. a characterization of the effect of surface defect on the system dynamic response and its controllability characterization.
4. a design for controllability methodology for PEM fuel cells.

1.4 Methodology

Based on the objectives mentioned above, the methodology used is as follows:

Phase 1: Parametric Electrochemical Model for PEMFC
In this phase, a 1D analytical model that represents the dynamic response of a fuel cell is proposed. The model is used to evaluate the impact of the properties of the materials that constitute the different components of the cell on its dynamic response in order to carry out a controllability analysis of the system and evaluate the performance of different control strategies.

The model consists of three nuclear components: (1) mass transfer model, (2) thermodynamic model, and (3) electrochemical model of the cell. Finally, in this phase, it is determined which are the variables that have the major theoretical impact on the fuel cell performance and the region where its response is optimal.

Phase 2: Design of a Test Bench to assess material impact
A test bench was designed to allow the characterization of a laboratory-scale PEM fuel cell. The process will include the sizing and selection of commercial equipment, instrumentation, fuel cells, and their membrane electrode assemblies (MEA), the data acquisition system, the gas supply system (air and hydrogen), and connections. The humidification system for the air pipeline was designed and manufactured.

Phase 3: Assessment of Materials Properties
To evaluate the fuel cell response in both steady and transient states, the data acquisition system was used. The steady-state test seeks to obtain the fuel cell polarization and power curves for different configurations and operational conditions. From the dynamic response of the cell, information was obtained to identify dynamic parameters like the time constants and settling times.

Experiments were designed to evaluate the impact of the fuel cell components on their dynamic response, both when their point of operation changes and when the load changes. The dynamics of the system will be crucial in the performance of control strategies. There are several components that in previous literature studies have been shown to have a significant impact on cell performance, such as channel design Catlin et al. [2011], because they affect the current distribution of the collecting plates, and the membrane, especially its moisture content Das and Weber [2013], Zhou et al. [2007].

Phase 4: Assessment of Materials Surface Defects
Using the same approach used in phase 3, with Microscope inspections defects are addressed, and its impact on dynamic performance is quantified. Experimentation

is used to identify defects on the GDL that have a significant impact on fuel cell performance.

Phase 5: Design of the Methodology
The information related to properties of the constituent materials of the fuel cell is correlated with its impact on the controllability using easy-to-read visual tools that facilitate the selection process of materials. Finally, each step of the methodology will be explained, and guidelines will be included to facilitate its use during the process of design and selection of PEM fuel cell materials.

1.5 Thesis Outline

In this chapter, it has been explained what the problem to be solved is, as well as the methodology proposed to complete the objectives. The rest of the document is divided as follows:

Chapter 2: The current status of the fuel cells and their evolution throughout history is briefly shown. It focuses mainly on PEM stationary fuel cells. It also includes a brief review of nonlinear control strategies and current trends in energy conversion systems.

Chapter 3: The parametric model is fully detailed and tested. All the parameters for its correct operation are included.

Chapter 4: Dynamic response of the fuel cell is linked to material properties. Test bench characterization is used to validate the dynamic model predictions. The use of advanced characterization techniques for the GDL morphology study is shown. The relation between the GDL morphology and the fuel cell performance is explained. In this chapter, it is also presented the design of the test bench used for the experimental stages.

Chapter 5: Dynamics variables correlations are developed using a DOE approach. It includes design, operation, and disturbances variables.

Chapter 6: A DFC methodology is proposed to merge the material selection process with the system dynamic response data obtained in the firsts stages of the research.

Chapter 7: Conclusions

Chapter 8: Future work

Chapter 2

Fuel Cell Technology and Control Background

The need to find new energy sources as an alternative to fossil fuels has boosted fuel cell research, mainly because of their low (almost zero) emission levels and high efficiencies [Wang et al., 2011]. The development of new materials that reduce prices, improve durability, and control strategies that allow operating them in regions of maximum performance are areas of interest at present. This literature review includes the current state of the technology of fuel cells in general, followed by a review focused on the low-temperature PEM fuel cells and, finally it includes a review of the most commonly used techniques for the identification and control of PEM fuel cell systems.

Fuel cells share features with the batteries that convert chemical energy into electrical energy and with the engines which produce energy continuously consuming some fuel. Unlike a battery, a fuel cell does not need to charge, and unlike the engines, they work quietly and efficiently. Furthermore, as the fuel is hydrogen they only generate energy and water, that is why they are also called *"zero emission engine"*[Hoogers, 2003]

2.1 Fuel Cell History

Fuel Cells principles studies began in the XIX century. These are some of the milestones the technology has had [1].

In the XIX century

1801: The principle of what will be called fuel cell (the galvanism) is demonstrated by Sir. Humphry Davy in London [Holmes, 2008].
1839: The first fuel cell, the "Gas Battery" is invented by William Groove[Grove, 1839]
1889: Ludwig Mond and his assistant Charles Langer improved the "Gas Battery" invented by William Groove and the name "fuel cell" was coined. [SAE, 2016].
1893: Friedrich Wilhelm Ostwald provided the fundamentals to understand the role of the components of the fuel cells (electrodes, electrolyte, oxidizing and others)

In the XX century

1950's: The PEMFC is invented in General Electric by William Thomas Grubb (1955) and improved by Leonard Niedrach also in General Electric (1958). Francis Bacon worked on a 6 kW alkaline fuel cell (1959)
1960's: For the first time the NASA uses a fuel cell in a space mission (Apollo mission) (1964) and also for the Gemini Project (1965)
1970's: The PAFC is developed. The principle dates from Groove experiments, but it was until researches at Los Alamos National Laboratory designed a golf cart powered by a phosphoric acid fuel cell. In 1979 Ballard Power System was founded
1980's: Naval applications of the fuel cell in submarines. In Japan began the *Moonlight Project* one of the largest fuel cell research programs (1981)
1990's: Stationary power supply for commercial applications and transportation.

In the XXI century

2000's: Improvements in efficiency and durability. Applications on electric vehicles. PEMFC and DMFC dominate the market. In 2005 a world record was

[1] Where is not stated in this section the reference is FuelCellToday and Cleveland and Morris [2014]

established (a vehicle with 5,285 km per liter of gasoline performance) by the *Swiss Federal Institute of Technology*. Also, a PEMFC based system powered an airplane (2008).

2.2 Fuel Cell Types

Fuel cells are clasified based on the electrolyte they use. The change in the electrolyte will affect the chemical reactions that take place in the cell, the operation temperature, and the fuel.

- Alkaline Fuel Cell (AFC)
- Phosphoric Acid Fuel Cell (PAFC)
- Molten Carbonate Fuel Cell (MCFC)
- Solid Oxide Fuel Cell (SOFC)
- Direct Methanol Fuel Cell (DMFC)
- Proton Exchange Membrane Fuel Cell (PEMFC)

2.2.1 Alkaline Fuel Cell (AFC)

AFCs are one of the earliest fuel cells, developed in the middle of the XX century, although the technology dates back to the 30s. NASA improved it for the space mission Apollo. This type of fuel cells is one of the most open ranged fuel cell, which can operate within a wide range of conditions, and use several catalysts like Pt, Au, and Ni. The reactions in the anode and cathode are:

Anode reaction:

$$H_2 + 2OH^- \rightarrow 2H_2O + 2e^- \tag{2.1}$$

Cathode reaction:

$$O_2 + 2H_2O + 4e^- \rightarrow 4OH^- \tag{2.2}$$

The electrolyte used is potassium hydroxide, which is an advantage due to its low cost, but it has a significant challenge: intolerance to CO_2.

2.2.2 Phosphoric Acid Fuel Cell (PAFC)

Developed in the 1970s, as it said by its name, the electrolyte used in this type of fuel cell is phosphoric acid. They are middle range cells with powers ranging between 50 kW and 1 MW. The reactions in the anode and cathode are:

Anode reaction:

$$H_2 \rightarrow 2H^+ + 2e^- \tag{2.3}$$

Cathode reaction:

$$2H^+ + \frac{1}{2}O_2 + 2e^- \rightarrow H_2O \tag{2.4}$$

One crucial advantage of PAFC is the ability to operate in the presence of CO; that is why this fuel cell type can use different fuels without a complex CO cleaning system. It has some challenges, including the warmup time (the electrolyte is not conductive below 160°C [Mench, 2008]

2.2.3 Molten Carbonate Fuel Cell (MCFC)

These are cells designed for stationary or maritime applications where the size and slow star up of these cells is acceptable.The reactions in the anode and cathode are:

Anode reaction:

$$H_2 + CO_3^{2-} \rightarrow H_2O + CO_2 + 2e^- \tag{2.5}$$

Cathode reaction:

$$O_2 + 2CO_2 + 4e^- \rightarrow 2CO_3^{2-} \tag{2.6}$$

Unlike other fuel cells, the MCFC uses CO as fuel (it is usually a poison), then it does not require a hydrogen infrastructure, and due to the high operation temperature (about 650°) it does not require noble metals catalysts. [Mench, 2008]. The maintenance and durability are still challenges for these cells applications.

2.2.4 Solid Oxide Fuel Cell (SOFC)

SOFCs are one of the more efficient energy conversion devices [Singhal et al., 2003]. Their power ranges between 5 kW and 3 MW in stationary applications and between 1 kW and 5 KW in auxiliary power systems used in vehicles. There are different geometries, including planar and tubular designs. The reactions in the anode and cathode are:

Anode reaction:

$$H_2 + O_2^{2-} \rightarrow H_2O + 2e^- \tag{2.7}$$

Cathode reaction:

$$O_2 + 4e^- \rightarrow 2O^{2-} \tag{2.8}$$

Due to the high operation temperatures (800-1000°), there is no need for noble-metal catalysts, and therefore, the cost is lower. Also, the high temperatures make it possible to use the waste heat in a cogeneration system, increasing the system efficiency [Mench, 2008]. The thermal stress in the materials is still a challenge.

2.2.5 Direct Methanol Fuel Cell (DMFC)

Unlike the other fuel cells, this cells uses liquid fuel (a solution of methanol and water) which have a global reaction with the form $H_2 + \frac{1}{2}O_2 \rightarrow H_2O$, the global electrochemical reaction in a DMFC is:

$$CH_3OH + \frac{3}{2}O_2 \rightarrow 2H_2O + CO_2 \tag{2.9}$$

And the reactions in the anode and cathode are:

Anode reaction:

$$CH_3OH + H_2O \rightarrow 6e^- + 6H^+ + CO_2 \tag{2.10}$$

Cathode reaction:

$$6H^+ + \frac{3}{2}O_2 + 6e^- \rightarrow 3H_2O \tag{2.11}$$

The use of a liquid fuel reduce the energy loss in the flow, compared with a gas flow [Mench, 2008] and simplify the storage, requiring smaller containers. There is also a complete distribution infrastructure for methanol; for the hydrogen, this is still a challenge. Methanol toxicity is an issue.

2.2.6 Proton Exchange Membrane (PEMFC)

These are one of the most promising technologies. Due to their low operation temperature, they can power stationary, transportation, or mobile applications. Equations 2.12 and 2.13 define the reactions taking place inside the cell. There is a reduction reaction in the cathode and oxidation reaction in the anode.

Anode reaction:

$$H_2 \rightarrow 2H^+ + 2e^- \tag{2.12}$$

The Hydrogen Oxidation Reaction (HOR) taking place in the anode side split the hydrogen molecule. The proton will now travel through the polymeric membrane, while an external circuit which includes the load collects the electrons.

Cathode reaction:

$$O_2 + 4H^+ + 4e^- \rightarrow 2H_2O \tag{2.13}$$

In the cathode side, the Oxygen Reduction Reaction takes place, there, the oxygen molecules react with the hydrogen protons coming from the anode side and with the electrons coming from the load circuit to form water.

Figure 2.1 shows the main components of a PEMFC. Each one o the components requires materials with specific properties and configurations that affect the cell performance. The main components are:

1. Membrane
2. GDL (including the catalyst layer)
3. Gas distribution channels
4. Sealing materials[2]

[2]This is beyond the scope of this investigation

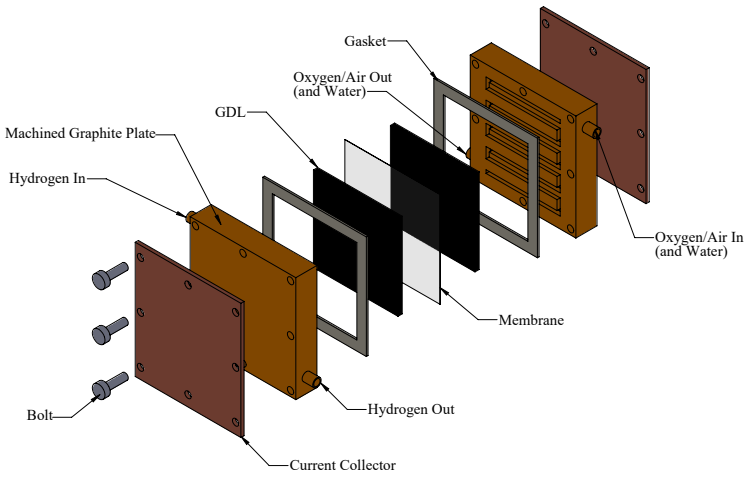

FIGURE 2.1: Simplified schematic of a PEMFC

2.2.6.1 Flow Field Channels

According to [Zhang et al., 2013] this component is responsible for multiple functions:

1. providing gas channels with their respective electrodes
2. provide channels to remove moisture in the cell
3. provides mechanical support to the electrodes.
4. operate as a current collector.
5. electrically connect a cell with the contiguous cell inside a stack of fuel cells
6. serves as a separator between the flows of the reactive gases; avoids that the hydrogen mixes with the oxygen and with the cooling fluids.

The design of these patterns is a complex process due to the high interaction of electrochemical, mass transfer, and heat transfer phenomena. Figure 2.2 shows some of the commonly used designs. Each one of them has its advantages and disadvantages in terms of pressure drops, condensate removal, machinability, cost, and reagent distribution.

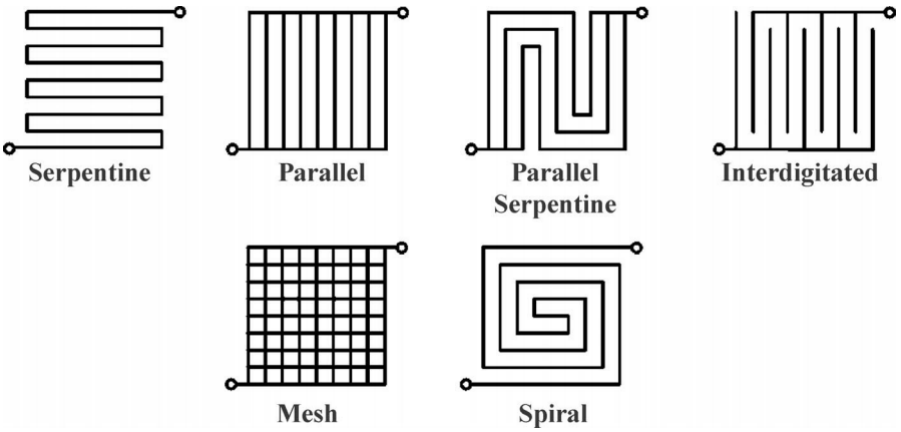

FIGURE 2.2: Flow field design used in the distribution channels [Mench, 2008]

2.2.6.2 Gas Diffusion Layer (GDL)

Inside a fuel cell are located two GDLs, one located on the anode side and the other located on the cathode side. Being a porous media serves mainly as a support for the catalyst as well as media for the flow of gases and water. According to [Park et al., 2012], typically the GDLs are manufactured with carbon-based materials since they are stable in acidic media and provide high gas permeability and good electrical conductivity.

The use of catalysts (typically platinum-based) is a prerequisite for oxidizing the hydrogen at the anode and reducing oxygen at the cathode, especially in the latter, where the reaction rate is usually lower. They must be designed to minimize the amount of the required catalyst. Ideally, this layer should:

1. maximize the active area
2. minimize obstacles that restrict the flow of reactants to the catalyst
3. allow the flow of protons
4. facilitate the removal of moisture

2.2.6.3 Membrane

The membrane of the fuel cell is the nuclear component and is the electrolyte of the fuel cell and is at the same time alongside the catalyst most of the cost of the system. The “iron triangle” (performance, durability, and cost) as K. Martin and

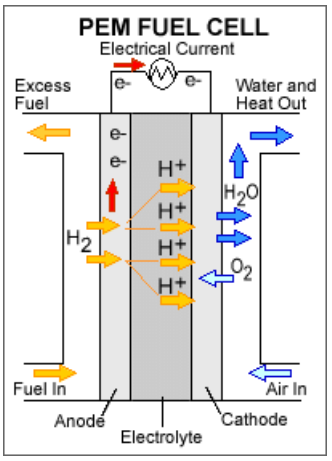

FIGURE 2.3: Simplified reactions inside a PEMFC [EERE, 2016]

J. Kopasz[Martin and Kopasz, 2010] call it is the main research objective. The ionic exchange membrane usually made of Nafion^{TM}, which is a perfluorosulfonic acid polymer (see Figure 2.4) made by Dupont. A membrane suitable for use in a fuel cell must have the following characteristics:

1. High proton conductivity. The membrane has to allow the H^+ to cross from the anode side to the cathode side to complete the reaction.

2. Thermal and mechanical stability. The membrane mechanical properties have to allow the polymer to form films that can sustain stress due to change in reactants pressures and temperatures.

3. Electronic insulator. Figure 2.3 shows that the electrons need to follow a specific path through the collectors and the load to avoid a short circuit in the cell.

4. Act as a physical barrier to the reactants. The thermodynamic activity difference between the anode and the cathode induce the voltage potential difference [Mench, 2008]

2.3 PEMFC Literature Review

With an automated review of nearly 5000 publications included in Web of Science, the network shown in figure 2.5, it shows that the major areas of research related to fuel cells are modeling, research into new membrane materials, catalysts and

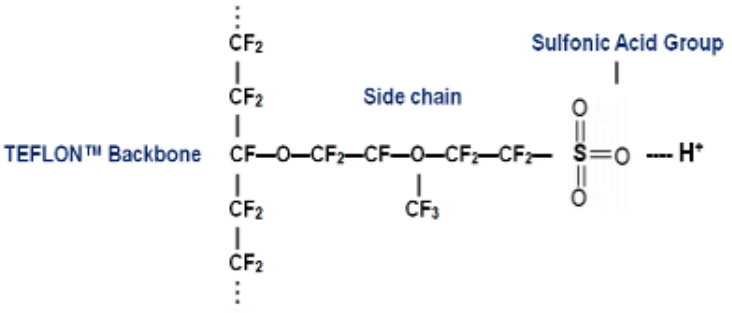

FIGURE 2.4: Nafion^{TM} molecule [Nafion Store, 2016]

the integration of systems including control strategies, hydrogen production and storage systems, auxiliary equipment and costs.

The areas of most significant development in fuel cells have been in the automotive sector and in the area of portable devices for domestic use and the commercial sector [Cele et al., 2010] although there are barriers limiting the incursion of fuel cells [Cottrell et al., 2011, Wang, 2015]. The **first barrier** is mainly technical limitations associated with the durability and reliability of the components, not only the cell but also the auxiliary equipment required for operation (sensors, controllers, power output conditioning system, and moisture modifiers equipment), the storage system still requires much research so that the autonomy of the systems increase. The **second barrier** is the cost; this is perhaps one of the main limitations for fuel cells can compete in the market of power generation systems. The **third barrier** to consider is the fuel flexibility in what can be called as "hydrogen economy", i.e., it is required to develop an entire infrastructure to ensure the availability of hydrogen, similar to what happens with oil and its derivatives. Finally, and not least, the **fourth barrier** is public acceptance. The perception of people who are

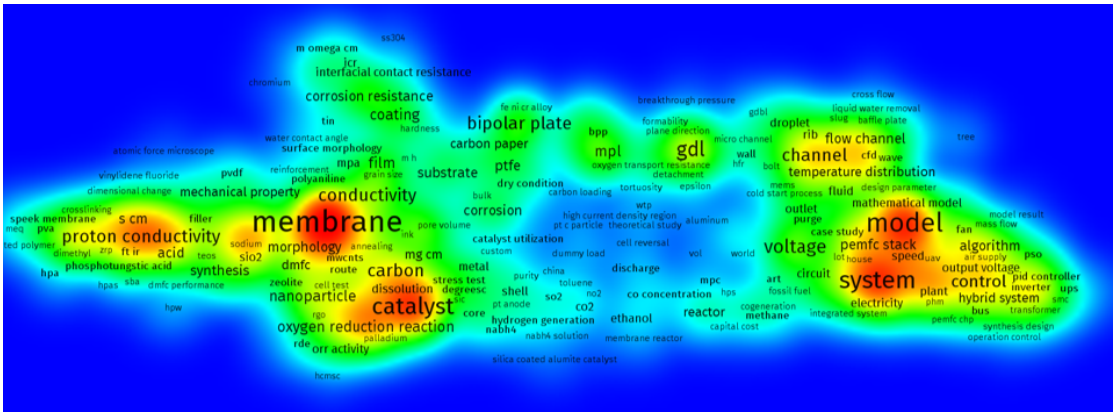

FIGURE 2.5: State of the art research areas

not familiar with this type of energy sources is that technologies using hydrogen are not safe for use by the average citizen, it is, therefore, necessary to sensitize them in order to change the perception.

In the case of the flow channels geometry, [Manso et al., 2012] present a comprehensive review of various studies until 2012. This study evidence that one of the primary goals is to find geometries that guarantee a better uniformity in the distribution of gases, i.e., arrangements that maintain restrictions as possible uniform flow and operating conditions that allow avoiding possible two-phase flow (avoid condensation of moisture).

2.3.1 Membrane

There are three research areas related to membranes. **the first** is modified Nafion^{TM} membranes in which polymer chains are modified by adding, for example, the sulfonic acid group $-CF_2SO_3H$. **the second** is non-fluorinated membranes typically made from aromatic structures as benzene, which stand as promising options due to their lower costs compared with Nafion membranes. Finally, **the third** group corresponds to composite acid-base membranes, i.e., membranes that incorporate an acid component in an alkaline membrane, this latter type of membranes has a great conductivity at high temperatures without suffering from the problems of dehydration suffered for example by Nafion^{TM} membranes.

2.3.2 Gas Diffusion Layer (GDL)

The GDL consists of two large zones (excluding the catalyst) which are (1) a macroporous layer and (2) a microporous layer; both regions are currently of interest for research. Several additives are being tested as well as support materials and catalyst types and loadings in order to improve the achievement of the GDL requirements indicated in section 2.2.6.2.

2.3.3 Dynamic Modeling and Control

In order to analyze the fuel cell dynamics many models have been developed with different levels of complexity, this complexity depends on the number of volumes

considered within the cell, the analyzed physical phenomena and dimensions into consideration. In general, the models can be used to test advanced control strategies and optimize cell performance. It is important to validate the models through experimentation under different operating conditions [Ziogou et al., 2013]. It is crucial that the model properly represent the fuel cell nonlinearities since these are the challenge in designing a control system [Meidanshahi and Karimi, 2012]. A 1D dynamic model was proposed by [Ziogou et al., 2011]. It takes into account the mass dynamics under the assumption the gases follow the ideal gas laws. It also includes a detailed water transport model, a thermal analysis, and a semi-empirical electrochemical model with parameters estimated from experimental data.

The fuel cell itself alone is not enough because the output is DC; therefore, the system includes DC-DC and DC-AC converters. [Al-dabbagh et al., 2010] present a dynamic model that includes those auxiliary systems and the control system they require, in this particular case a fuzzy logic controller for the DC-DC converter and a Pulse Width Modulation (PWM) for the DC-AC converter. Different strategies have been proposed to improve control of the fuel cells. There are many control objectives in a fuel cell system, and different strategies have been used to accomplish them.

Different strategies have been proposed to improve the control of fuel cells, taking into account the different control objectives within the system, each of them with their specific requirements.

1. Stack/Fuel Cell temperature.
2. Stack/Fuel Cell pressure
3. Power
4. Voltage
5. Reactant supply
6. Membrane conductivity

2.3.3.1 Stack/Fuel Cell Temperature

The temperature of the system needs to be regulated because it could decrease the durability of the fuel cell [Cheng et al., 2015]. The temperature is also related

to the cell potential and water balance. It is usual to control the temperature as a dependent variable, for example, [Panos et al., 2012] designed an MPC to control the fuel cell voltage, but at the same time controls the fuel cell temperature. Classic control strategies like PID regulates the temperature, while an MPC controls variables like power and excess ratios [Ziogou et al., 2013]. This approach is possible due to the slow dynamics of temperature. This strategy also works in mobile applications like buses. [Cheng et al., 2015] proposes a strategy that includes a state feedback controller with a feedforward module that monitors the stack current and voltage and the ambient temperature to help the feedback loop control of the fuel cell cooling system.

2.3.3.2 Stack/Fuel Cell Pressure

During the transients, it is possible that the pressure in anode and cathode to be different. This difference could damage the membrane; therefore, there is a control loop for the pressures or the pressure difference. [Matraji et al., 2012] used a second order sliding MIMO controller under the assumptions of uniform and constant temperature inside the fuel cell stack, proper humidification and the gases behave like an ideal gas.

2.3.3.3 Power

Power generation is the main purpose of a power source; a fuel cell is meant to provide the necessary power to operate a load. The fuel cell alone is not usually enough to operate a dynamic load. Therefore, the system includes batteries and supercapacitors to sustain the FC power output during the transients. Those hybrid systems need intelligent systems that switch from a power source to another. In other scenarios, the FC is the back like in work presented by [Hatti et al., 2011] where the main generator is a photovoltaic generator, and the support is a PEMFC, and the two generators can operate in parallel. A challenge in this hybrid systems is the change of the system itself when the switch between a power source to another happens, at that moment the whole dynamic changes and the control system has to be able to adapt to that change. As is stated by Hatti, an option is the use of artificial neural network called Maximum Power Point Tracker (MPPT) in order to adjust the system when the solar irradiation changes, and to complete the transition from a generator to another power source. The system requires a

control layer that manages the flow of energy. This system takes into consideration the different variables that can affect the system, like the weather, the load, among others, in the end, it will determine which power source should be active at any moment of the operation, trying to use the fuel cell the minimum time possible along the day. The power of the system is proportional to the voltage and the current $P = VI$. In the case of fuel cells, the voltage range is narrow and strongly related to other variables of the system, that is a reason to consider the current as an indirect control variable to the power through the auxiliary conditioning systems like the DC/DC converters [Segura et al., 2011].

2.3.3.4 Voltage

The fuel cell voltage relates strongly to the current demanded by the load. The polarization curve represents that relataionship in a voltage vs. current plot, which starts with the theoretical cell potential followed by the different potential drops (activation, ohmic, and concentration). After developing a dynamic model and its simplified version using state space model representation, [Panos et al., 2012] propose a multi-parametric model predictive controller which controls the voltage and the temperature manipulating the coolant mass flow rate and its temperature and the voltage of the compressor used to feed the air required for the cell.

2.3.3.5 Supply of Reagents

Usually, there are mass flow controllers installed on each line (oxygen and hydrogen), but the real problem is to define the mass flow required to operate within the safe zone of the fuel cell. There must always be a reactant excess in the fuel cell to avoid the "starvation" phenomena which could cause irreversible damage in the cell, reducing its performance, and durability. Starvation is a significant problem during transients [Sanchez et al., 2014], where sudden changes in the load (current) require a rapid response in the mass flow control loop. The use of supercapacitors is another way to protect the PEMFC against "starvation" during the transients [Zhan et al., 2012], but this requires a MIMO control strategy that involves a power switching control in order to supply the lacking power of the PEMFC from the batteries.

2.3.3.6 Membrane conductivity and Humidity

Membrane humidity is a temperature and water content dependant property [Fărcaş and Dobra, 2014] and a highly non-linear key factor in the performance of the fuel cell. Farcas proposed an adaptive controller using two PID with adaptation rules based on gain scheduling method, which is required due to the high nonlinearities in the relationship between temperature, humidity, and conductivity.

TABLE 2.1: Modeling and Control Previous Studies

	Fuel Cell Dynamic Model		Control		Optimization	Experimental Validation	Reference
			Strategy	Objective			
1	Analytical	Fluid dynamics Thermodynamics Electrochemical static model	Mamdani Fuzzy Control	Power density	Differential Evolution	No	Meidanshahi and Karimi [2012]
2	Analytical (Space State)	Fluid dynamics Thermodynamics Electrochemical static model	Constrained MPC	Voltage Temperature	Off Line QP	Yes	Panos et al. [2012]
3	No	-	Adaptive (Fuzzy) neural-network	Optimal Air Supply	On-Line Instantaneous learning rule	Yes	Sanchez et al. [2014]
4	Analytical (Transfer Functions)	Electrochemical static model	2 PID with direct gain scheduling	Membrane Conductivity	-	No	Fărcaş and Dobra [2014]
5	No	-	sliding mode control	Power	-	Yes	Kunusch et al. [2013]

Continued on next page

TABLE 2.1: Modeling and Control Previous Studies

	Fuel Cell Dynamic Model		Control		Optimization	Experimental Validation	Reference
			Strategy	**Objective**			
6	Analytical (Simplified)	Electrochemical static model Auxiliary Systems Fluid dynamics	Static-feedforward LQR optimal control Gain-scheduling	Voltage Oxygen excess ratio	LQR	Yes	Özbek et al. [2013]
7	Analytical (Simplified)	Thermodynamics Electrochemical static model Auxiliary Systems Fluid dynamics	Feedforward fuzzy PID	Oxygen excess ratio	Fuzzy optimization	Yes (Electrochemical model)	Ou et al. [2015]
8	Analytical	Thermodynamics Electrochemical static model Auxiliary Systems	Non linear MPC	Oxygen excess ratio	Sequential quadratic programming	Yes	Schultze and Horn [2016]
9	Analytical (Simplified cooling system)	Electrochemical static model Auxiliary Systems	Feedforward and state feedback	Temperature	LQR	Yes	Cheng et al. [2015]

Continued on next page

TABLE 2.1: Modeling and Control Previous Studies

	Fuel Cell Dynamic Model		Control				
			Strategy	**Objective**	**Optimization**	**Experimental Validation**	**Reference**
10	Analytical (Simplified)	Fluid dynamics Electrochemical static model	PID (Temperature and Humidity) Non linear MPC (Power and Excess ratios) second order sliding mode multi-input multi-output (MIMO)	Temperature Humidity Power Reactant excess ratio	reduced gradient based solver (MINOS) quasi-Newton algorithm	Yes	Ziogou et al. [2013]
11	Analytical	Fluid dynamics Electrochemical static model		Pressure difference	-	No	Matraji et al. [2012]
12	Analytical (s domain)	Fluid dynamics Thermodynamics Electrochemical static model Power Converters Battery	PID (Pressure) Fuzzy PI (H2 mass flow) Pi + logic selection of control law (Air mass flow)	Power	-	Yes	Zhan et al. [2012]

Continued on next page

Table 2.1: Modeling and Control Previous Studies

	Fuel Cell Dynamic Model		Control		Optimization	Experimental Validation	Reference
			Strategy	**Objective**			
13	Analytical	Fluid dynamics Thermodynamics Electrochemical static model Auxiliary Systems	-	-	-	Yes	Ziogou et al. [2011]
14	Analytical (simplified)	Basic power calculations	MPTT method neural network	Power	-	No (Simulation with experimental input data)	Hatti et al. [2011]
15	No	-	Analog control	Current	-	Yes	Segura et al. [2011]

Concluded

2.4 Controllability Theory

Controllability is an essential feature of a control system and is one of the most important concepts of modern control theory. In a very general way, one can say that:

"...a controllable system is a system in which the state variables can be driven to any position with a finite value of performance measure..." Müller and Schiehlen [1985]

A system defined by:

$$\begin{aligned} \dot{x} &= Ax + Bu \\ y &= Cx \end{aligned} \tag{2.14}$$

where,
x : state vector [n dimensional]
u : control vector [r dimensional]
y : output vector [p dimensional]
A,B,C: matrices of dimensions [n x n, n x r, p x n]

According to Kalman [1959], Müller and Schiehlen [1985], the system will be controllable if the system is in a state x_0 at time $t = 0$, then for a finite time $T > 0$ there is a control signal $u(t), t \in [0, T]$ such that $x(T) = 0$.

Kalman [1959], Müller and Schiehlen [1985], Pickl and Krabs [2010] state that the solution of equation 2.14, with $x(0) = x_0$ is of the form:

$$x(t) = e^{tA}\left(x_0 + \int_0^t e^{-sA}Bu(s)ds\right), \; t \in \mathbb{R} \tag{2.15}$$

According to Kalman [1970], the desired state of the plant is identical to zero for all t. Also, for the system to be controllable Kalman criteria must be met

$$rank\left(B|AB|\ldots|A^{n-1}B\right) = n \tag{2.16}$$

The range of the matrix is the number of linearly independent rows, which is usually estimated using the SVD (singular value decomposition) method.

The controllability analysis is not limited to whether the system is controllable or not, but also to evaluate how well the control system performs. As stated by Smith and Corripio [2005], some parameters that can be taken into account to analyze the system response are the following:

1. Percentage of the time that the controllers are saturated
2. Standard deviation of the controlled variable
3. IAE (Integral Absolute Error)
4. Rise time and Settling time.
5. Overshoot

2.5 Materials Characterization Techniques

Many experimental techniques can be used to have an assessment of the main characteristics of a PEMFC. This research includes data from two techniques, the Brunauer–Emmett–Teller (BET) method, and the x-ray diffraction (XRD).

2.5.1 Braunauer-Emmett-Teller (BET)

This method, developed by Brunauer et al. [1938], is used to characterize powders and porous media.

In figure 2.6, the typical equipment schematic is shown. The sample is cooled down with liquid nitrogen to 72 K, and a well-known mass flow rate of a particular gas goes inside the chamber. Based on the gas absorption, the method can estimate the porosity and pore size distribution of the sample.

2.5.2 X-Ray Difraction (XRD)

It is used to analyze the atomic and molecular structure of a sample. Its use is suggested in the proposed methodology to assure the quality of the catalyst used in the electrodes. In figure 2.7, the principle of operation is shown. The

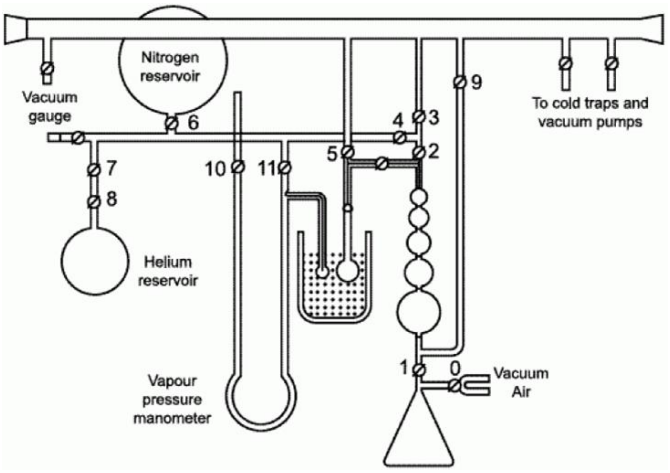

FIGURE 2.6: BET equipment schematic *From: Particle Analytical*

measurement of the diffraction beams angles and their intensities are used to analyze the crystalline structure of the test sample. In literature, typical curves for well know materials can be found and used to verify the materials found in the tested material.

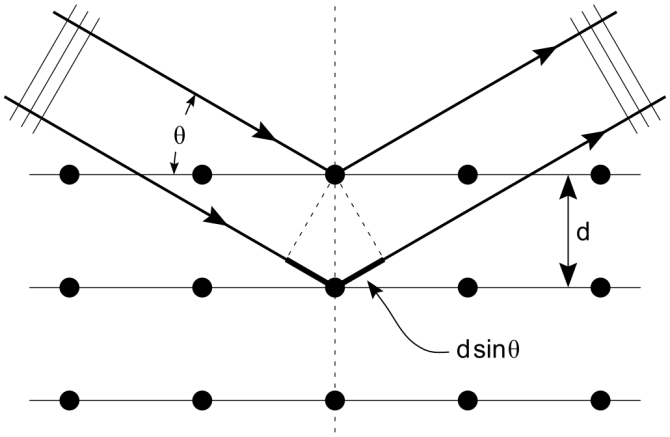

FIGURE 2.7: XRD - Bragg diffraction *From: Hydrargyrum*

Chapter 3

PEM Fuel Cell Modeling

In this chapter includes a 1D parametric model that can be used to simulate the control system using Matlab or similar software. It only includes the main equations (mass and energy balances, and the electrochemical model) for the other equations, please refer to the appendix A.

3.1 1D Model

The fuel cell model is built integrating fluid dynamics, heat transfer, and electrochemical phenomena occurring inside a PEM cell. A fuel cell consists of two electrodes (anode and cathode) separated by a solid electrolyte (polymer membrane).

The Fuel Cell will be analyzed using the following domains (see Figure 3.1): Cathode and Anode (Channels and GDL) and the Membrane.

From Figure 3.2 it can be seen that its main inputs are the heating resistance power fraction (x_R) and the reference temperature T_{ref} which is usually the ambient temperature. This model is linked to the mass transfer model by the mass flows of reagents and byproducts of the electrochemical reaction. The mass transfer model is defined over three main volumes: anode, membrane and cathode. For each one of these volumes mass balances are used to calculate the masses of each species inside them, and also the transfer of water vapor between them. This flow will be defined mainly for the difference of concentrations (strongly related with the partial pressures of the gas p_v^{GDL}) and electro-osmotic drags (N_v^{mem}) through the

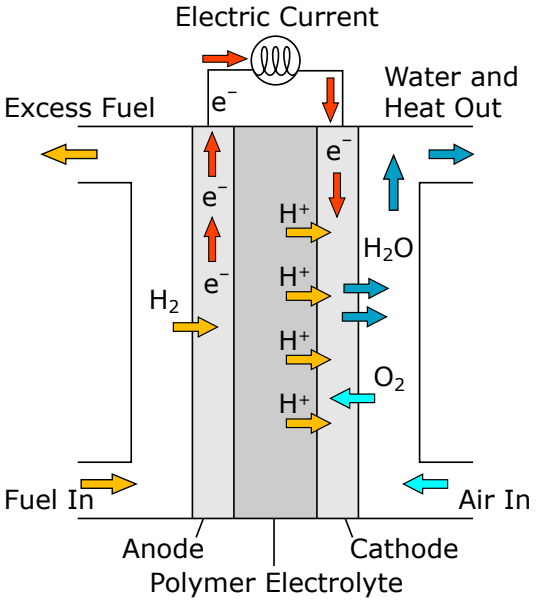

FIGURE 3.1: PEM Fuel Cell Domains

membrane. Also from the mass transfer model the partial pressures of H_2 and O_2 are calculated, which are also linked to the electrochemical model by means of the Nernst equation, used in the cell voltage calculation.

3.1.1 Mass Transfer Model

In each side of the fuel cell, different species are transferred due to inlets and outlets flows and also due to internal mass transfer phenomena, like diffusion and electro-osmotic drags.

3.1.1.1 Mass Balances

The model begins with the mass balances for the internal domains previously defined.

Cathode The mass balances of the different gases (oxygen, nitrogen and water vapor) entering from the cathode side are the following:

For the oxygen

$$\frac{dm_{O_2}^{c,ch}}{dt} = \underbrace{\dot{m}_{O_2,i}^{c,ch}}_{\text{Eq. A.5}} - \underbrace{\dot{m}_{O_2,o}^{c,ch}}_{\text{Eq. A.21}} - \underbrace{\dot{m}_{O_2,reac}^{c,GDL}}_{\text{Eq. 3.14}} \tag{3.1}$$

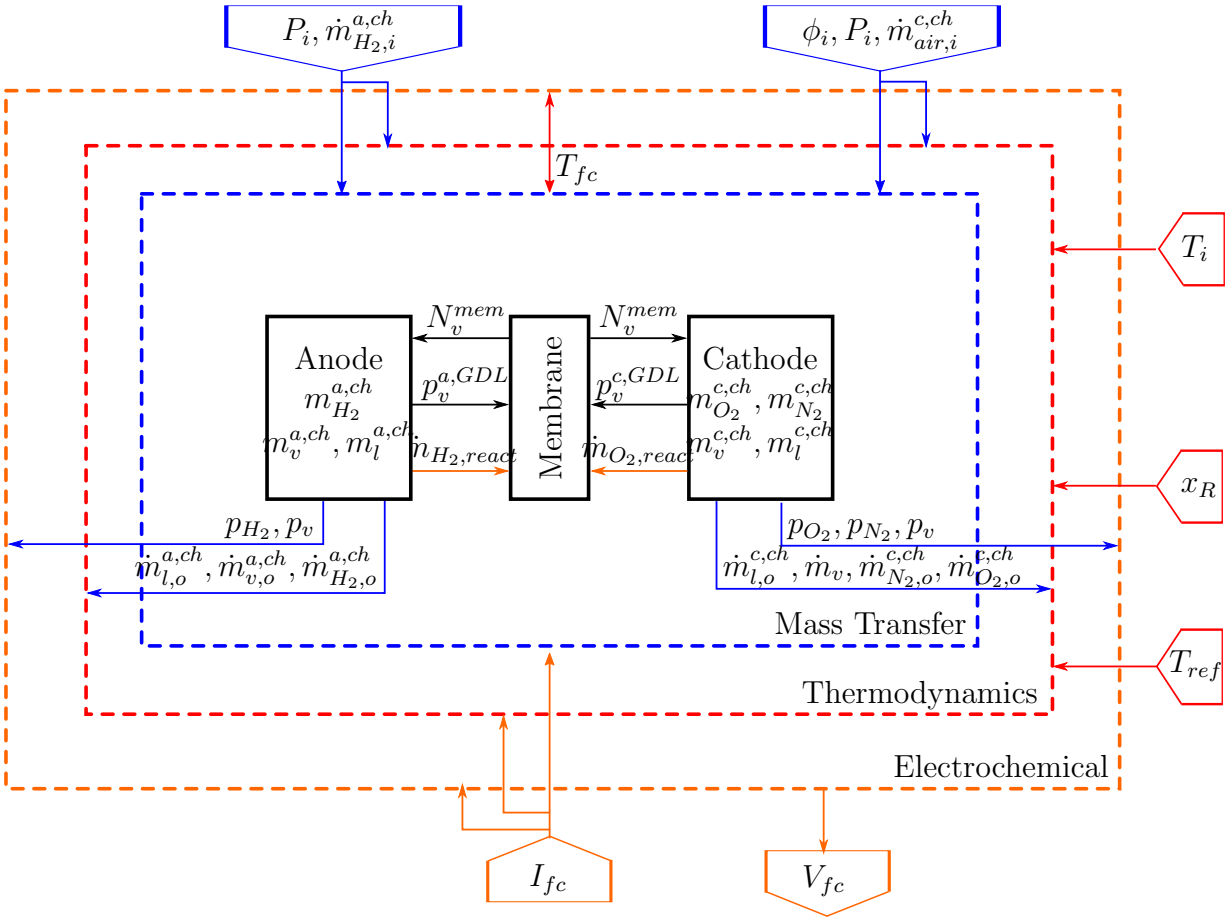

FIGURE 3.2: Fuel cell model diagram

For the nitrogen

$$\frac{dm^{c,ch}_{N_2}}{dt} = \underbrace{\dot{m}^{c,ch}_{N_2,i}}_{\text{Eq. A.6}} - \underbrace{\dot{m}^{c,ch}_{N_2,o}}_{\text{Eq. A.21}} \tag{3.2}$$

For the water vapor

$$\frac{dm^{c,ch}_{v}}{dt} = \underbrace{\dot{m}^{c,ch}_{v,i}}_{\text{Eq. A.4}} - \underbrace{\dot{m}^{c,ch}_{v,o}}_{\text{Eq. A.21}} + \underbrace{\dot{m}^{c,GDL\to c,ch}_{v}}_{\text{Eq. A.9}} + \underbrace{\dot{m}^{c,ch}_{evap}}_{\text{Eq. A.15}} \tag{3.3}$$

For the liquid water

$$\frac{dm^{c,ch}_{l}}{dt} = \dot{m}^{c,ch}_{v,i} - \dot{m}^{c,ch}_{l,o} - \underbrace{\dot{m}^{c,ch}_{evap}}_{\text{Eq. A.15}} + \underbrace{\dot{m}^{c,GDL\to c,ch}_{l}}_{\text{Eq. A.17}} \tag{3.4}$$

Where the terms $\dot{m}^{c,ch}_{v,i}$ and $\dot{m}^{c,ch}_{v,o}$ refer to the mass vapor flows entering and leaving the cell with the feed currents of reagents and discharge currents of the products

respectively. The terms $\dot{m}_v^{c,GDL}$ are due to the diffusion of the water vapor generated in the catalyst layer (where the electrochemical reaction occurs) and that will later be transported by diffusion through the GDL which is a porous medium; the direction of mass transfer will depend on the concentration gradient (see equation A.9). The term $\dot{m}_{evap}^{c,ch}$ is the mass flow of vapor that occurs when the liquid water contained in the cathode evaporates. The model assumes that there is no liquid water entering the fuel cell with the humidified air, i.e., $\dot{m}_{l,i}^{c,ch} = 0$, and that one purge cycle is enough to remove all the liquid water inside the channels. Then, equation A.7 define the liquid water flow leaving the cell.

Membrane The term associated with the flow through the membrane in eq. 3.10 is due to two phenomena (a) an electrochemical drag osmotic and (b) diffusion by the difference of concentrations. It could be modeled according to Ziogou et al. [2011] by means of the following equation:

$$N_v^{mem} = n_d \frac{I}{A_{fc}F} - \alpha_{H_2O} D_{H_2O} \frac{c_v^c - c_v^a}{\delta^{mem}} \tag{3.5}$$

Where the factor n_d is the electro-osmotic drag coefficient defined by Dutta and Shimpalee [2001]. See appendix A for more details.

Anode On the anode side, the fuel (hydrogen) will enter, whose mass balance is as follows:

For Hydrogen:

$$\frac{dm_{H_2}^{a,ch}}{dt} = \dot{m}_{H_2,i}^{a,ch} - \underbrace{\dot{m}_{H_2,o}^{a,ch}}_{\text{Eq. A.40}} - \underbrace{\dot{m}_{H_2,reac}^{a,GDL}}_{\text{Eq. 3.13}} \tag{3.6}$$

For vapor:

$$\frac{dm_v^{a,ch}}{dt} = -\dot{m}_{v,o}^{a,ch} + \underbrace{\dot{m}_v^{a,GDL}}_{\text{Eq. A.33}} + \underbrace{\dot{m}_{evap}^{a,ch}}_{\text{Eq. A.37}} \tag{3.7}$$

For Liquid water:

$$\frac{dm_l^{a,ch}}{dt} = \underbrace{\dot{m}_l^{a,GDL\to a,ch}}_{\text{Eq. A.36}} - \underbrace{\dot{m}_{evap}^{a,ch}}_{\text{Eq. A.37}} - \underbrace{\dot{m}_{l,o}^{a,ch}}_{\text{Eq. A.41}} \tag{3.8}$$

$$\rho_l^{H_2O}\frac{dV_l^{a,GDL}}{dt} = \underbrace{\dot{m}_l^{a,GDL\to c,ch}}_{\text{Eq. A.36}} - \underbrace{\dot{m}_{evap}^{a,GDL}}_{\text{Eq. A.38}} \tag{3.9}$$

3.1.1.2 Pressures

The variations of pressures inside the cell are important since the electrochemical potential depends on them, as well as the integrity of the electrolyte; if the pressures at the anode and the cathode are different, the membrane will sustain stress that could cause damage to its structure. The accumulations and losses in the cell produce pressure changes that, depending on the operating temperatures and the gases contemplated, can be estimated using the ideal gas equation.

Cathode

$$\frac{dp_v^{c,GDL}}{dt} = RT_{fc}\left(\frac{\overbrace{N_v^{mem}}^{\text{Eq. 3.5}} - \overbrace{N_v^{c,GDL\to c,ch}}^{\text{Eq. A.9}} + \overbrace{N_v^{gen}}^{\text{Eq. 3.15}}}{\delta_{GDL}} + \frac{\overbrace{\dot{m}_{evap}^{c,GDL}}^{\text{Eq. A.19}}}{M_{H_2O}V^{GDL}}\right) \tag{3.10}$$

Where N_v^{gen} depends on the load demanded from the cell (see equation 3.15)

Anode

$$\frac{dp_v^{a,GDL}}{dt} = RT_{fc}\left(\frac{\overbrace{N_v^{a,GDL\to c,ch}}^{\text{Eq. A.33}} - \overbrace{N_v^{mem}}^{\text{Eq. 3.5}}}{\delta_{GDL}} + \frac{\overbrace{\dot{m}_{evap}^{a,GDL}}^{\text{Eq. A.38}}}{M_{H_2O}V^{GDL}}\right) \tag{3.11}$$

3.1.2 Heat Transfer Model

The energy balance includes the exothermic electrochemical reaction, and the transfer of heat to the air that passes through the cathode and that surrounds the cell. Based on Dalton's law Müller and Stefanopoulou [2006], the model assumes that the change of the enthalpy in the system is equivalent to the sum of the enthalpies of each gas contained in the fuel cell.

Assuming a uniform distribution, so that the calculations are simplified in the simulation, the following energy balance is proposed.

$$m_{fc}c_{fc}\frac{dT_{fc}}{dt} = \dot{H}^{reac} - \Delta\dot{H}^{pur}_{H_2} - \Delta\dot{H}^{pur}_{H_2O} - \Delta\dot{H}^{cool}_{ma} - \dot{W}^{elec} \tag{3.12}$$

3.1.3 Electrochemical Model

In order to model the electrochemical phenomenon in the fuel cell, the model includes the stoichiometric reagent, and products flow, the theoretical cell potential, and the main voltages drop.

In Figure 3.3 the main electrochemical parameters are shown. A different mechanism governs each voltage drop. A t low loads the polarization is dominated by the activation potential, which is a function of the exchange current (i_0^{ref}), the reference temperature (T_{ref}), the activation energy (ΔG_c^j) and the roughness factor (f_r). In the middle range, ohmic losses are the main source for the potential drop, where the electrical resistance of the materials (r_j) and the conductivity of the membrane (σ^{mem}) operate as series resistances. (σ^{mem}) changes with the humidity levels, therefore, the vapor saturation pressure ($p_{sat}^{H_2O}$) and the vapor partial pressure (p_v) are included in its parameters.

3.1.3.1 Molar Flows

The reagent flows required by the fuel cell are a function of the current demanded by the system as indicated in the Eq. 3.13 and Eq. 3.14. As a product of the reaction, water vapor is generated in the catalyst layer at a rate calculated with Eq. 3.15

$$\dot{m}^{a,GDL}_{H_2,reac} = n_{fc}M_{H_2}\frac{I}{2F} \tag{3.13}$$

$$\dot{m}^{c,GDL}_{O_2,reac} = n_{fc}M_{O_2}\frac{I}{4F} \tag{3.14}$$

$$N^{c,GDL}_{v,reac} = n_{fc}\frac{I}{2F} \tag{3.15}$$

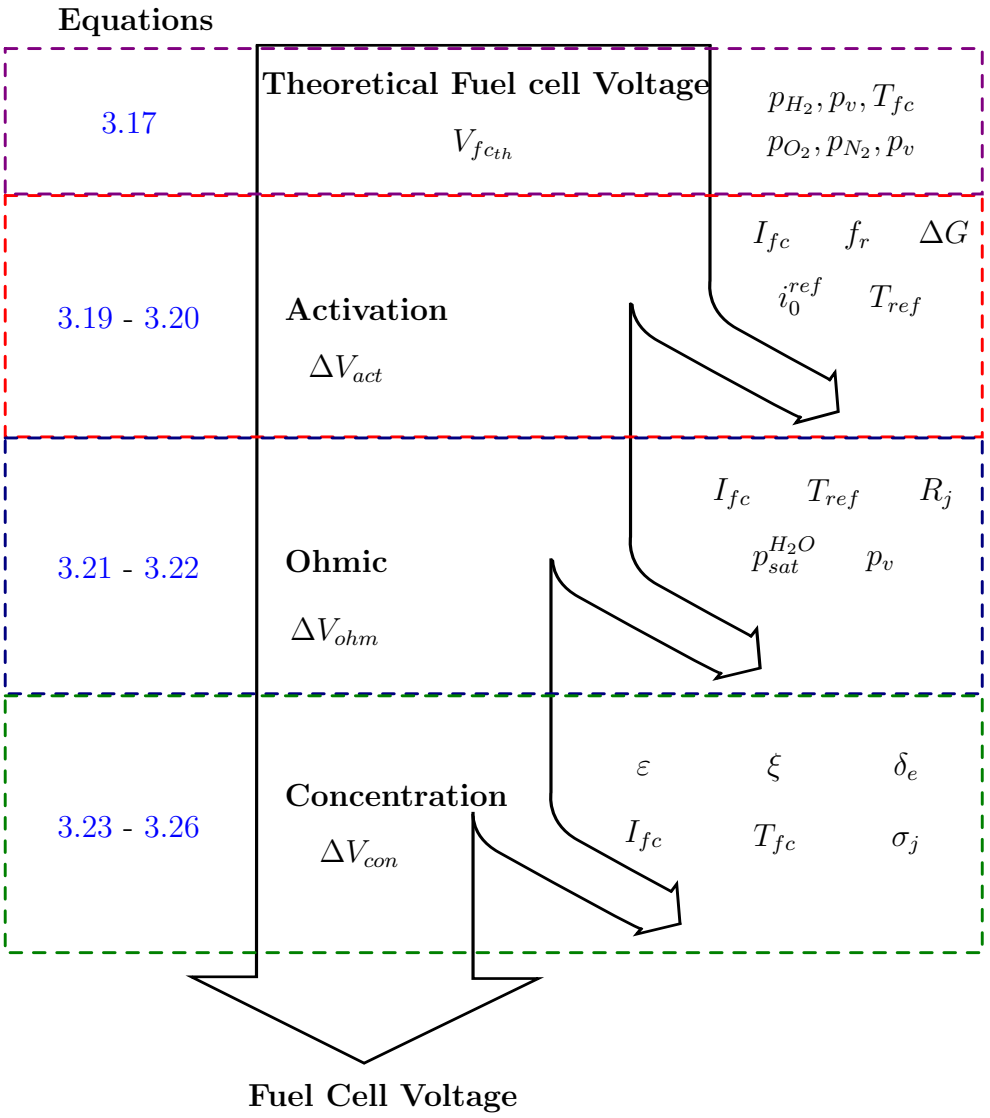

FIGURE 3.3: Fuel cell polarization main parameters; from theoretical potential towards the real output voltage. Operational (pressures p, temperatures T, and load current I), electrochemical (Activation energy ΔG, exchange current i_0^{ref}, electrode roughness f_r and material (electrical resistances R_j, conductivity σ_j, porosity ε, tortuosity ξ), thickness δ_e) parameters

3.1.3.2 Fuel Cell Voltage and Power

The fuel cell voltage, defined in Eq. 3.16, will depend on the theoretical voltage and the polarization voltages due to activation, ohmic and concentration.

$$V_{fc} = V_{fc_{th}} - \Delta V_{act} - \Delta V_{ohm} - \Delta V_{con} \tag{3.16}$$

where, the Nernst equation (Eq. 3.17) define the theoretical voltage as $f(p,T)$

$$V_{fc_{th}} = -\left(\frac{\Delta H}{nF} - \frac{T\Delta S}{nF}\right) + \frac{RT}{nF}\ln\left(\frac{p_{H_2}p_{O_2}^{0.5}}{p_{H_2O}}\right) \tag{3.17}$$

Equation 3.18 calculates the fuel cell power, where I is the current flowing through the fuel cell stack whose cells are connected in series so that all of them have the same current.

$$\dot{W}_{elec} = V_{fc}I \tag{3.18}$$

3.1.3.3 Voltage Drops

The real fuel cell voltage departs from the theoretical potential due to the potential losses described below.

Activation Loss This is the loss due to the energy required to depart the reaction from the equilibrium point. Butler - Volmer equation can be used to represent this potential loss.

$$\Delta V_{act} = \frac{RT}{\alpha_c F}\ln\left(\frac{i}{i_o^c}\right) + \frac{RT}{\alpha_a F}\ln\left(\frac{i}{i_o^a}\right) \tag{3.19}$$

The exchange current density can be calculated using Eq. 3.20. The higher the exchange current density is, the lower the voltage drop will be, and according to Barbir [2013], the roughness factor defined $f_r = L_{cat}a_{cat}$, where (a_{cat}) is the catalyst specific area.

$$i_0^j = a_{cat}L_{cat}\exp\left[-\frac{\Delta G_{cat}^j}{R}\left(\frac{1}{T} - \frac{1}{T_{ref}}\right)\right] i_0^{ref} \qquad \text{for } j = a, c \tag{3.20}$$

Ohmic Loss Conductivity of the materials and their contact induces a voltage drop due to Ohm's law, Eq. 3.21.

$$\Delta V_{ohm} = i\left(r_{ion} + r_e + r_c\right) \tag{3.21}$$

According to Springer et al. [1991] the membrane conductivity can be calculated with Eq. 3.22 (for $\lambda > 1$), therefore the resistance through the membrane can be calculated after knowing its thickness $r_{ion} = \delta^{mem}/\sigma^{mem}$. Here λ is the same water content in the membrane, mentioned in section A.1.1.2.

$$\sigma^{mem} = (0.005139\lambda - 0.00326)\left[\exp\left(\frac{1}{T_{ref}} - \frac{1}{T}\right)\right] \tag{3.22}$$

Concentration Loss Mass transfer of reagents in the electrodes is limited at high current densities. It is required that the mass flow rate reaching the catalyst layer to be at least equal to mass flow consumed in the reaction. Eq. 3.23 quantify the limitation in the concentration at the catalyst layer.

$$\Delta V_{con} = \frac{RT}{nF}\ln\left(\frac{C_B}{C_S}\right) \approx B\ln\left(\frac{C_B}{C_S}\right) \tag{3.23}$$

where, C_S is the reagent concentration over the electrode surface at the membrane and C_B is the bulk concentration in the anode and cathode channels, n_{reac} is the molar flow per area of the reagents; hydrogen in the anode and oxygen in the cathode and D^k is the effective diffusion coefficient.

$$C_S = C_B - \frac{\delta_{el} * n_{reac}}{D^k} \text{ For } k = an,\ ca \tag{3.24}$$

The effective diffusivity (Bosanquet formula) can be calculated using Eq. 3.25 and 3.26. This diffusivity represents the combined effect of the Knudsen mechanism and the molecular diffusion. In these equation ε is the electrode porosity, and ξ is its tortuosity. The tortuosity of the GDL is reported as 3 ($\varepsilon = 0.6$) Liu et al. [2013], 3.3 ($\varepsilon = 0.7$) Robin et al. [2015] and 6 ($\varepsilon = 0.3$) Ni et al. [2006]; for simulation purposes the tortuosity was fixed in a value of 4 in order to reduce the model departure from manufacturer experimental data. '

$$\frac{1}{D^{an}} = \frac{\xi}{\varepsilon}\left(\frac{1}{D_{H_2-H_2O}} + \frac{1}{D_{H_2O}}\right) \tag{3.25}$$

$$\frac{1}{D^{cat}} = \frac{\xi}{\varepsilon}\left(\frac{1}{D_{O_2-H_2O}} + \frac{1}{D_{H_2O}}\right) \tag{3.26}$$

The binary diffusion coefficient (D_{j-H_2O}) can be calculated using the Chapman-Enskog theory Cussler [2009], and the effect of the Knudsen diffusivity, using Eq.

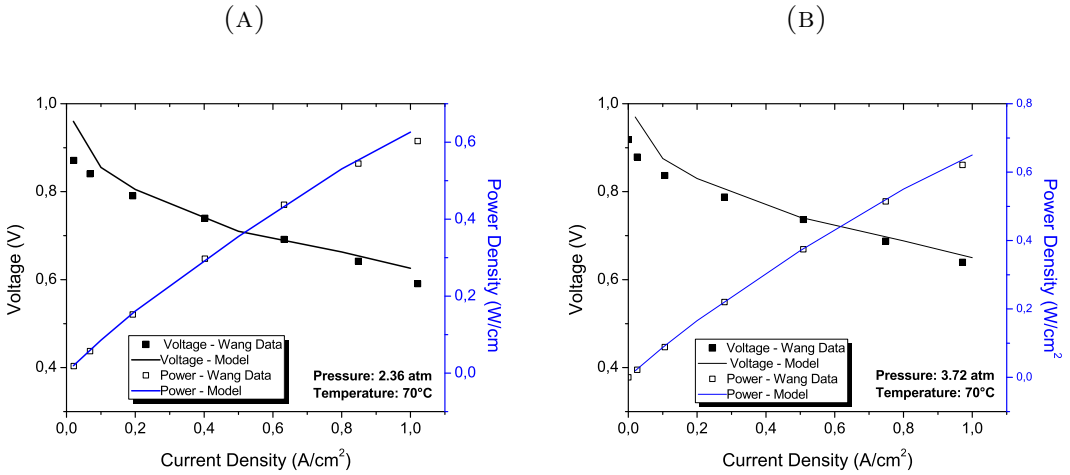

FIGURE 3.4: Polarization curve when the operation pressure is (a) $p = 2.36\ atm$ and (b) $p = 3.72\ atm$

3.27. This takes into account the collisions of molecules with the GDL pores and the cell walls. For details on the Cahpman-Enskog theory refer to appendix B

$$D_{H_2O} = \frac{d}{3}\sqrt{\frac{8RT}{\pi M_{H_2O}}} \tag{3.27}$$

where, d is the mean porous radius.

The diffusion will be dominant not only at higher loads but also during the purges when the excess ratios will drop, and a faster mass transfer is desirable. Limited mass transfer leads to reactant depletion at the membrane, even when sufficient concentrations are present in the channels.

3.1.3.4 Electrochemical Model Validation

The model validation used data from the experimental work of Wang [2003] under two pressure operation conditions and a fixed temperature of 70 $°C$. The fuel cell operated under several current densities ranging from 0.02 to 1 A/cm^2. In each step, after the cell reached the steady-state, the magnitude of voltage was recorded.

Figures 3.4a and 3.4b show how the model fits the fuel cell polarization curve in most of the middle range of the current densities. The model slightly departs from the experimental data only at extremely low and high currents densities.

3.1.4 Mass Flow Controllers (MFC) modeling

For the two MFC (see Figure 3.5), the flow through them will be modeled according to the standard ISA - 75.01.01 - 2007 ISA [2007]. Each MFC is sized according to the max flow requirements of hydrogen and oxygen, therefore in Table A.1 two flow coefficients (maximum value) will be indicated. N_9 is a numerical constant found in the ISA standard at a reference temperature $t_s = 15°\ C$. p_1 is the supply line pressure; if there is no pressure sensor before the cell, it can be assumed it is the cylinder discharge pressure. M is the gas molar mass, T is the supply temperature in Kelvin, and Z is the compressibility factor.

$$\dot{\mathbb{V}} = K_v^j N_9 p_1 Y \sqrt{\frac{\Delta p_i}{p_1 M T_1 Z}} \tag{3.28}$$

The expansion factor $Y = 1 - \frac{\Delta p_i}{3 p_1 F_y x_T}$ is included to take into account the compressibility effects expected for a gas (ie. changes in density). x_T is the pressure differential factor, which is related to the choked flow (increases in Δp_i will not increase the flow), where Δp_i is the pressure difference between the supply line and the fuel cell channels. $F_y = \gamma / 1.4$ is the specific heat ratio factor; this is used to adjust pressure differential ratio factor of a control valve with attached fittings at choked flow (x_T) when the gas is different of air.

Between the purges, the pressure difference across the valve is close to zero; therefore, there will be no flow (see Eq. 3.28), for any valve position. Between the purges the system will be uncontrollable, so after the purges is the best moment to increase the concentrations of reagents (and partial pressures) and with that the voltage can be modified, increasing the Nernst potential (see. Eq. 3.17) and reducing the concentration losses (see. Eq. 3.23).

3.2 Control system dynamic response

The main objective of the control system will be the regulation of the PEMFC voltage. Increasing or decreasing the hydrogen mass flow rate, the control system regulates the fuel cell voltage.

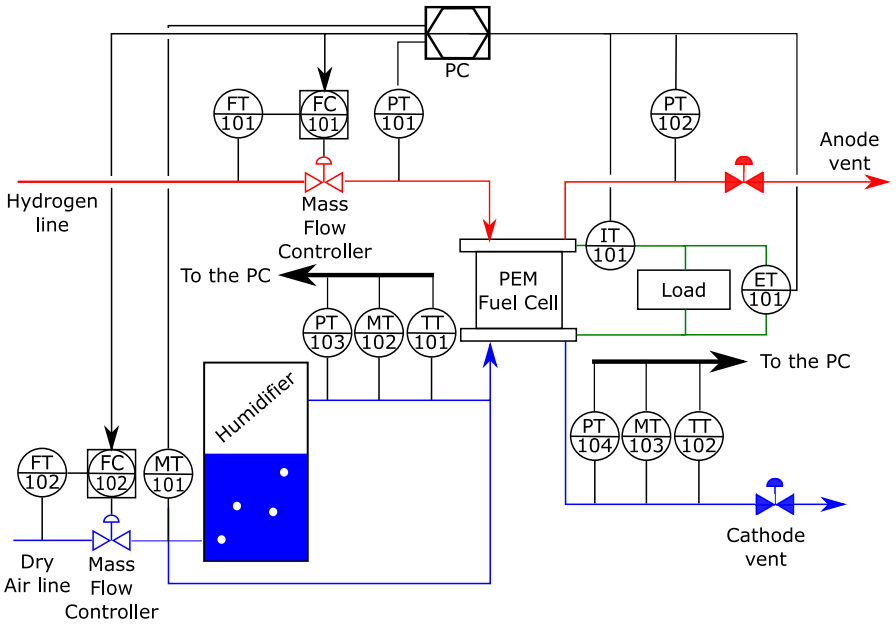

FIGURE 3.5: PEMFC system

The secondary control objective is to minimize the pressure difference between the anode and cathode to protect the membrane. The control system regulates the pressure difference modifying the air/oxygen mass flow rate.

For the system shown in Figure 3.5, there are two possible manipulated variables: the mass flow controllers, one per reagent line, and many controlled variables (e.g., pressures, moisture, and voltage). The two variables selected as the controlled variables are the cell voltage and the pressure difference between the anode and the cathode.

The load is assumed to be purely resistive, and for the humidity, it is assumed a fixed relative humidity in the air supplied to the anode and cathode. On/off purge valves are included at the anode and cathode discharges. Therefore, the fuel cell will operate in dead-end mode, under two operation scenarios: a) with no purges and b) with periodical purges.

Both controllers have an impact over the fuel cell voltage. Under a dead-end mode of operation, a reduction in the voltage can be achieved, reducing the hydrogen and oxygen concentrations in the membrane-catalyst layer interface, which occurs because fewer reagents are replacing the ones consumed in the reaction. Mass flows of hydrogen and oxygen are different; therefore, during transients, the pressure difference between the anode and the cathode is $\neq 0$. Thus the two controlled variables are coupled.

Multiple Inputs Multiple Outputs (MIMO) PID architecture is used to control the voltage and pressure difference between the cathode and anode electrodes. One controller is used to regulate the voltage manipulating the hydrogen MFC setpoint while the other one is controlling the pressure difference manipulating the air MFC setpoint.

According to Eq. 3.17 reagent partial pressures in the anode and cathode, and the fuel cell electric potential are strongly related, therefore, to compensate a voltage drop the hydrogen mass flow controller will try to increase the hydrogen partial pressure in the anode. On the other hand, the pressure difference is calculated as $\Delta P = P^c - P^a$, then, a positive ΔP occurs when the cathode pressure is higher than the anode pressure. The air mass flow control will open its valve to reduce ΔP. It means the air mass flow controller follows the hydrogen one.

3.3 Results

This section presents the results of the model simulation. Table A.1 contains the fuel cell PEM parameters and materials properties. For all the scenarios considered the mass of species, the partial pressures, the electrical variables, and the reagent concentrations in the channels and the catalyst layer (at the membrane interface) were studied. These results analysis includes open and closed loop operations. Open loop means that the controllers were deactivated, and the supply gas valves were in a fixed position all the time. For the closed loop operation, the analysis only includes the purge scenario.

3.3.1 No purges scenario

The first scenario to be analyzed is the cell under a load of 3 A when no purge is applied. The anode and cathode are both dead ends. Under this condition, for the specific cell simulated, the operation is stopped around 1 min, to prevent the starvation of reagents in the catalyst layer.

In Figure 3.6a the accumulation of water vapor is evidenced. There is also a gradual but sustained increase in the amount of nitrogen in the cathode. Nitrogen accumulates in the cathode because it does not participate in the reaction. After

pressurizing the fuel cell, only a small amount of new air will be able to enter the cathode corresponding to the reduction in pressure due to the oxygen consumption. Once new air comes inside the cell, just a fraction of that gas is oxygen (about 21% of the dry air). Over time, this will reduce the amount of oxygen in the cell until the reaction stops due to the lack of it. The water vapor produced inside the channels also accumulates, as can be seen in this same figure. This accumulation also reduces the volume available in the channels for the hydrogen and the oxygen, reducing the time until starvation. The starvation could be delayed using drier air, but this will affect the membrane humidity, and therefore its conductivity. The accumulated water vapor could condense once its partial pressure reaches the saturation pressure of water p_{sat}. If the process continues, there could be even *flooding*, a condition in which liquid water saturates the porous media reducing the available area for the reaction and decreasing the mass transfer coefficient. This flooding will also reduce the reagents in the catalyst layer. Notice that for the operational conditions in this first simulation, the fuel cell stops its normal operation due to the lack of reagents in the catalyst layer (interface with the membrane), although there are reagents in the channels, which means that the main voltage drop at the end is due to concentration losses.

In Figure 3.6b shows partial pressures for the different species, and the results are in agreement with the mass behavior (Figure 3.6a); the higher the amount of any gas, the higher its partial pressure is. With the operation in dead-end mode (no purges), the total pressure will be almost constant, around 4 *bar*. This means that inlets are still open, and the consumed reagents are being replenished, but the trend is the same as in Figure 3.6a; eventually there will be no space for new reagents and the cell will starve, that is the reason why for a constant load in an open loop operation without disturbances, the reagents partial pressures are decreasing.

In Figure 3.6c, the electrical variables are presented. As it was stated before, the system is working under a constant load and the purge valves are always closed ($\upsilon_0 = 0$). Once the oxygen is almost depleted in the cathode catalyst layer, as can be seen in Figure 3.6d, even when there is available oxygen in the cathode channels, the voltage will drop because mass transfer is limited in the porous media. If the cell is allowed to continue operating in this point, ($t = 50\ s$) for this particular system, there will be irreversible degradation of the membrane, the GDL, and the channels if they are made of graphite.

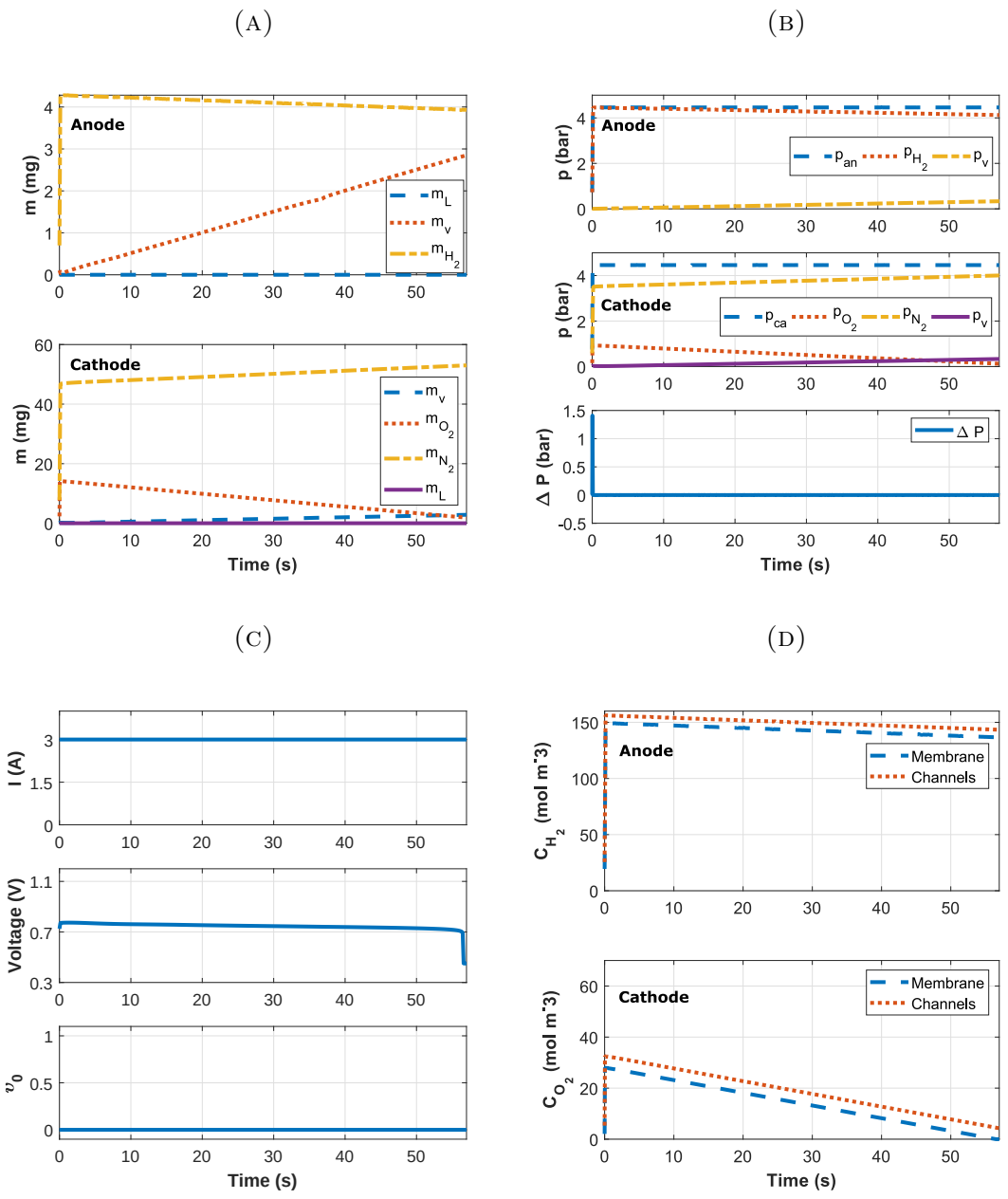

FIGURE 3.6: Fuel Cell dynamic response with no purge applied (load: $I_{fc} = 3\ A$)). a) Species in anode and cathode channels, b) Pressures in anode and cathode channels, c) Load, Current and Purge Valve Control Signal and d) Reagent Concentration

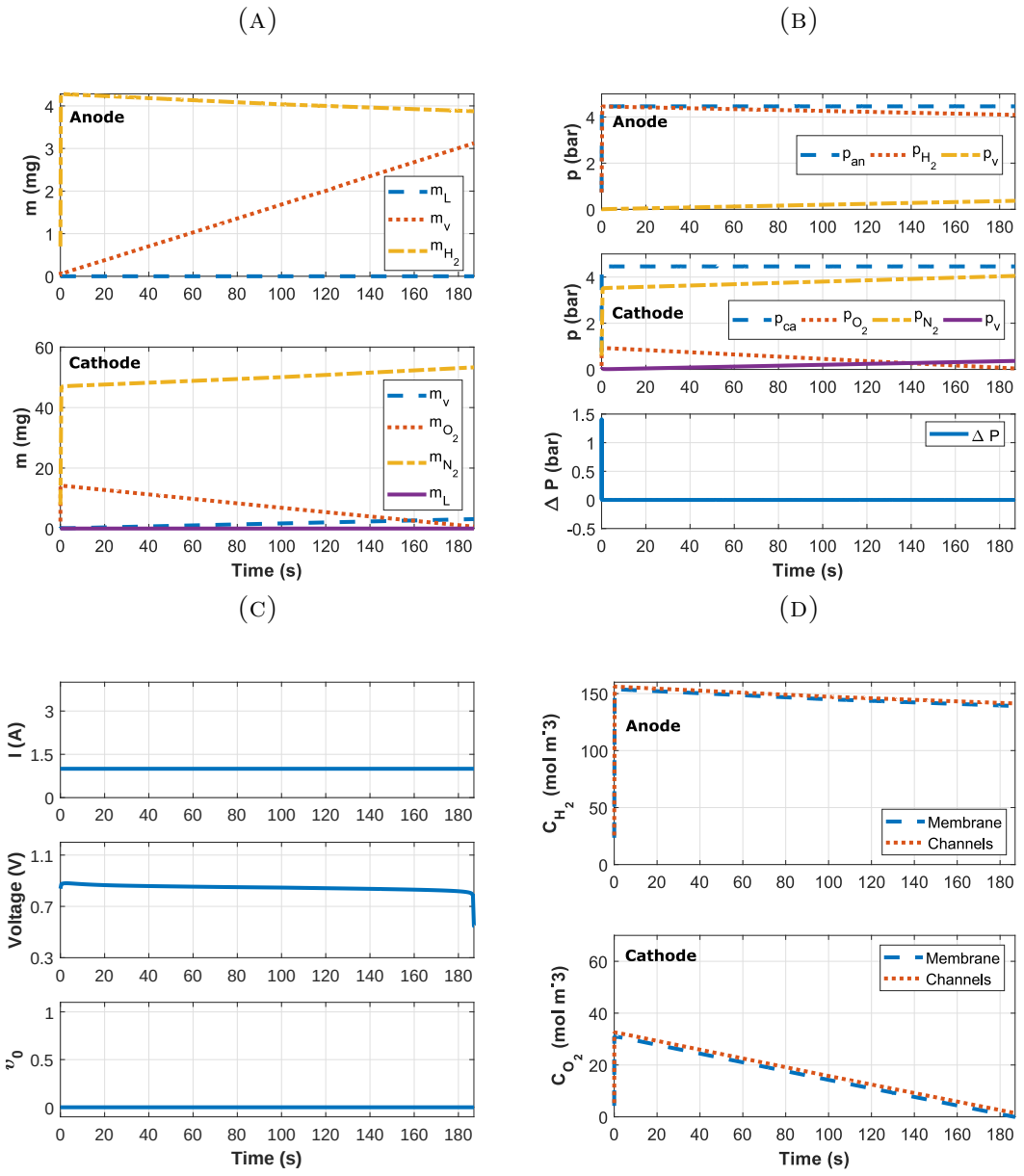

FIGURE 3.7: Fuel Cell dynamic response with no purge applied (load: $I_{fc} = 1\ A$). a) Species in anode and cathode channels, b) Pressures in anode and cathode channels, c) Load, Current and Purge Valve Control Signal and d) Reagent Concentration

Figure 3.7 shows the results for the system response under a lower load condition. In this case, the system worked for more than 150 s, but the trend of the oxygen concentration is to zero, so eventually, the cell will also be in starvation. The analysis of each one of the figures included in Figure 3.7 is the same as the ones shown for the higher load (Figure 3.6) with the longer operation time as mentioned earlier.

3.3.2 Continuous purges scenario

The system is now tested under a series of continues purges during its regular operation. The purges are done using discharge valves located at the outlets of the anode and cathode (see Figure 3.5). These valves have only two positions: fully open or closed and a single control signal is used to operate them, that means that it is assumed that they are synchronized. The timing of the valves is essential during the cell operation to avoid pressures differences over the membrane.

The purges are used in this scenario to allows the by-products and nonreactive gases inside the cell to get out of it and allow new reagents to replace them. The current is measured and integrated over the operating interval until it reaches a threshold to decide when to open the purges valves. For simulation purposes, the threshold is fixed in a value of 15 $A\ s$.

Figure 3.8a shows the dynamic response of the species inside the cell, both in the anode and the cathode. In these domains the reagents fills the cell in the first seconds and after that there is a reduction until about the time reaches 100 s, after this moment and for the next 50 s the mass of reagents and by-products remains stable, it means, it still oscillates because of the purges but the mean value remains constant.

Partial pressures of reagents and by-products are also stable, but due to the differences in the inlet mass flows in anode and cathode, it can be seen in Figure 3.8b that the pressure difference during the purges tends to be negative, that means a higher pressure in the anode, even when the timing of the valves is synchronized.

After 150 s of operation a sudden change in the load occurs and it changed from 3 A to 1 A (see Figure 3.8c, this leads to an increase in the output voltage, which is in accordance with the polarization curve (lowers currents densities have higher voltages) and the frequency of the purges is reduced because the threshold remained the same . In Figure 3.8d the effect over the concentration is evidenced, even with a lower frequency in the purges, the reagents availability is stable in the catalyst layers of both, anode and cathode, and its oscillations are reduced which is expected to improve the control system performance.

Pressures differences were critical in the start-up of the cell. In both scenarios without purge, the cathode pressurizes much faster than the anode, due to the

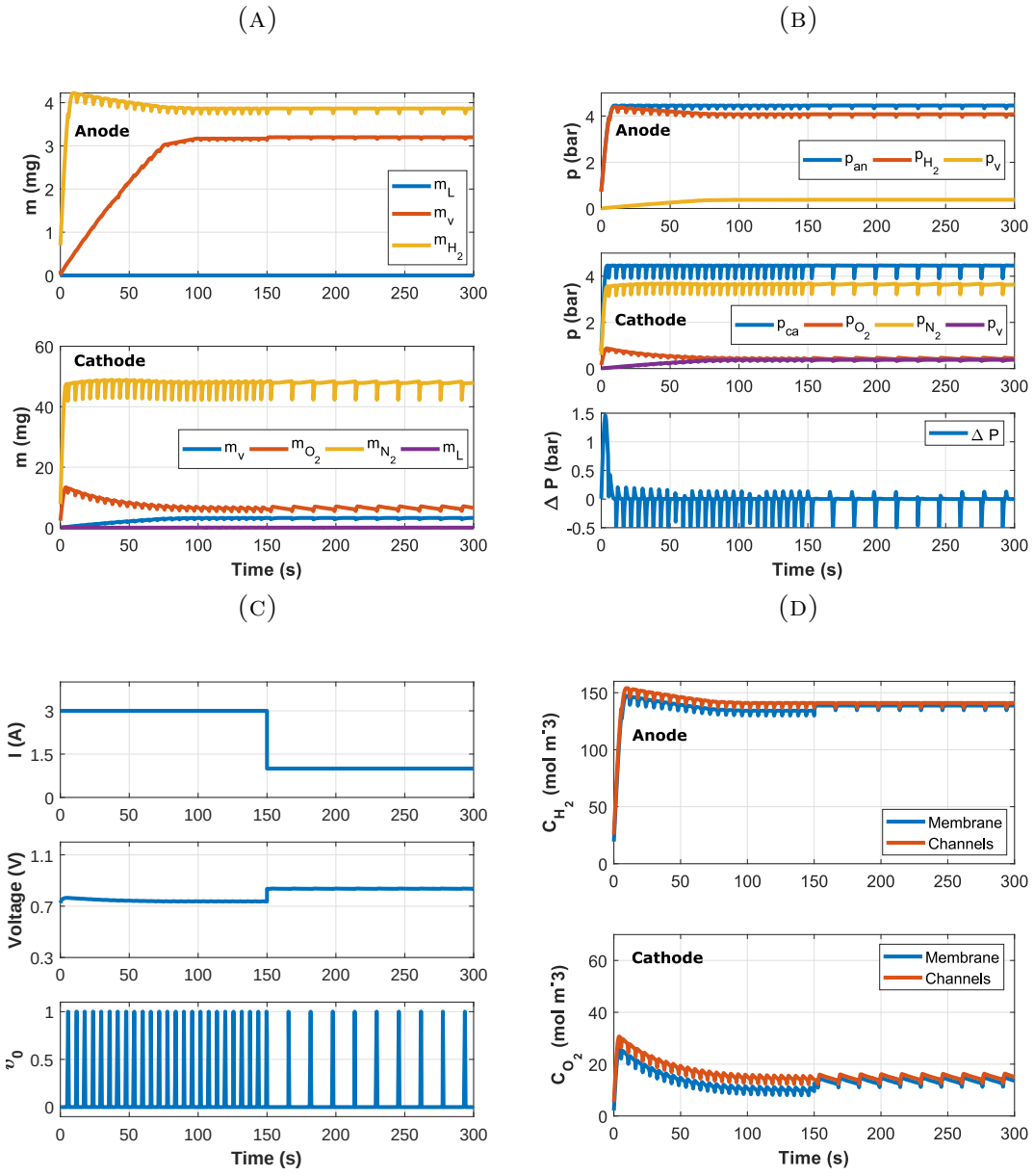

FIGURE 3.8: Fuel Cell dynamic response with purge applied periodically. a) Species in anode and cathode channels, b) Pressures in anode and cathode channels, c) Load, Current and Purge Valve Control Signal and d) Reagent Concentration

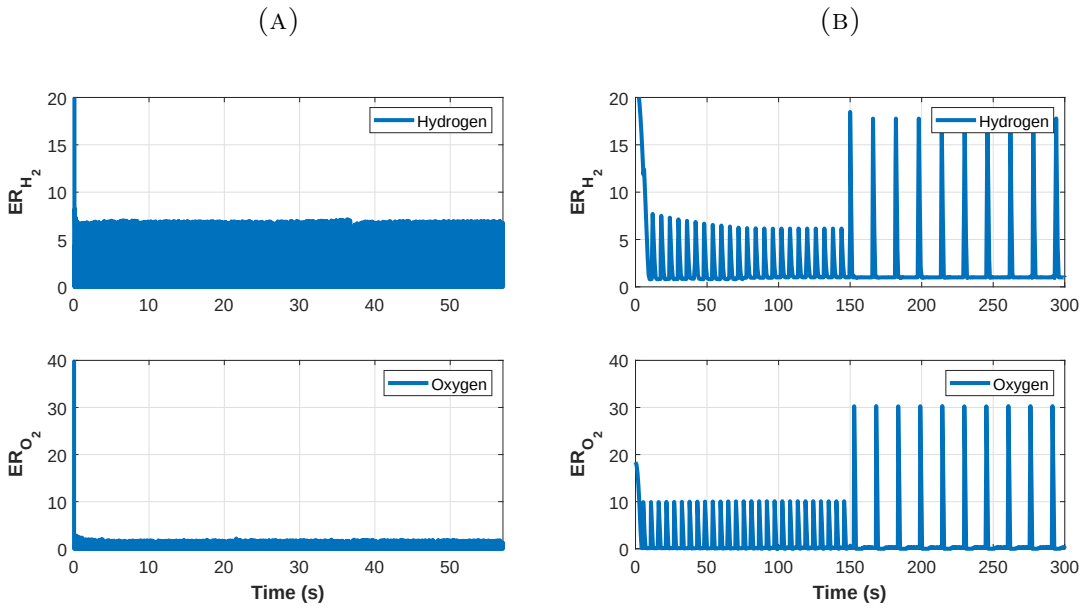

FIGURE 3.9: Excess Ratios when (a) no purge is applied ($I_{fc} = 3\ A$) and (b) purge is applied periodically.

differences in the size of the mass flow controllers. As a result, for about 5 s, the membrane sustained a pressure difference of $\approx 1.5\ bar$.

Another indicator of the normal operation of the fuel cell are the reagents excess ratios (See Figure 3.9) $ER_k = \frac{\dot{m}^{j,ch}_{k,i}}{\dot{m}^{j,GDL}_{k,reac}}$ for $j = a, c$ and $k = H_2, O_2$, which are the ratio between the reagent mass flow entering the channels and the theoretical flow consumed in the reaction for a particular electric load .

In Figures 3.9a and 3.9b the difference between the two previous scenarios is shown. It is desired that ER_k be greater than 1; otherwise, the reagents inside the flow will be depleted. In the case of air, the effect of purges is more noticeable. The main difference between those scenarios is that when no purges are applied, the only way more reagent enters the fuel cell (without changing the supply conditions) is to consume the oxygen inside the cells and therefore, reduce the pressure inside the cell. It means only when the reagent in the cathode is used to sustain the reaction, and there is enough pressure difference between the supply line and the cell, new air can come in, that is why the ER_{O_2} is highly oscillatory. On the other hand, in the case of the continuous purges scenario, in each purge a fast reduction in the pressure is produced in each purge, allowing the new reagent to come in. This behavior is also found in the anode side, although the difference is less notorious due to the use of a high purity gas.

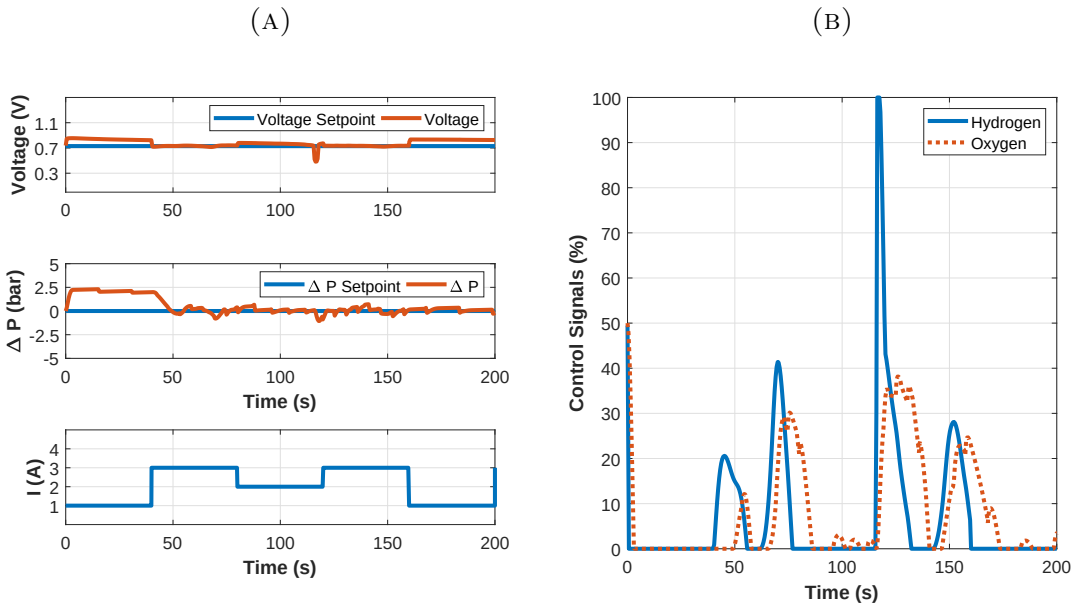

FIGURE 3.10: Closed Loop Response (a) Controlled variables and (b) Manipulated variables

3.3.3 Closed Loop

Finally, the system operation under closed-loop control is tested. The results of this test are shown in the Figures 3.10a and 3.10b. In Figure 3.10a the load profile used to induce a disturbance in the system is shown, in the first 40 seconds, the load is 1 A, and in this condition, the fuel cell is starting. It can be noticed that the small fuel cell volumes are filled quickly (around 2 s), after that the supply valves are closed (see Figure 3.10b). During this start-up, the pressure difference cannot be compensated because the voltage set up is below the actual voltage of the cell; therefore, the control system is waiting for the pressure to be reduced due to the electrochemical reaction with the subsequent reduction in voltage.

After the startup, the load increased until 3 A, and the control system regulates both voltage and pressure difference. Notice that oxygen supply (air line) tend to be lower than the hydrogen one, due to the initial positive pressure difference (pressure in cathode > pressure in anode). The hydrogen valve is used mainly to control the voltage, so if the output is above the setpoint, the control system will close this valve. The air valve will be used to control the pressure difference; if the $\Delta p > 0$ the control system will close this valve. There are two loops in the system, and they interact because once the pressure is reduced, the voltage is also reduced.

Notice how the second peak load, which occurs around the $t = 120\ s$ makes the hydrogen control signal jump to 100 % to compensate the sudden reduction in the voltage due to the load change. This action also induces a deviation of the pressure difference to the negative zone, meaning that now, the pressure in the anode side is higher than the cathode side. Now the pressure in the cathode is increased to compensate the anode pressure, and this is done opening the air valve; notice that this response came after the hydrogen signal.

The oscillations in the response are due to the purges valves which are still in operation. It can be seen that the pressure difference is affected in a stronger way than the voltage, but due to the interaction of the loops and the electrochemical model itself, the voltage is also affected. This also explains why the air control signal is more oscillatory than the hydrogen control signal.

Chapter 4

Materials and dynamic response characterization

The material properties have a direct effect on the performance of fuel cells. Using the model presented in a previous chapter, the impact of the following properties on the steady-state and dynamic response will be assessed. Typical material properties are included in appendix C. The dynamic model is able to include the effect of the GDL porosity, tortuosity and the membrane conductivity dependence on the humidity inside the cell. For pores size distributions and catalyst surface area, BET can be used to measure the sample GDL properties, as well as XRD, which can be used to estimate the chemical composition of the catalyst and particles sizes.

Initially in this chapter, it is assumed that the fuel cell components are studied with the electrodes "as received" from the manufacturer, and later the effect of imperfections in the GDL will be taken into consideration. For this analysis a test bench is designed to test the PEMFC dynamic response under MFC setpoints changes at a fixed load.

In the case of the membrane conductivity, it will be a function of the temperature and the relative humidity in the cell, therefore, these variables will be taken into consideration in the design of experiment (DOE).

(A) (B)

FIGURE 4.1: BET test (a) GDL sample and (b) BET test equipment

4.1 Material characterization

Two characterizations were completed on the GDL of the PEMFC. Initially, a BET test was completed for GDLs with and without microporous layers (MPL) on both sides to measure the porosity of the electrodes.

4.1.1 BET Test

For new materials it is necessary to assess its main properties, for example, the porosity is one of the most important parameters for the fuel cell GDL. One approach for the porosity measurement is the use of the Brunauer–Emmett–Teller (BET) method. In this method, the sample is cooled to $72K$ using liquid nitrogen, for then measure the absorption of pure gases. Based on that measurements the porosity of the media can be estimated.

For the pure catalyst, the pore size distribution was found (see figure 4.2). From this figure the pore size is in the range of $17-1500$ Å with an average value close to 150 Å. In the same figure is also reported the isotherm during de adsorption and desorption process. From the International Union of Pure and Applied Chemistry (IUPAC), the catalyst isotherm is classified as an isotherm type II Sing [1982]. This type of isotherm is typical of solids material with low porosity. At the point

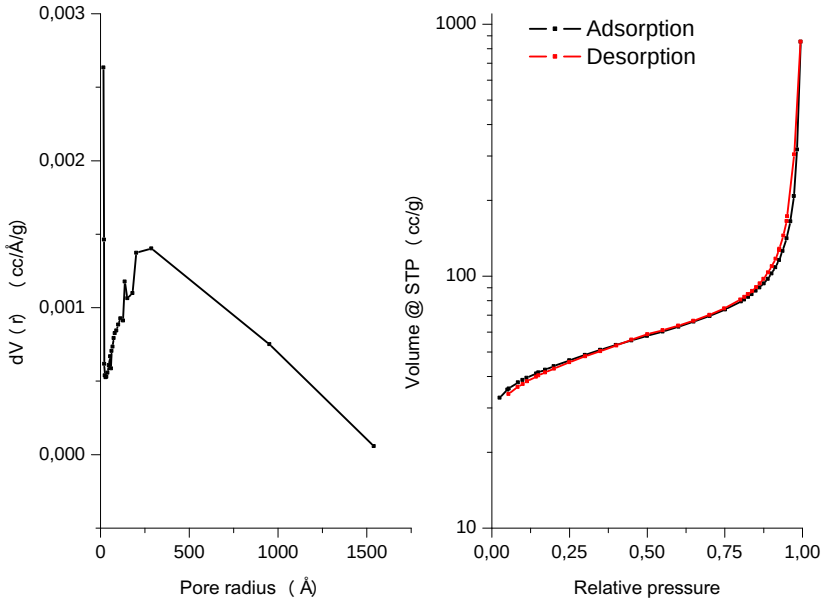

FIGURE 4.2: Catalyst pore size distribution (left) and isotherm (right)

of inflection (between 0 - 0.125 for the relative pressure) begins the multilayer adsorption.

The GDLs used in the test bench were also characterized using this technique. In figure 4.3 the results for the reference ELAT-2400W are presented. From the data of the manufacturer included in appendix C, this is a cloth type GDL with 2 MPL. From this figure it can be seen how most of the pores have a radius of around 450 Å, although the ranges go from $15 - 1700$ Å. In this sample, the isotherm can be classified as a type IV in the IUPAC classification. This type has a characteristic hysteresis loop, "which is associated with capillary condensation taking place in mesopores" Sing [1982].

For the second GDL type, the ELAT-1400W, also a BET test was completed and the results are reported in the figure 4.4. This is also a GDL with MPL, but only on one side, the side placed between the GDL and the membrane. The absence in the second MPL increased the dispersion in the pore size measurements, mainly due to the cloth free surface, although the pore size range $\left(17 - 1100\,\text{Å}\right)$ is similar to the values found for the ELAT-2400W, now the presence of microporosities ($d < 2\ nm$) compared with the mesopores ($2 \leq d < 50\ nm$) is reduced, and the pores are more uniformly distributed as micro and mesoporous. From Sing [1982], it can also be said that the isotherm is also an IV type with a hysteresis type H4

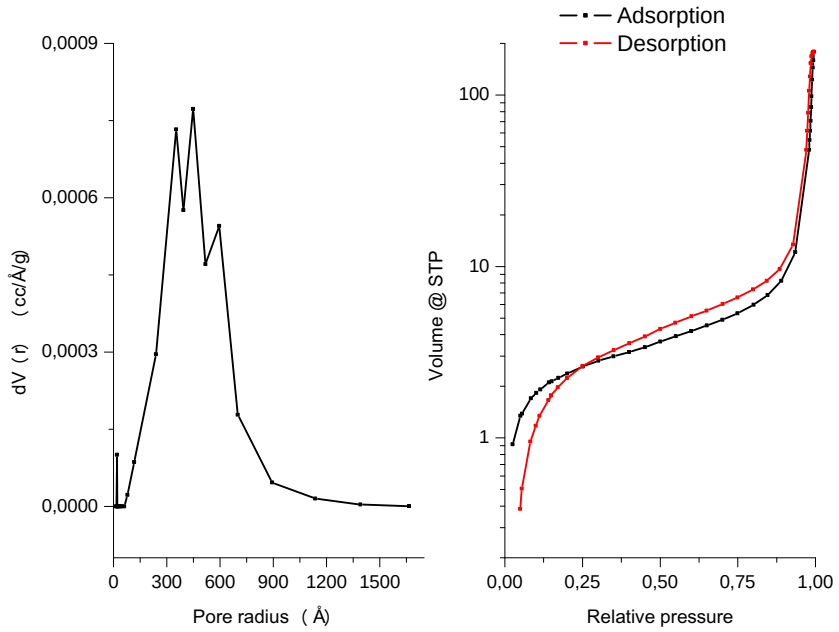

FIGURE 4.3: GDL ELAT - 2400W pore size distribution (left) and isotherm (right)

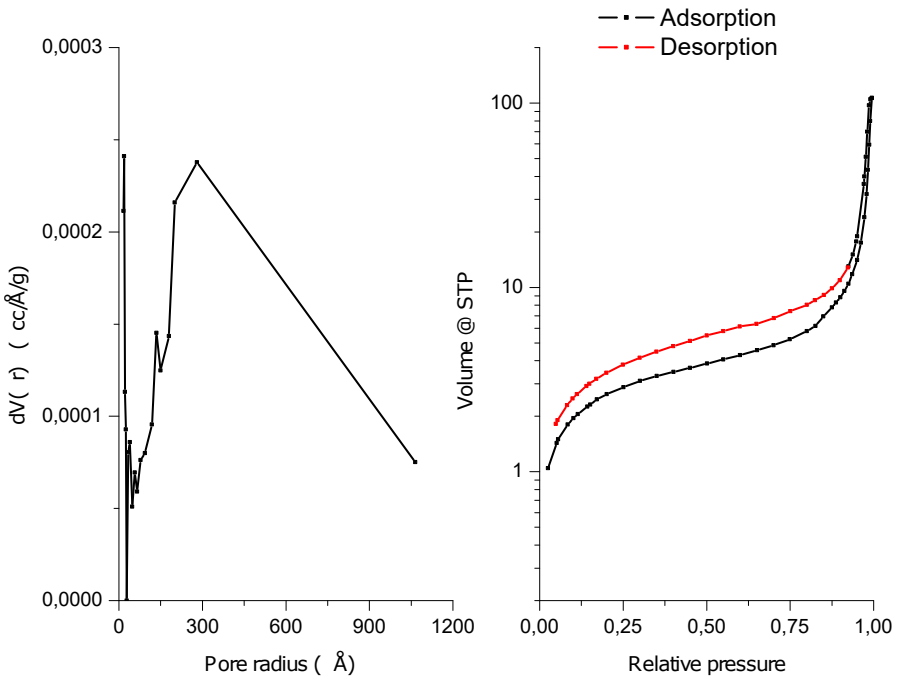

FIGURE 4.4: GDL ELAT - 1400W pore size distribution (left) and isotherm (right)

(A) (B)

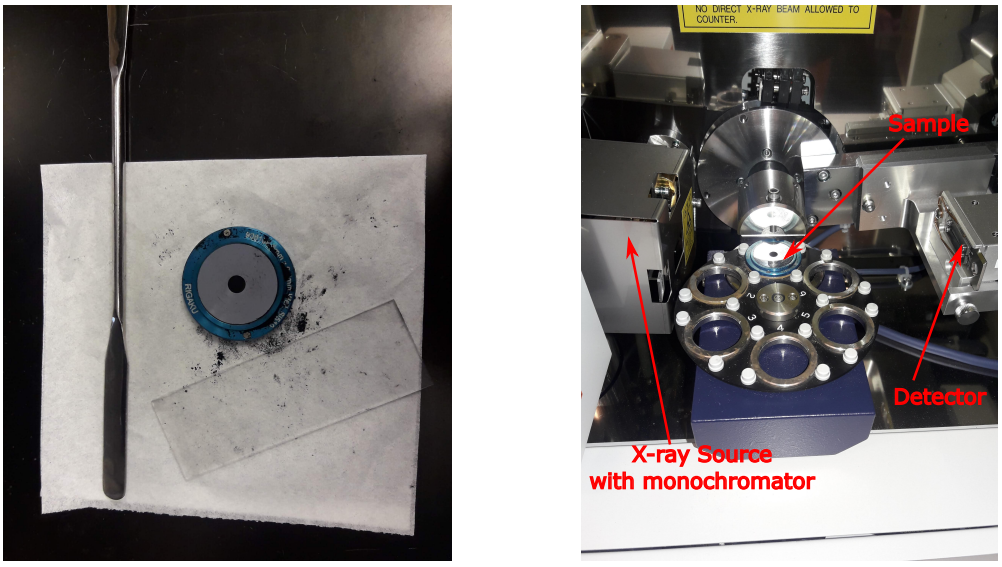

FIGURE 4.5: XRD test (a) Catalyst sample and (b) XRD test equipment

according to the IUPAC classification, confirming the presence of microporosity in the sample.

4.1.2 XRD Test

A catalyst sample was also tested in order to identify possible contaminants in the catalyst powder. The testing approach selected was a XRD test, which as it was mentioned in section 2.5.2, is a technique based on the measurement of the diffraction beam angles and their intensities from a X-Ray radiation applied to a sample.

In figure 4.5a the sample preparations is presented. The powder has to be evenly pressed in the sample holder, making its surface as flat as it can be done. Once the sample is correctly mounted in the disc sample holder, it has to be placed inside the XRD equipment shown in figure 4.5b

This technique requires previous knowledge about the typical material response, then using the positions of the peaks shown in figure 4.6 and comparing it with literature data as the one found in the work of Liu et al. [2004], where for this type of catalyst it is expected to found peaks at $25, 40, 45, 68, 82°$, it can be said that no contaminants are present in the sample. Also, it is suspected that the catalyst was heat treated, due to the size of the peak at $40°$.

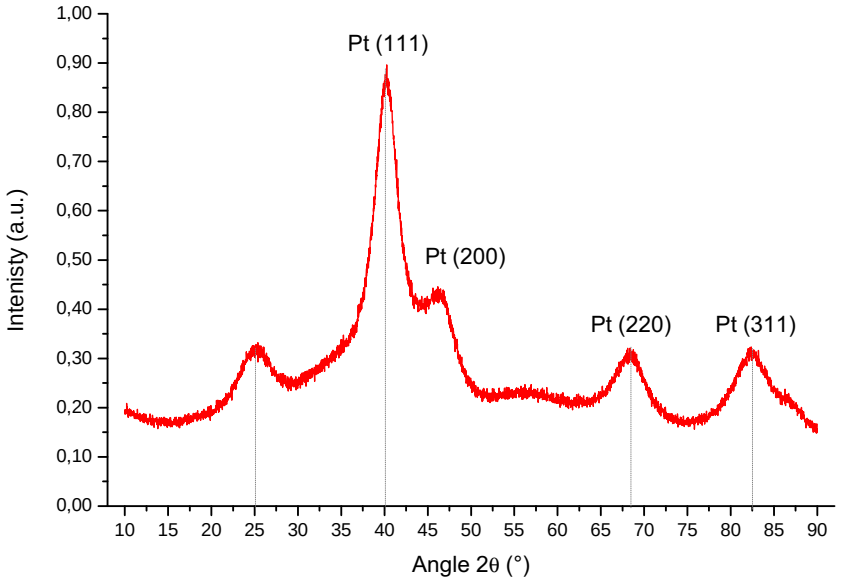

FIGURE 4.6: Catalyst powder XRD test

4.2 Model-based Dynamic characterization

Two approaches were used for the dynamic characterization of the fuel cell system. The first approach was simulation-based, using the dynamic model presented in chapter 3 and appendix A. The second one is based on experimentation, using the test bench.

Regarding the first approach, using the 1D model, the following dynamic variables, and parameters can be included in this stage.

4.2.1 Design variables

In this category are the material properties. Mainly the properties of the assembly of the electrodes and membrane (MEA). Typical GDL materials are included in the appendix C. The pore size range was defined using the BET results and literature data from Oh et al. [2015]. The GDL tortuosity is reported in the literature with values in the range $3 - 6$ according to Liu et al. [2013], Ni et al. [2006]. For the membrane, Nafion 211 and Nafion 117 were taken as a reference (data from FuelCellStore).

TABLE 4.1: Design variables levels

Variable	**Low level**	**High level**
GDL porosity	31%	61%
GDL average pore size (nm)	60	120
GDL tortuosity	3	6
GDL thickness (μm)	250	500
membrane thickness (μm)	25	183
roughness factor	5	15

4.2.2 Operation variables

These are the main controllable operation variables. Mass flows were not included here due to their strong relationship with the pressure inside the FC and the supply pressure.

TABLE 4.2: Operation variables levels

Variable	**Low level**	**High level**
temperature set point ($°C$)	30	60
air supply pressure (bar)	4.5	6
hydrogen supply pressure (bar)	2.5	4.5
air inlet HR (%)	20	60

4.2.3 Disturbances variables

Only the electric load is referenced as a disturbance variable, although there could be others, like surroundings temperature. The model includes a simple temperature control loop which guarantees a fairly constant operating temperature. From the developed model, it can be seen (for example figure 3.8c) the voltage system response to changes in the load is almost dynamic free, therefore, it will be used only as a variable for the test of the control system.

4.2.4 Response variabless

The response variables correspond to electrical and mass transfer variables. It was assumed that the fuel cell temperature can be held constant.

The dynamic response of the fuel cell system is defined by the following variables: reagent concentration in the cathode catalyst layers and fuel cell voltage. These

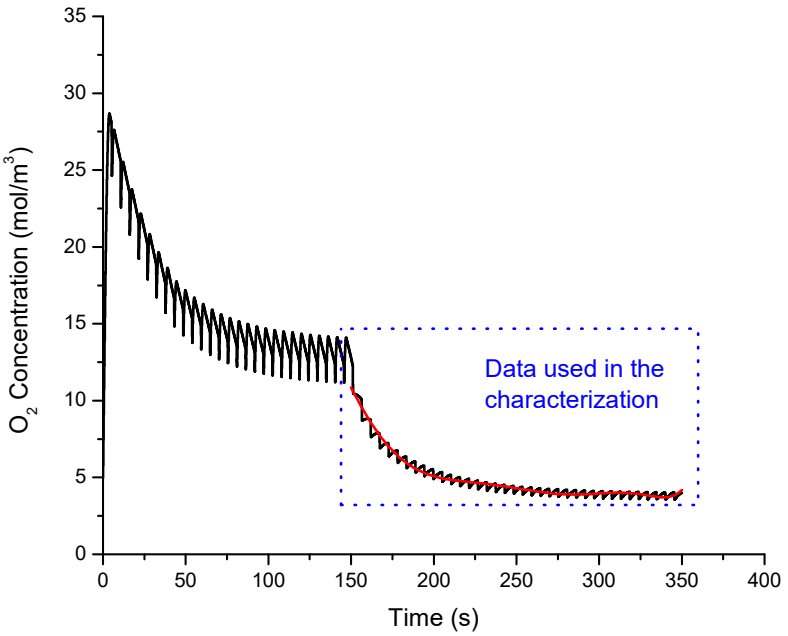

FIGURE 4.7: Sample O_2 concentration (mol/m^3) in the cathode catalyst layer dynamic response

variables were selected due to their strong relationship with the electrochemical model. In fact, the concentration will affect not only the open loop voltage, defined by the Nernst potential (see equation 3.17) but also the polarization potentials (see equation 3.23). For the voltage, which is a function not only from the operation variables but also from the design variables, the average steady-state value was analyzed, and the settling time is analyzed.

For the aforementioned variables dynamic and steady-state parameters are identified. The selected dynamic parameters are: a time delay and settling time; only the variables with a significant impact on the fuel cell performance are taken into consideration after the first stage.

A typical result in the simulation is presented in figure 4.7, where the input step was applied at $t = 150\ s$. The data before the step time were used to allow the model to find its steady state point because, in the model, it is assumed that the PEMFC starts in a shut-down condition, i.e. there is no fuel inside the cell. Due to the continuous purges detailed in section 3.3.2, the response is oscillatory, therefore, the data were fitted to their central trend using a polynomial fit, which is only used to approximate the response to a smooth function; this ease the process of reading the response data.

4.2.5 One-factor-at-a-time (OFAT) DOE

In this first stage, the pure effect of the factors on the dynamic response of the fuel cell is analyzed. Taking into consideration that the cathode in the PEMFC is the slowest one, for the dynamic response it was analyzed the concentration of oxygen in the catalyst layer and the cell voltage. For all the factors defined before in tables 4.1 and 4.2, no time delay was observed. Due to the purges during the operation, the responses were fitted to smooth the response and ease it analyze, and then they were approximated to a first order plus dead time (FOPDT) model (equation 4.1), using the FIT 3 method proposed by Smith and Corripio [2005].

$$FOPDT : G(s) = \frac{Ke^{-t_0 s}}{\tau s + 1} \tag{4.1}$$

From figure 4.8, it can be seen that the pore size has no significant effect on the dynamic response of the oxygen concentration and the voltage. Also, the porosity has no significant effect on the O_2 concentration, but it has it on the voltage. There is also a significant impact on voltage and concentration due to the changes in tortuosity and GDL thickness. In figure 4.9 the effect of the membrane

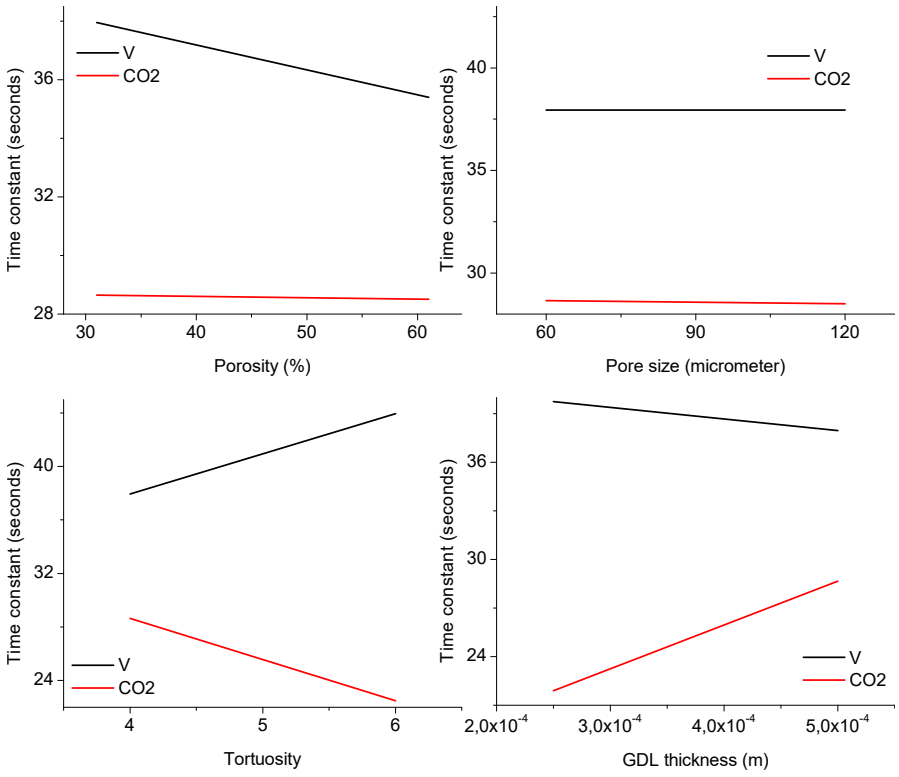

FIGURE 4.8: Design parameters impact on the system time constant

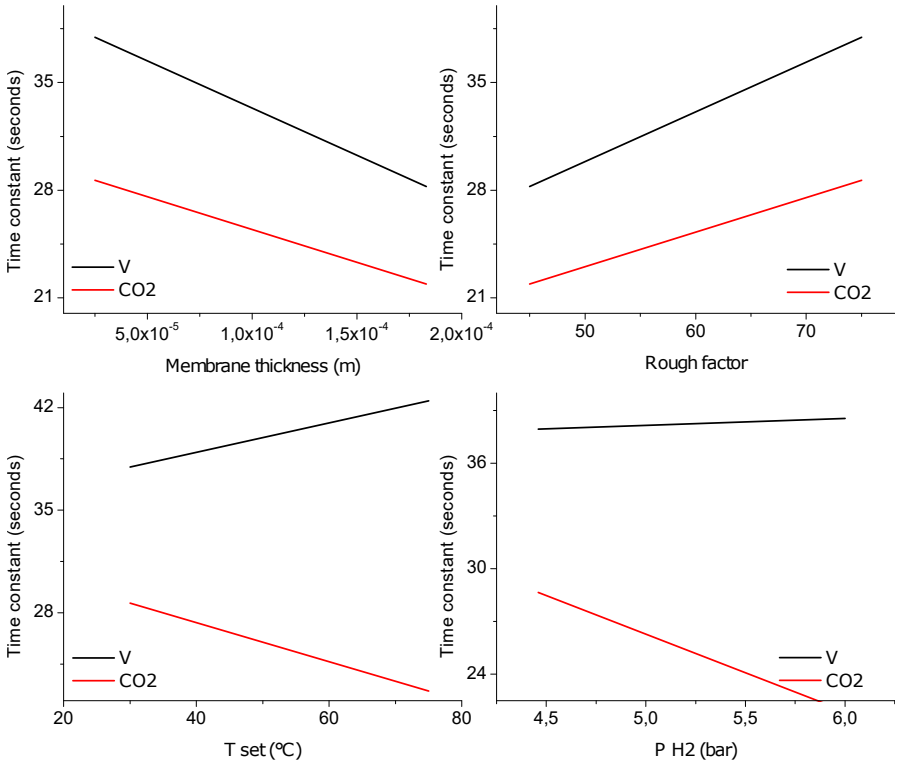

FIGURE 4.9: Design and operation parameters impact on the system time constant

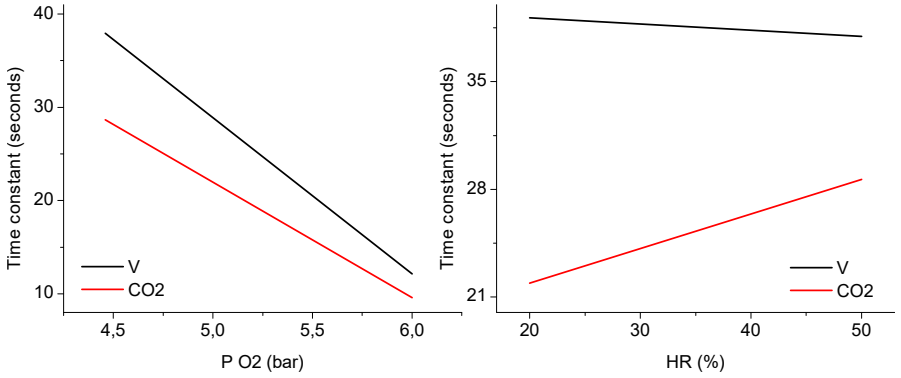

FIGURE 4.10: Operation parameters impact on the system time constant

and rough factor are presented. They have a significant impact on the system dynamic.

Figures 4.9 and 4.10 show the operational parameters results. All of them seems to have a significant impact on the system dynamic response, being the supply air pressure the parameter with the highest impact, both on the voltage and the O_2 concentration.

It was found that not every factor affects both of the responses analyzed, moreover, there are factors that have opposite effects on the dynamic response of the voltage

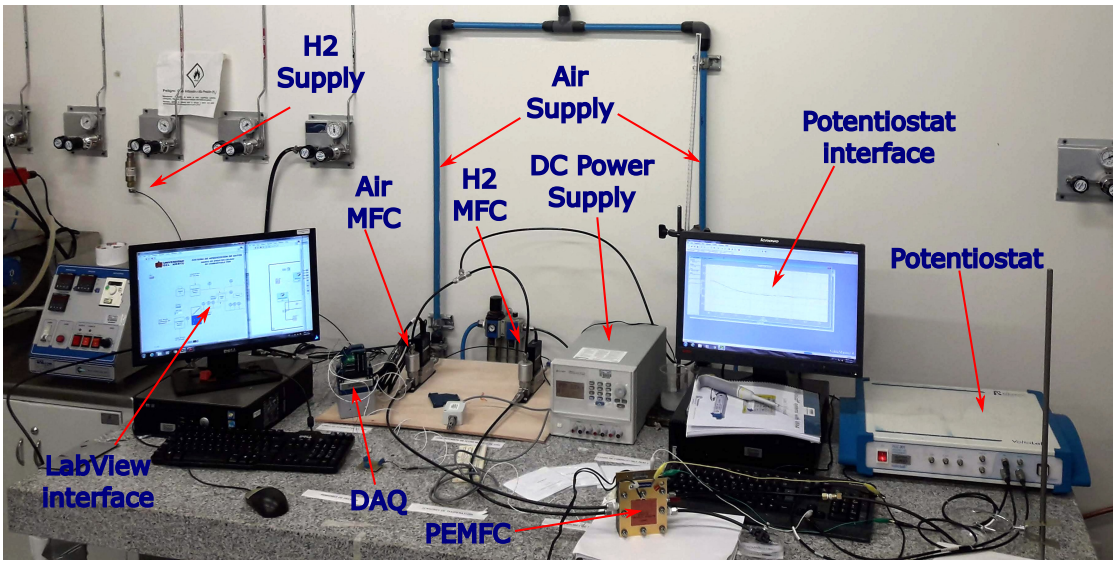

FIGURE 4.11: PEMFC Test Bench

and the concentration, like the operation temperature, the tortuosity, and the GDL thickness.

4.3 Experimental dynamic characterization

During the execution of this research, a test bench was constructed that allows the characterization of fuel cells (PEM Fuel Cells). This system is of vital importance in the design process of systems that integrate fuel cells, since it allows the dynamic characterization of the same under different loading conditions, as well as measuring the impact of different materials used in the electrodes of these devices on the dynamics of the cell, and its response in steady state. It is necessary to have a dynamic characterization of the cell and its auxiliary components for the appropriate design of the cells (selection of materials and geometries), as well as control strategies that allow their integration with other systems of electric power generation: hybrid systems. It is necessary to perform dynamic characterizations of the fuel cells, in order to give experimental support to the recommendations raised within the developed methodology and include the effect of possible defects on the performance of generation systems, which in the most general case they are hybrid systems.

4.3.1 Test Bench Design

Figure 3.5 presents the typical components required for the PEMFC operation in the experimental stage. Now the simulated system is constructed (see figure 4.11) for the experimental stage. For this system, the following equipment were defined.

TABLE 4.3: Test bench equipment

Components	**Qty**	**Manufacturer**
PEM Fuel Cell	2	Electrochem
Instrumentation		
Pressure sensor	2	Honeywell
Temperature sensor	2	Omega
Current sensor	2	
Voltage sensor	2	National Instruments
Humidity sensor	2	Omega
Mass flow controller (hydrogen)	1	Omega
Mass flow controller (air)	1	Omega
DAQ	1	National Instruments
Auxiliary components		
Humidifier	2	Uninorte
PCB's	6	Uninorte

4.3.1.1 PEM Fuel Cell

PEM fuel cell is the core equipment in the test bench. It was selected a 5 cm^2 with serpentine channels and column channels. In figure 4.12 the connections are shown. The operation pressure was restricted to the range $0 - 50$ $psig$ with a pressure difference between the anode and cathode at most ± 30 $psig$. For the test four different MEA are available.

4.3.1.2 Instrumentation

The following sensors were selected to measure the main dynamic variables in the test bench.

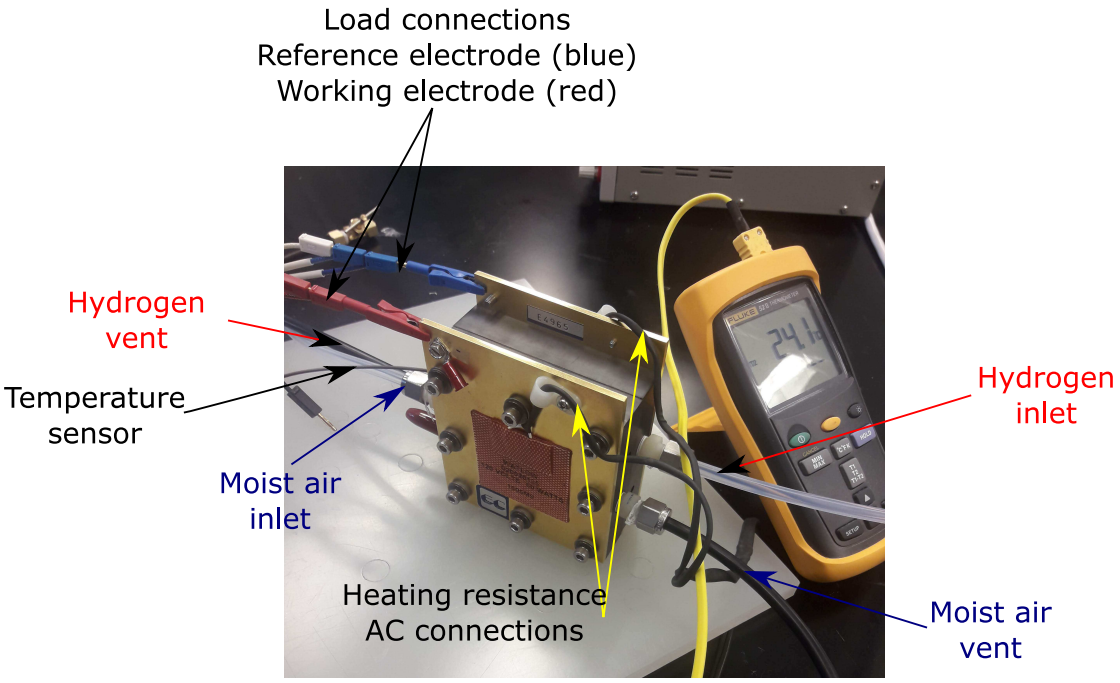

FIGURE 4.12: PEMFC connections

Pressure sensor A Wheatstone bridge-based sensor is used for the pressure measuring at the PEMFC inlets.

For the voltage amplification the circuit shown in figure 4.14 was used. The amplification will be defined by equation 4.2. The selected resistances are included in the circuit diagram. R_g is a variable resistance to adjust the voltage sent to the

26PC SERIES PERFORMANCE CHARACTERISTICS
at 10.0 ±0.01 Vdc Excitation, 25 °C

	Min.	Typ.	Max.	Units
Excitation	—	10	16	Vdc
Response Time	—	—	1.0	ms
Input Resistance*	5.5 k	7.5 k	11.5 k	Ohm
Output Resistance*	1.5 k	2.5 k	3.0 k	Ohm
Weight		2		gram

* Measured using a 1 mA current

ENVIRONMENTAL SPECIFICATIONS

Operating Temperature	-40 °C to 85 °C [-40 °F to 185 °F]
Storage Temperature	-55 °C to 100 °C [-67 °F to 212 °F]
Compensated Temperature	0 °C to 50 °C [32 °F to 122 °F]
Shock	Qualification tested to 150 g
Vibration	MIL-STD-202, Method 213 (0 kHz to 2 kHz, 20 G sine)

Note: For media compatibility specifications, refer to catalog or web site: www.honeywell.com/sensing

Honeywell

26PC CIRCUIT TERMINATION

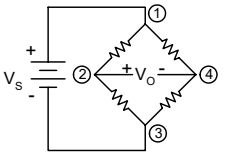

Pin 1 = Vs (+)
Pin 2 = Output + (V2)
Pin 3 = Ground (-)
Pin 4 = Output - (V4)
Pin 1 is notched
Pin 2 is next to Pin 1, etc.

FIGURE 4.13: Pressure sensor technical data. *Taken from:* manufacturer datasheet

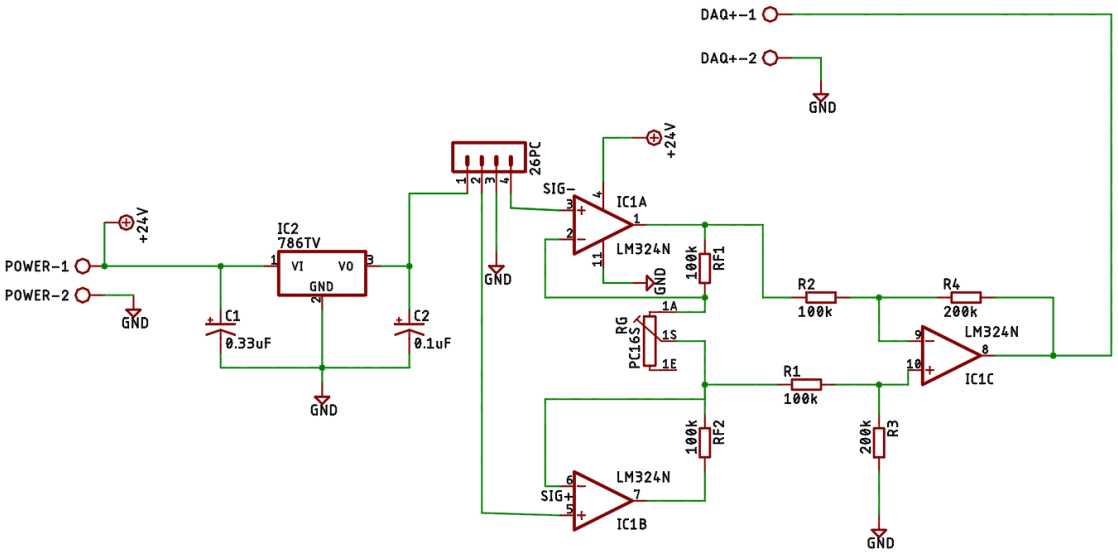

FIGURE 4.14: Pressure sensor signal conditioning circuit.

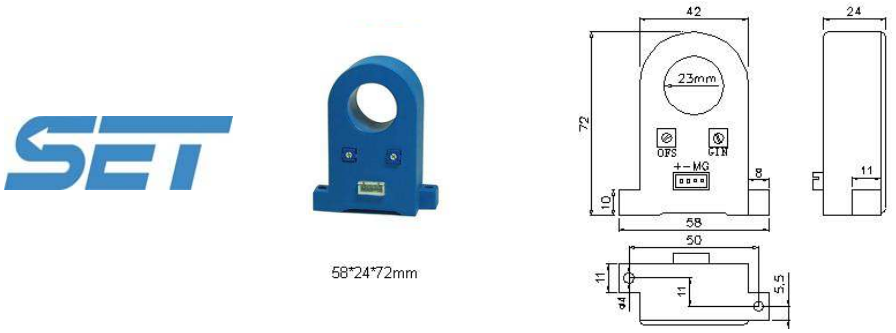

FIGURE 4.15: Current sensor size. *Taken from:* Manufacturer datasheet

DAQ, which at most can be 10 V.

$$V_{DAQ} = [(SIG+) - (SIG-)] \left[\frac{R_4}{R_2} \left(\frac{2R_f}{R_g} + 1 \right) \right] \tag{4.2}$$

Temperature sensor RTDs are used to measure the temperature in the PEMFC. They are placed in ports designed for that purpose in the graphite machined plates of the PEMFC. For this application Omega RTD with reference RTD-2-F3105-72-T-B, were used.

Current sensor A Hall-effect sensor was selected to minimize joints in the load connections which could increase the resistance losses in the system.

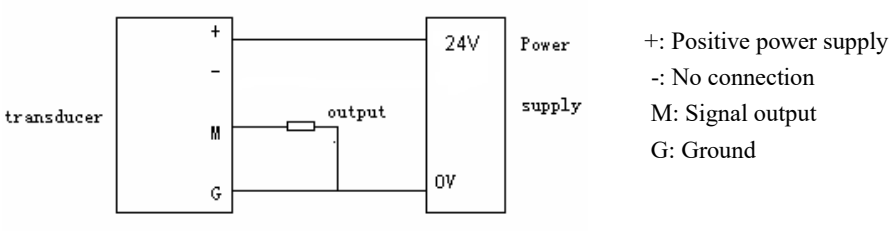

FIGURE 4.16: Connection diagram for the current sensor. *Taken from:* Manufacturer datasheet

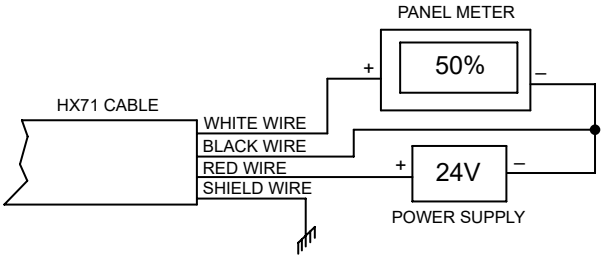

FIGURE 4.17: Humidity sensor connection diagram *Taken from:* Manufacturer datasheet

From the manufacturer, SET, the connection of this sensor is as shown in figure 4.16. Connections will be done using a PCB which machined routes to avoid using extra cables. This sensor will be connected to the NI-9205 DAQ analog inputs module.

Voltage sensor Voltage is directly measured with the NI - 9205 module or with a potentiostat. The advantage of using a potentiostat lies in that it is also the load for the fuel cell. The connections will be explained in section 4.3.1.2.

Humidity sensor To measure humidity the sensor available is an Omega relative humidity sensor, with reference HX71. This sensor works at atmospheric pressure, therefore, a measuring chamber is designed to expand the air, reducing its pressure. This implies that the humidity is characterized only in steady state.

Connections of this sensor are shown in figure 4.17, where the "PANEL METER" is the DAQ module NI - 9205.

Mass flow controllers The test bench uses two mass flow controllers (MFC), one for each gas inlet. Their size is based on the reaction mass flow rates required of hydrogen and oxygen, which can be calculated using equations 3.13 and 3.14.

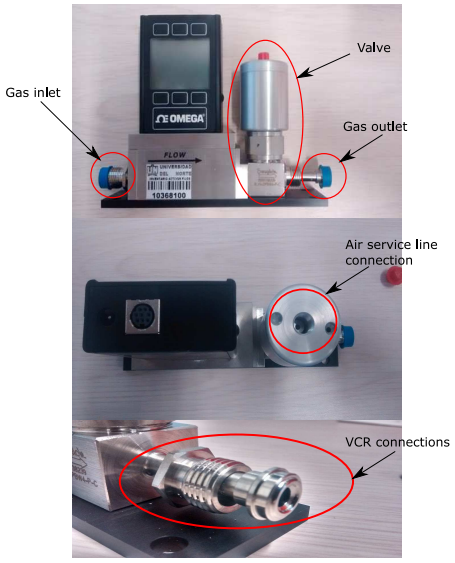

FIGURE 4.18: Mass flow controllers gas connections

In this research the PEMFC always worked with compressed air, instead of pure oxygen, for this reason, the mass flow controller of air is sized with the equation 4.3, which assumes the dry air is 21% oxygen.

$$\dot{m}_a = \frac{M_a}{0.21 M_{O_2}} \dot{m}_{O_2} \tag{4.3}$$

Finally, using the standard condition ($0°C$ y 101.325 kPa), for a max load of 6 A, the required mass flows are 41.875 $SCCM$ for the hydrogen, and 20.905 $SCCM$ for the oxygen (99.521 $SCCM$ of air). The selected controllers for H_2 and air have twice the nominal capacity to ease the control loop operation. In figure 4.18, the gas connections are shown. These controllers require an additional air input to open the outlet valve, which otherwise will remain closed.

These controllers accept remote set points which will be set by the LabView interface designed for the test bench data acquisition and control.

The electrical connections are detailed in section 4.3.1.2.

DAQ A National Instrument DAQ is used in the test bench (see figure 4.19) for the measurement and control of the PEMFC system dynamic variables. The NI cDAQ - 9174 was selected with the following modules:

1. NI - 9216 used for the RTD temperature measurements

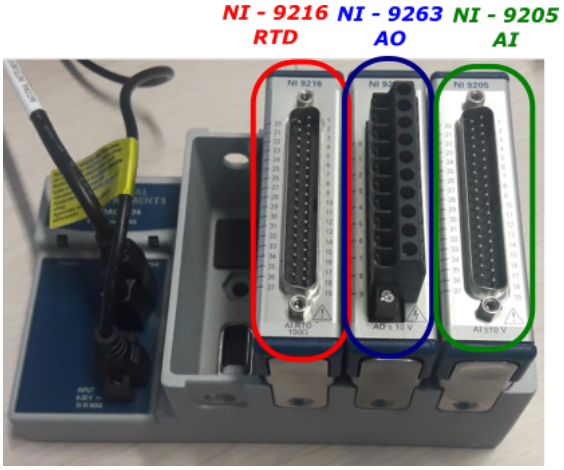

FIGURE 4.19: National Instruments DAQ

2. NI - 9263 used to measure all the analogs inputs in the range $\pm 10\ V$
3. NI - 9205 used for the analog outputs, used mainly to assign the MFC remote setpoints.

The connections of the instrumentation elements are shown in figure 4.20. With the exception of the cell voltage, all other analog inputs are referenced to a common the ground with the NI-9205 module (see figure 4.20 (left)). In the case of the NI-9216 module, the connection of a three-wire RTD is shown. The color code is the one used by OMEGA. No calculation is necessary for this sensor since the transformation of the voltage in a temperature reading is part of the functionality of the equipment. Finally, the setpoints of the mass flow controllers can be applied remotely. For this, the NI-9263 module with the connections as shown in figure 4.20 (right) is used.

4.3.1.3 Auxiliary components

The humidifiers, humidity measurement chamber, and PCB are described in the following sections.

Humidifiers The moisture content in the feed of the inlet gas lines of the fuel cell can be modified by this device. The bubbling column style was chosen because of the simplicity of its design. The principle of operation is by mass transfer between the water and the air bubbles that are injected in the lower part

of the column. It is desirable that the bubbles be of small diameters to increase the total area in contact since the mass transfer is favored by this variable, for this reason, a diffusor is installed in the humidifier inlet.

The humidifier has the dimensions shown in the drawing (see figure 4.21). The manufacture of this equipment was carried out in the manufacturing workshop of the Universidad del Norte.

During the research internship in the United States, a new humidifier was built, with the difference that it was built in PVC to avoid the complications associated with steel corrosion. In this case, the blueprints and the device are shown in figure 4.21. In this case, the connections were made through tank couplings that have the necessary NPT threads and seals to reduce leaks. Due to the applied pressure, it was necessary to apply epoxy to the joints to eliminate water and air leaks.

In this case, the air came from a bottle of completely dry compressed gas. After passing through the humidifier, humidities of the order of 60% were recorded.

Printed Circuit Board (PCB) To facilitate the electrical connection of the sensors, a circuit with screw terminals was printed. This card is suitable for both humidity and current sensors. The Autodesk Eagle software was used to define the tracks, and the CNC milling machine shown in figure 4.22 was used for the layout. In this same figure, the final product (top view) on the right is detailed, as well as the machined tracks before the terminals are welded (center).

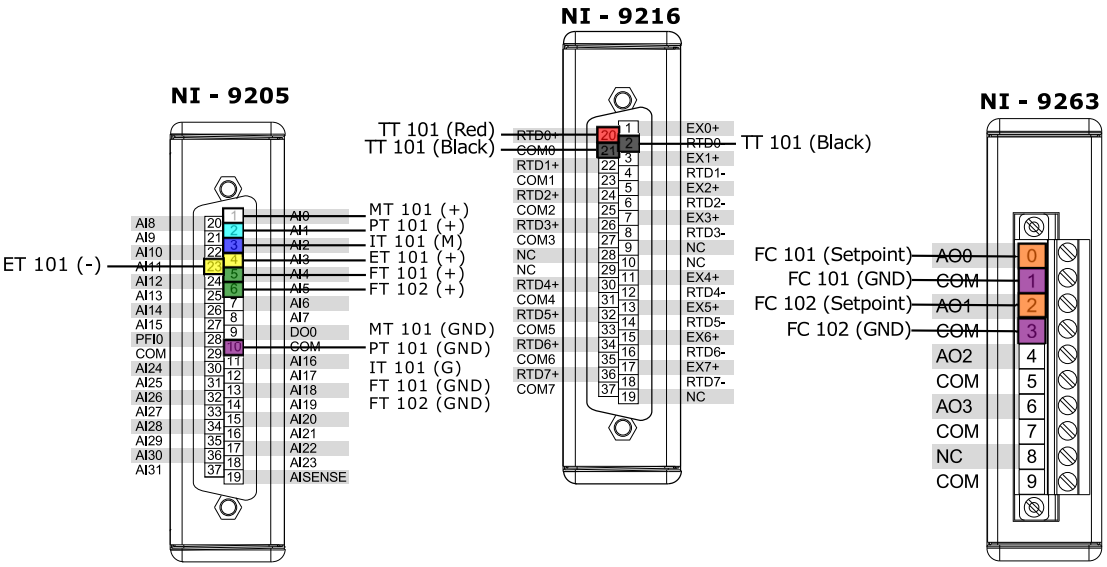

FIGURE 4.20: Instrumentation connection with the NI DAQ

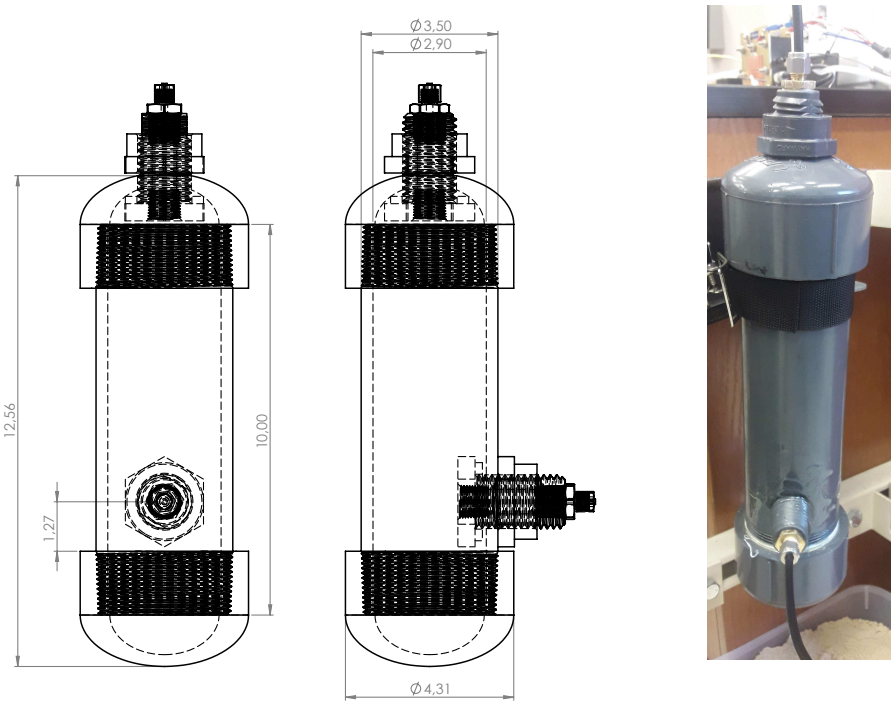

FIGURE 4.21: Air humidifier used in the international research program (units: inches)

With this card, it is guaranteed that the earth of the DC source is the same reference of the sensor and of the DAQ, necessary condition for a correct reading of the instruments, both of humidity and current.

Potentiostat To have better control on the load applied to the cell, and due to limitations in the load available to test the cell, a potentiostat was included in the system as an alternative current sensor/load. This system was used to fix a stable current on the cell while the PEMFC reagents supply are controlled by the National Instrument DAQ. This improvement leads to more reliable experimental conditions, but lead to a limitation in the max current that could be applied to the cell, which in this case is near to 1 A. This equipment can be seen at the right of the figure 4.11.

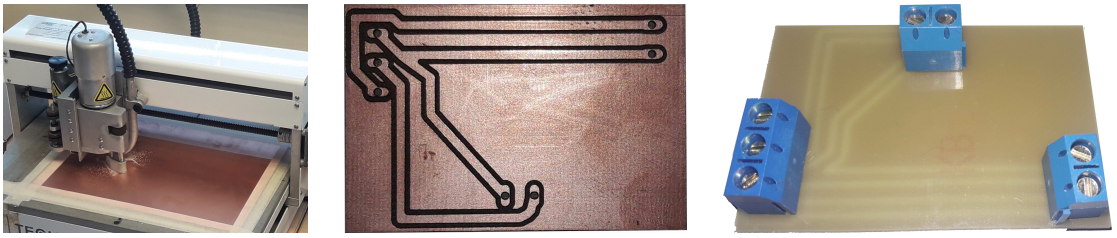

FIGURE 4.22: PCB for humidity and current sensors connection.

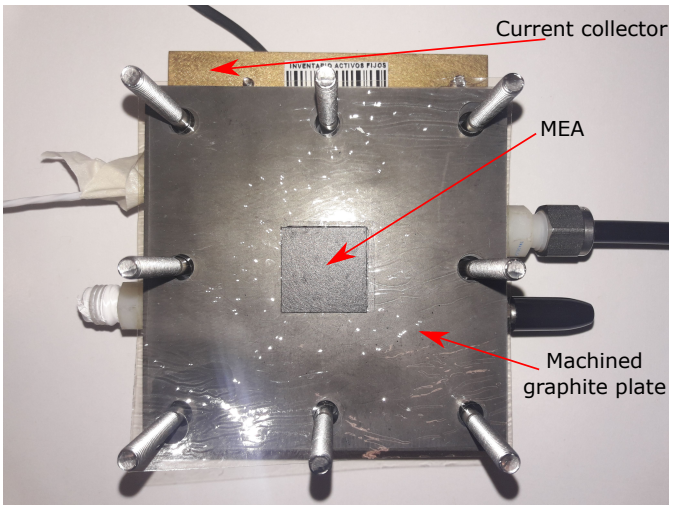

FIGURE 4.23: Open PEMFC showing a carbon paper based MEA

4.3.2 Test bench characterization

Using the test bench designed in section 4.3.1, the dynamic response of a 5 cm^2 PEM fuel cell is completed. To achieve this, an OFAT design of experiment approach is used to characterize the system dynamic response.

Initially, the air humidity was measured. The environment in the lab has a humidity close to 60%, but for the operation of the fuel cell, the compressed air line is used. This line operates close to 20% of HR which is a value too low to humidify properly the Nafion membrane in the cell. For this reason, the humidifier (this equipment is described in section 4.3.1.3) is used to increase the HR to values close to 85%, according to off-line measurements.

To test the samples, it was decided to operate at ambient temperature, which is controlled by the air conditioning system. This was done to reduce the external perturbations due to changes in the temperature of the cell because for the heating of the cell only a control ON/OFF was available.

4.3.2.1 Samples

Different GDL materials were tested on the test bench. In figure 4.23 the open cell with an installed MEA is shown. For each test, only the MEA is changed while the rest of the components remains the same.

The available samples on the market are of two types: Carbon paper type, and cloth type. During this research, the carbon paper was tested, although the presence of possible surface defects on the cloth type was also evidenced.

Two scenarios were studied. In the first experimental stage, undamaged MEAs were used and their dynamic response was studied. Later, defects on the GDL were induced, and the MEAs were tested again to study the effect of the defects on the PEMFC dynamic response.

4.3.2.2 Preliminary inspection

The MEAs were inspected under an optical microscope to complete the characterization of its surface. It was analyzed at the interface between the GDL and the distribution channels and in the catalyst layer. Figure 4.24 presents the typical defects that can be found in the electrode.

In figure 4.24a a cloth type GDL is shown. In this GDL small particles of what it seems to be catalyst ink, were found at the surface which is in contact with the flow channels. The presence of this ink in this surface is considered a defect on the MEA. The MEA is designed to work as a distribution media for the reactants in order to improve the homogeneity of the concentration distribution on the membrane. In the best case scenario, this ink will behave as a blockage to the gas flow decreasing the mass transfer coefficient, and therefore increasing the concentrations loses. From the inspection of different cloth type GDL it was concluded that this is common phenomena in GDLs, of this type. This could be there due to a lack of control during the assembly of the MEA. Also, excesses in the amount of

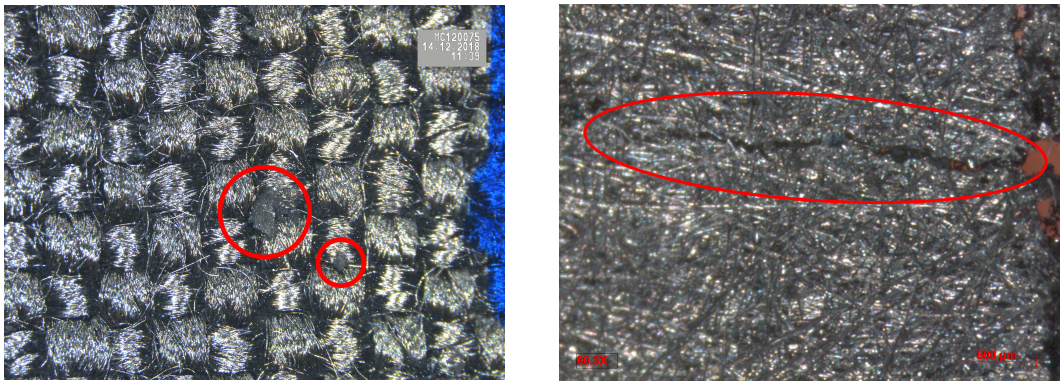

(A) ink drops in a carbon cloth type GDL (B) Cracks in a carbon paper type GDL

FIGURE 4.24: Defects on the GDL found in the preliminary inspection.

catalyst ink applied on the GDL could travel through the fibers due to excesses in the pressure of assembly of the fuel cell.

In figure 4.24b a carbon paper GDL is inspected. In this GDL a crack was found near to one of its corners. After completing the test the GDL was separated from the membrane, and it was found that the crack in most of its length is not just a surface defect but a volumetric defect, i.e. the fracture goes through all the GDL thickness. Cracks work as a void in the porous media, modifying drastically the porosity and tortuosity of the zone. This also can lead to further peeling of the GDL from the membrane increasing the contact resistance, leading to a major loss in performance.

Both of the previous defects will have an impact on the local porosity where they appear, for these reason, distortion in the GDL is artificially created to emulate the porosity variations in the electrode at its surface.

4.3.2.3 GDLs "as received"defects test

For the testing, a sudden reduction on the supply air MFC was applied, maintaining a constant load, then the voltage was recorded. For the carbon paper-based GDL shown in figure 4.25 the following response was found:

In the first 100 s the cell is in its start-up process after the load was applied. Once the system reaches its first steady state, the MFC setpoint change is applied remotely using the LabView interface and the DAQ after 7 min approximately of the cell operation. After this point, the voltage behavior is analyzed using the same approach described in section 4.2.5. The last 200 s are averaged to get a final voltage of reference, required to apply the FIT3 identification method.

From the results, for this first test, it was found a time constant $\tau \approx 13.5$ and time delay $t_0 \approx 0.5$ s. Part of the time delay is due to the MFC once the setpoint is changed in the LabView interface, due to two main reasons, its own valve dynamic, and the sample time in the DAQ. Some oscillations are observed after in the steady-state zone, this is due to external and uncontrollable parameters like some pressure fluctuations in the air supply line. Also, there could be fluctuations in the supply HR due to small changes in the water level inside the humidifier.

A second MEA, also carbon paper-based but with 1 mg/cm^2 of the catalyst was tested. The response exhibits, in this case, a significant *"undershoot"*, not only

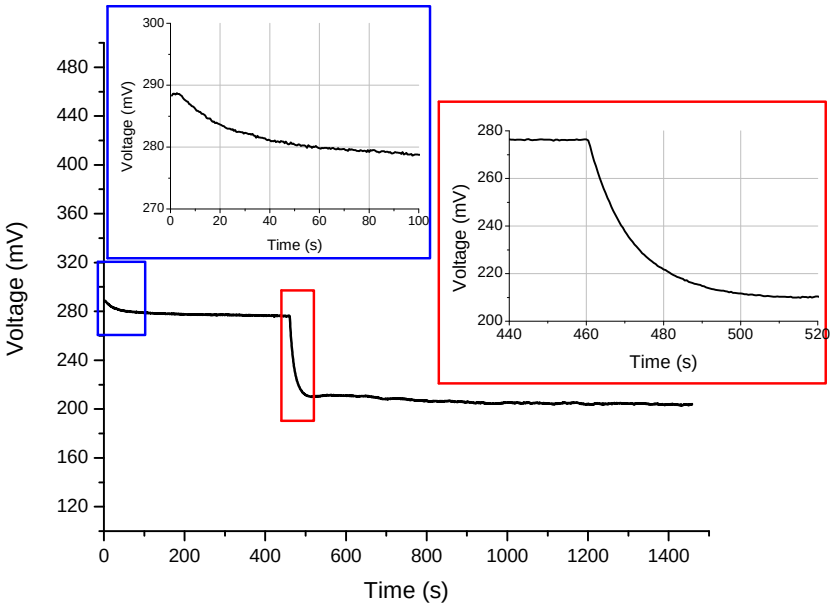

FIGURE 4.25: PEMFC with a carbon paper based MEA and 4 mg/cm^2 of catalyst dynamic response

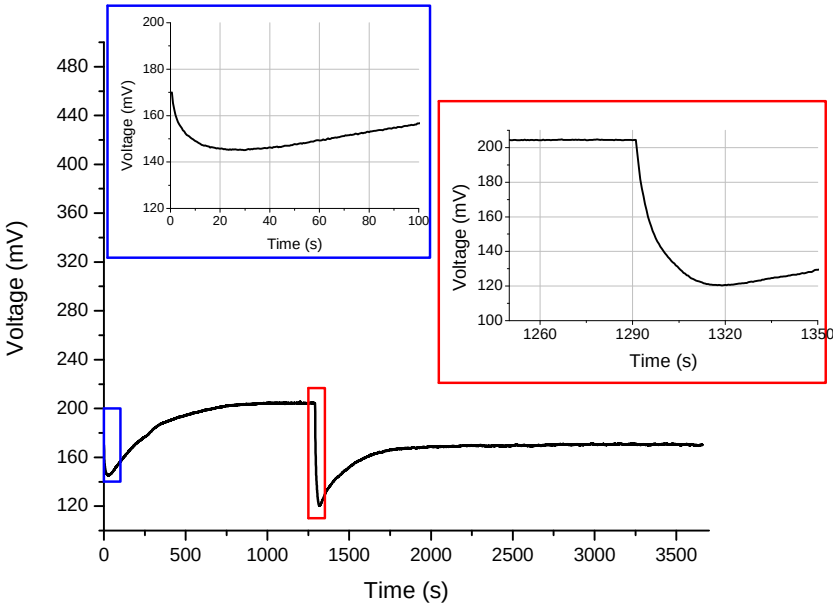

FIGURE 4.26: PEMFC with a carbon paper based MEA and 1 mg/cm^2 of catalyst dynamic response

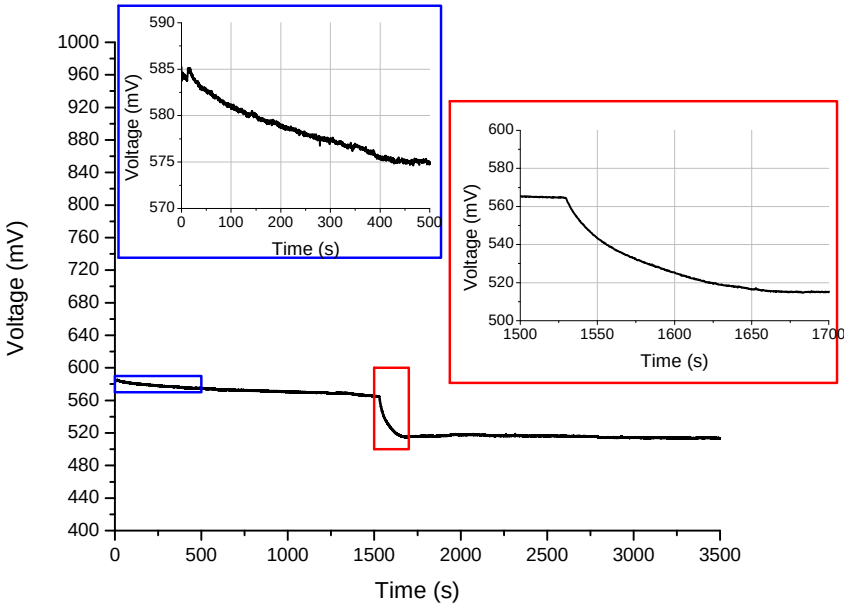

FIGURE 4.27: PEMFC with a carbon cloth based MEA and 1 mg/cm^2 of catalyst dynamic response

during the identification stage but also during the start-up as can be seen in figure 4.26, which has a duration of around 12 *min*. After this first steady-state is reached, the MFC setpoint is changed to assess its impact on the fuel cell output voltage. This change is applied at the time $t = 21.5$ *min*. In figure 4.26, in the red detailed zone, it can be seen that there is a small time delay in the cell voltage. This phenomenon follows the same explanation presented above for the previous sample.

Due to the *"undershoot"* which resembles a *lead-lag* dynamic response, the stabilization time will be associated with the "lag" time, thus the dynamic response after the sudden voltage drop is analyzed. For this sample, a time constant $\tau \approx 189$ *s*, with a time delay close to 20 *s* which means an approximated settling time around 950 *s*, which is in accordance with the dynamic response obtained for this sample.

Finally, figure 4.27 presents the results for a carbon cloth type MEA that was tested. For the same load, it was noticed a higher operation voltage, and an almost free, *undershoot* response. This type of response is an advantage during the operation of the control system, due to a less complicated dynamic response under a step change in the MFC input, reducing the system settling time.

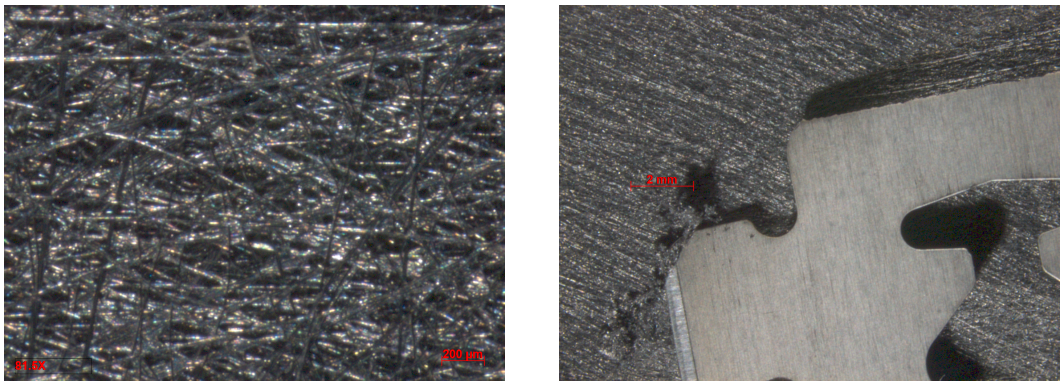

(A) "Healthy" surface (B) Induced surface crack

FIGURE 4.28: Defects preparation on the Carbon paper GDL with 1 mg/cm^2

4.3.2.4 GDLs defects "induced" test

Some defects are observed in the MEAs. Poor contact between the GDL and the membrane, for example, increase the polarization losses due to Ohm's law, making the flow of electrons towards the load harder, as well as the flow of protons through the membrane.

In figure 4.28a the reference condition for a carbon paper-based GDL is shown. This surface although smooth to the naked, exhibit a complex pattern that works as a support for the catalyst layer. As mentioned before and shown in figure 4.24b, cracks can be found in the GDL. To evaluate the effect of this defect, a crack was fabricated in the 1 mg/cm^2 GDL using a blade as illustrated in figure 4.28b. Special attention was taken to not cut through the GDL, an only create a surface "scratch". To do that a microscope was used to have a better view of the defect fabricated in real time.

After the preparation of the GDL with the defect, the fuel cell was tested again with similar operational conditions, as defined for the test presented in figure 4.26. The first thing that was noticed is the absence of the *"lead-lag"* effect both in the start-up, as well as in the step change. Also, the time required to reach an approximated initial steady - state increased in around four times. After 1 hour and 21 minutes, a sudden reduction in the MFC set point was applied, and the system dynamic response was analyzed. The system exhibit a time constant for changes in the MFC set point close to $\tau = 800\ s$ if we consider all the stabilization time (until the system reaches 2.5 h of operation in the test), if we only analyze the sudden step, it is similar to the one observed during the first step in the lag

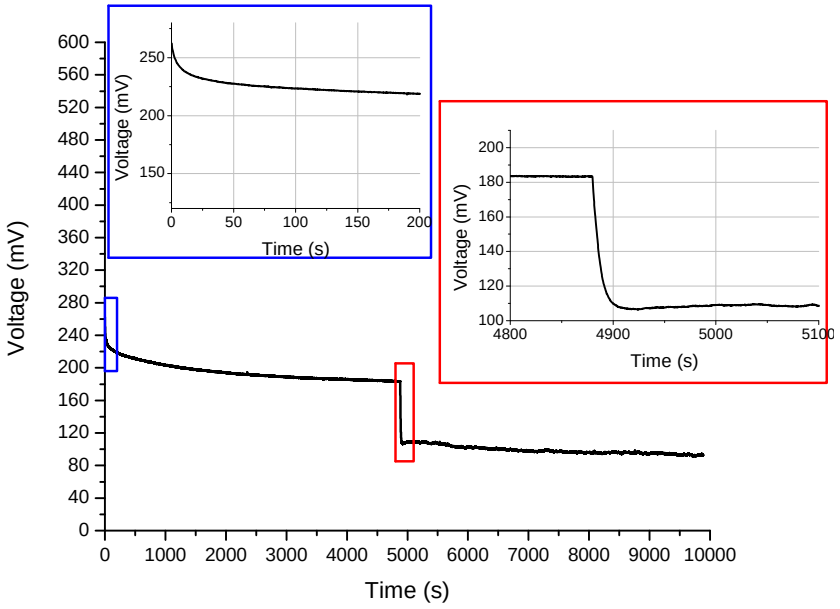

FIGURE 4.29: PEMFC with a carbon paper based MEA and 1 mg/cm^2 of catalyst dynamic response after the defect is prepared

shape in figure 4.28a. In conclusion, the system change rate is now faster in the first moments after a perturbation, but after an initial fast response, a second stage starts with a much more slower dynamic than the exhibited for this MEA before the defect. Regarding the steady states values, it starts at a relatively close potential in both scenarios (with and without defect) but the system is now more sensitive to the disturbances, this can be seen in a lower final steady state for the potential, which went from 170 to 126 mV. Therefore in a stack, it would be expected to lose around 50 mV per cell in the stack, due to this kind of defects.

Finally, figure 4.30 presents the results for the carbon cloth GDL after a defect was prepared. In terms of operating voltage it was lost around a 15 mV after the step change in the MFC, but the dynamic of the cell was significantly increased at lower loads, where it was required around 1.4 h to reach the first steady state. The trend is similar to what was found in carbon papers GDL, but the voltage loss was lower, this could be due to the GDL structure, being the carbon cloth mechanical stronger due to the fiber disposition, making the cracks harder to go through all its thickness.

Results in this section are representative of repeated measurements. For each GDL between 3 - 5 measurements repetitions were performed. For the open circuit voltage (OCV) less than 5% variations were found. For example, for the carbon

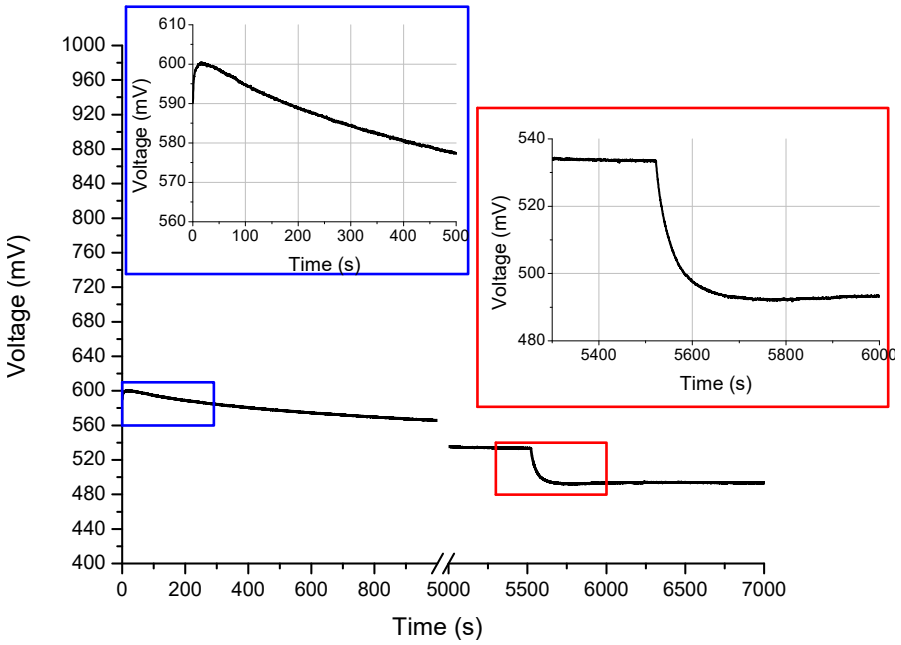

FIGURE 4.30: PEMFC with a carbon cloth based MEA and 1 mg/cm^2 of catalyst dynamic response after the defect is prepared

cloth GDL it was observed an average OCV of 838.2 mV with a standard deviation of 9.38 mV.

Chapter 5

Dynamic variables correlations

From the characterization completed in Chapter 4 correlations between system parameters (design and operation) are correlated with the dynamic response in this chapter.

5.1 DOE

From the OFAT results, the pore size was excluded from the analysis on the fuel cell dynamic response, although it has an impact on the voltage polarization due to concentration losses in the steady-state operation. For the 9 remaining factors, a factorial DOE is proposed in this stage. This stage will now introduce possible interactions between factors that could be missed in the OFAT DOE. Due to the nature of the simulation, there is no variability in the measurements so, there is no need for replication.

In table 5.1, the required runs for an IV resolution DOE design are shown. For each factor, two levels were chosen to measure the effect they could have on the dynamic response of the fuel cell. The simulation and data processing described in section 4.2.5 are also used here, therefore, the responses variables are still the result of a FOPDT fitting for the system dynamic response.

TABLE 5.1: Resolution IV DOE for the fuel cell system response. Factors, and response variables.

Factor 1 **A:GDL Porosity**	**Factor 2** **B:GDL Tortuosity**	**Factor 3** **C:GDL Thickness**	**Factor 4** **D:Membrane Thickness**	**Factor 5** **E:Roughness Factor**	**Factor 6** **F:Temperature**	**Factor 7** **G:Air Supply Pressure**	**Factor 8** **H:Hydrogen Supply Pressure**	**Factor 9** **J:Air Supply HR**	**Response 1** τ_V	**Response 2** τ_{cO_2}
31.00	6.00	500.00	25.00	75.00	75.00	4.50	4.50	20.00	44.55	22.5
31.00	4.00	250.00	25.00	75.00	30.00	4.50	4.50	50.00	40.65	22.65
61.00	4.00	500.00	25.00	75.00	75.00	4.50	6.00	50.00	35.85	21.3
31.00	6.00	500.00	183.00	75.00	30.00	6.00	6.00	50.00	15.6	9.9
61.00	6.00	250.00	25.00	75.00	75.00	6.00	4.50	50.00	11.25	8.7
31.00	4.00	250.00	183.00	75.00	75.00	6.00	6.00	20.00	9.75	9.6
31.00	6.00	250.00	25.00	45.00	75.00	4.50	6.00	50.00	44.55	22.5
61.00	6.00	250.00	183.00	75.00	75.00	4.50	4.50	50.00	37.2	21.6
31.00	4.00	500.00	183.00	45.00	75.00	6.00	4.50	50.00	13.65	9.75
61.00	4.00	250.00	183.00	45.00	30.00	6.00	6.00	50.00	13.8	9.75
61.00	6.00	500.00	183.00	45.00	75.00	6.00	6.00	20.00	11.4	9.6
31.00	6.00	250.00	183.00	45.00	30.00	6.00	4.50	20.00	13.95	24.9
61.00	4.00	250.00	25.00	45.00	75.00	4.50	4.50	20.00	36.45	21.3
31.00	4.00	500.00	183.00	45.00	30.00	4.50	6.00	20.00	41.25	22.5
61.00	6.00	500.00	25.00	45.00	30.00	4.50	4.50	50.00	41.4	22.2
61.00	4.00	500.00	183.00	75.00	30.00	6.00	4.50	20.00	13.65	9.75
31.00	4.00	500.00	25.00	45.00	30.00	6.00	6.00	20.00	13.35	9.9
61.00	6.00	250.00	25.00	75.00	30.00	4.50	6.00	20.00	40.35	22.05

TABLE 5.2: ANOVA results for the V_{fc} dynamic response

Source	**Sum of Squares**	**df**	**Mean Square**	**F Value**	**p-value Prob >F**
Model	3449.71	6	574.95	390.83	<0.0001
A-GDL Porosity	30.50	1	30.50	20.73	0.0008
B-GDL Tortuosity	18.90	1	18.90	12.85	0.0043
F-Temperature	14.43	1	14.43	9.81	0.0095
G-Air Supply Pressure	3319.53	1	3319.53	2256.49	<0.0001
AF	15.02	1	15.02	10.21	0.0085
AG	12.68	1	12.68	8.62	0.0135
Residual	16.18	11	1.47		
Cor Total	3465.89	17			

5.1.1 Voltage dynamic response

Table 5.2 presents the Analysis of Variance (ANOVA) for the significant effects obtained from the results in table 5.1. It was found that the GDL thickness (Factor C), membrane thickness (Factor D) and the roughness factor (Factor E) had no significant effect on the voltage dynamic as a main effect nor as an interaction. For the design variables, GDL material properties and their interaction with operation variables (AG) had a significant effect on the voltage dynamic response.

From the ANOVA a regression model is proposed in equation 5.1. This model has an adjusted R^2 close to 99%. Using this model response surface for the interaction are presented in figures 5.1 and 5.2.

$$\boldsymbol{\tau_V} = 26.79 - 1.32A + 1.04B - 0.917F - 13.79G - 0.92AF + 0.85AG \qquad (5.1)$$

It was found an interaction between a material property (GDL porosity) and an operation condition (temperature). From figure 5.1 it can be seen that a higher GDL porosity can improve the fuel cell system response when the system operates at higher temperatures, while at lower temperatures, increasing the porosity has little improvement on the fuel cell time constant, and therefore, its settling time will be almost unaffected.

The interaction between GDL porosity (a material property) and air supply pressure (operation parameter) was also significant, although due to the strong effect of the air supply pressure, this interaction is almost ruled by the operation factor. From figure 5.2, the voltage dynamic response will be faster for higher pressure

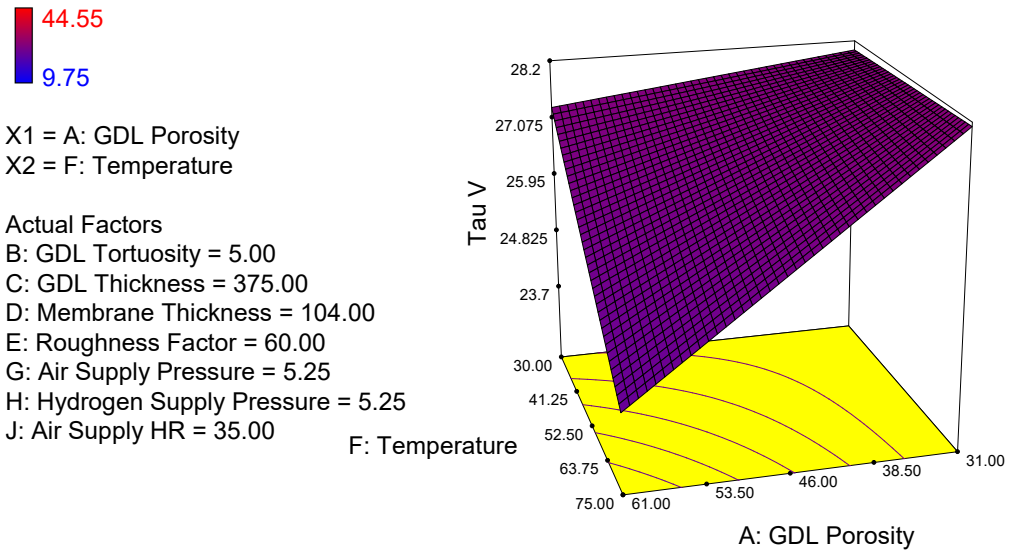

FIGURE 5.1: Interaction between GDL porosity and operation temperature effect on the voltage dynamic response

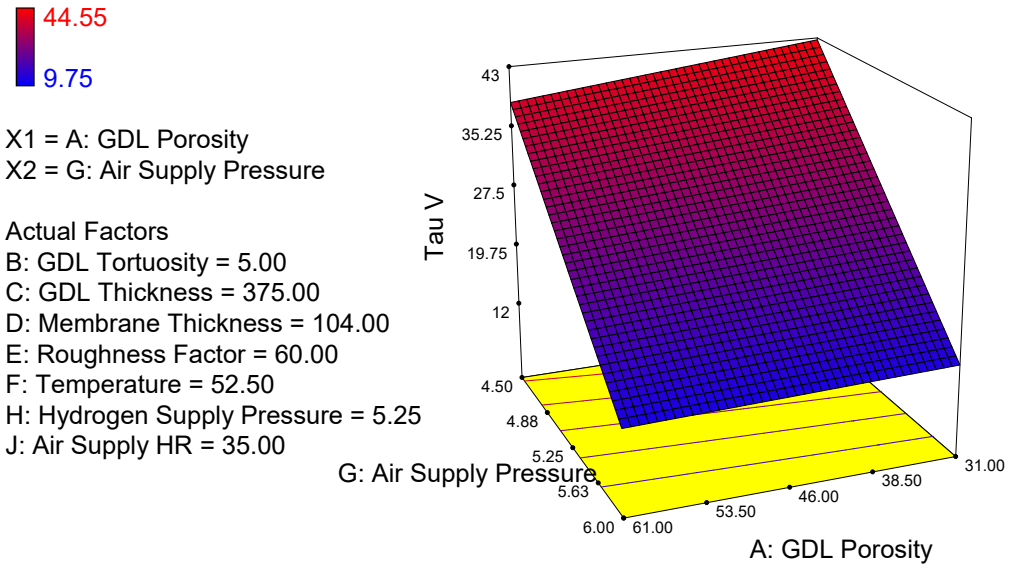

FIGURE 5.2: Interaction between GDL porosity and operation air supply pressure effect on the voltage dynamic response

operations, and this effect is slightly improved also for GDLs with higher porosity.

From all the factors then, the air pressure supply was the most important variable, appearing not only as a main effect but also in a second order interaction. The conclusion is the same for the pressure main effect and its interactions, higher pressures will lead to faster responses. The hypothesis is that at higher pressures the oxygen is replenished faster at the cathode, leading to a steady state value for the O_2 partial pressure in a shorter time. Also, a higher temperature, based on

TABLE 5.3: ANOVA results for the c_{O_2} dynamic response

Source	**Sum of Squares**	**df**	**Mean Square**	**F Value**	**p-value Prob >F**
Model	730,73	14	52,19	642,40	<0,0001
A-GDL Porosity	19,76	1	19,76	243,22	0,0006
B-GDL Tortuosity	21,98	1	21,98	270,57	0,0005
C-GDL Thickness	17,84	1	17,84	219,62	0,0007
D-Membrane Thickness	4,49	1	4,49	55,25	0,005
E-Roughness Factor	12,37	1	12,37	152,19	0,0011
F-Temperature	17,10	1	17,10	210,52	0,0007
G-Air Supply Pressure	407,79	1	407,79	5018,92	<0,0001
H-Hydrogen Supply Pressure	19,18	1	19,18	236,01	0,0006
J-Air Supply HR	11,30	1	11,30	139,09	0,0013
AB	37,81	1	37,81	465,32	0,0002
AC	41,07	1	41,07	505,48	0,0002
AG	39,93	1	39,93	491,40	0,0002
DE	44,74	1	44,74	550,69	0,0002
DG	17,82	1	17,82	219,35	0,0007
Residual	0,24	3	0,08		
Cor Total	730,97	17			

the Chapman-Engskog theory (see Appendix B), will improve the mass transfer in the porous media, in the fuel cell. The pressure in conjunction with a higher porosity in the electrode also proved to improve the dynamic performance; the porosity according to equation 3.26 also enhances the mass transfer phenomena in the electrodes.

5.1.2 O_2 concentration dynamic response

From the ANOVA in table 5.3, the important factors with a significant effect on the O_2 concentration dynamic response are presented. In this case, the material properties (GDL porosity, tortuosity, and thickness) has an impact on the dynamic response. Also, the membrane thickness and roughness factor are included in the model as design parameters. The operation parameters were also significant, both supply pressures, temperature and supplied air humidity turned out to be significant. Moreover, the interaction between design parameters and operation parameters (AG,DG) were also significant.

Using the ANOVA a regression model is proposed in equation 5.2. This model has an adjusted R^2 close to 99%. Using this model response surface for the interaction

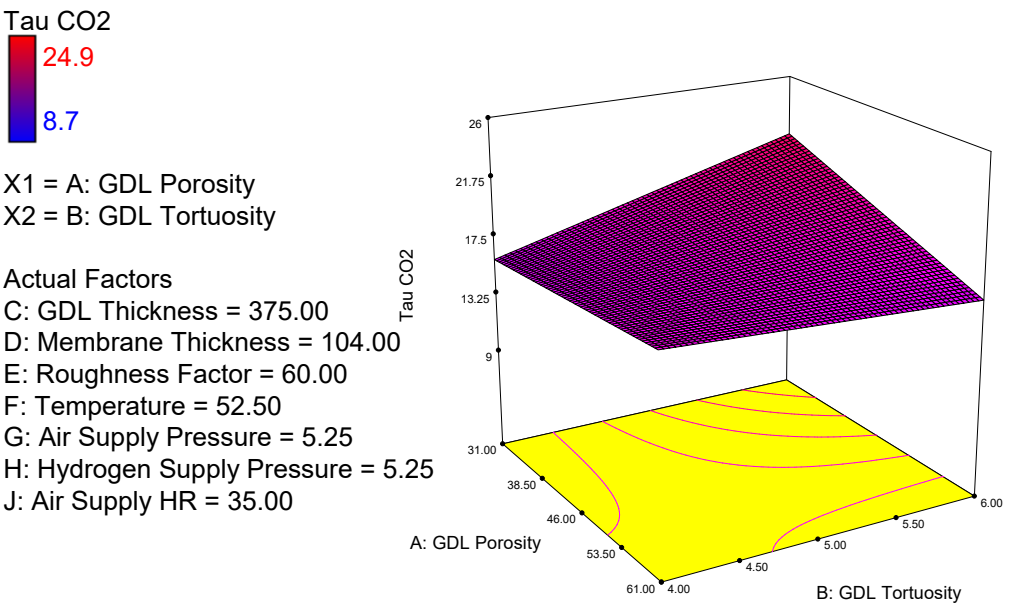

FIGURE 5.3: Interaction between GDL porosity and GDL tortuosity effect on the c_{O_2} dynamic response

are obtained and presented in figures 5.3 - 5.7.

$$\begin{aligned}\tau_{c_{O_2}} = {} & 17.63 - 1.08A + 1.14B - 1.02C + 0.61D - 0.85E - F - 5.77G \\ & - 1.06H - 0.81J - 1.77AB + 1.85AC - 1.71AG - 1.81DE - 1.67DG\end{aligned} \tag{5.2}$$

For the interaction between the GDL porosity and the GDL tortuosity (AB) two possibles approaches were found to be able to reduce the transients time: 1) reducing the porosity and the tortuosity, or 2) increasing both of them. The worst scenario is a GDL with low porosity and a high tortuosity.

The interaction between the GDL porosity and its thickness is also important. Its behavior is similar to the AB interaction, although the effect is more notorious at the lower thickness, in this case, it is recommended to increase the porosity of the electrode.

Unlike previous interaction, the interaction AG (GDL porosity - Supply air pressure) is an interaction between design and operation parameters. This interaction is dominated by the air supply pressure at higher pressures, at lower pressures, a higher porosity can improve the dynamic response.

The membrane thickness and the electrode roughness factor, which is directly related to the catalyst layer between the membrane are also related due to interaction DE. In this case, increasing the membrane thickness will require an increase

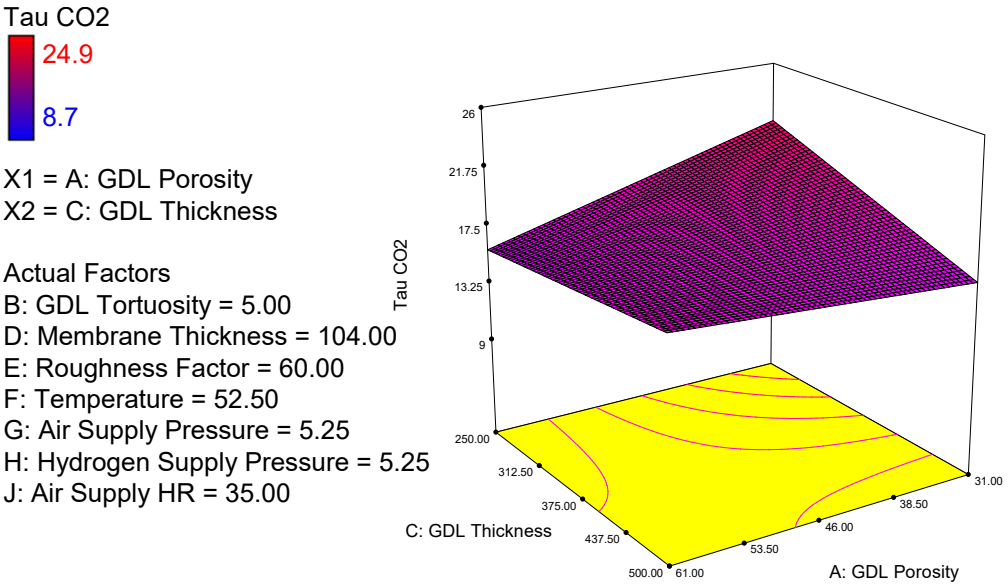

FIGURE 5.4: Interaction between GDL porosity and GDL thickness effect on the c_{O_2} dynamic response

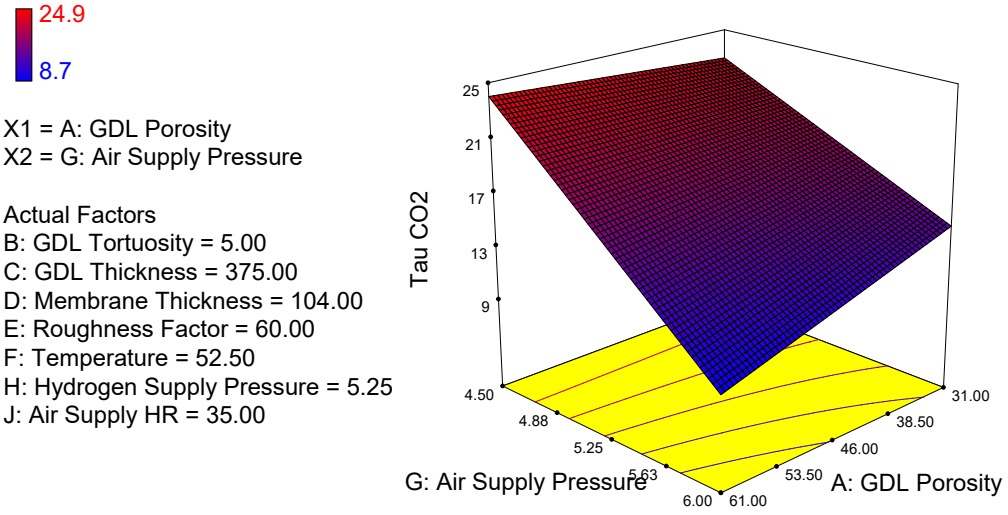

FIGURE 5.5: Interaction between GDL porosity and operation air supply pressure effect on the c_{O_2} dynamic response

in the roughness factor; for example a higher catalyst load.

The last interaction relates the membrane thickness with the supply air pressure. It can be seen from figure 5.6 that for thicker membranes there is a greater impact on the dynamic response due to the pressure level. In this scenario is suggested to increase the operating pressure in the cathode.

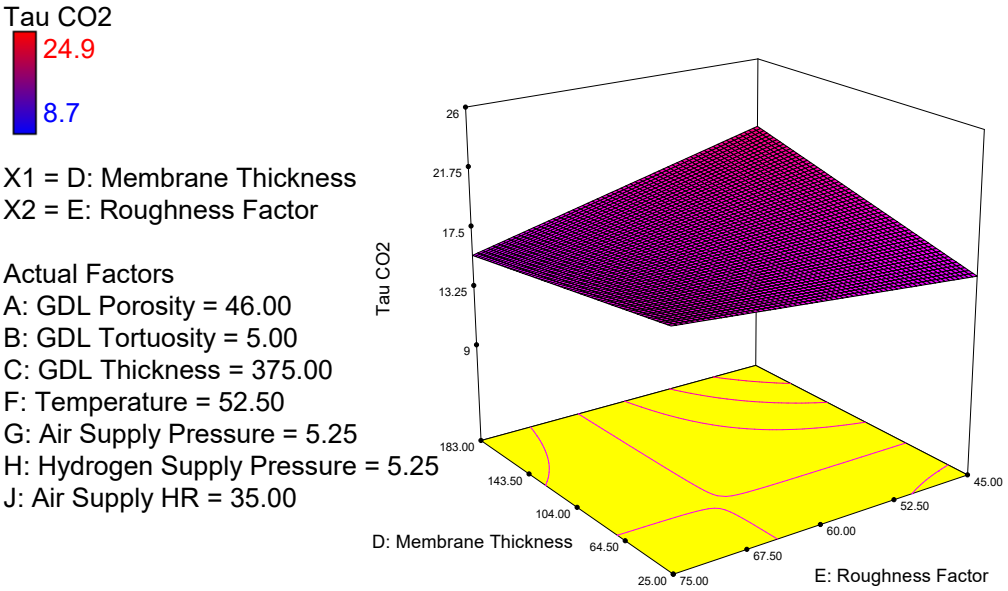

FIGURE 5.6: Interaction between the membrane thickness and the electrode surface factor effect on the c_{O_2} dynamic response

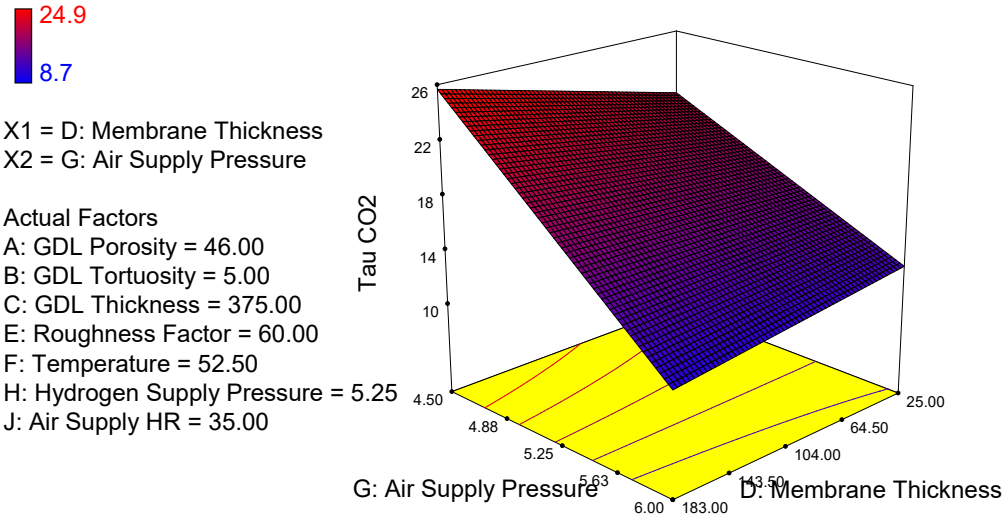

FIGURE 5.7: Interaction between the membrane thickness and operation air supply pressure effect on the c_{O_2} dynamic response

Chapter 6

Design of the Methodology

In this chapter, the design methodology is formulated and each step will be discussed. This method is the result of the integration of the previous results found during the assessment of the materials properties and electrodes surface defects impact on the fuel cell dynamic response and performance.

The design of a PEMFC requires of multidisciplinary tools, including design of the geometries that enhance the mass transfer processes and the materials selections that reduce electric resistances and catalyst that allows the electrochemical reaction to take place. In fuel cells used under variable loads like hybrid systems or transportation applications, the dynamic response is also critical and it has an important impact on the control system design.

Concurrent engineering (CE) should be applied in this multidisciplinary environment, where DFX (Design for X) tools have proven to be effective to this kind of tasks. Many methodologies of this kind have been developed for different fields, like DFM (Design for Manufacturability), DFP (Design for Portability), DFMA (Design for Manufacture and Assembly), among others.

The proposed methodology is intended to balance the pragmatism and the formality in the design process of PEM fuel cells oriented to improve its controllability.

6.1 Design for Controllability (DFC)

The intention of this methodology will be to asses the controllability of the system in terms of easily findable data, thus, it will be avoided too formal definitions of controllability like the mentioned in section 2.4, in exchange simulation of non linear systems, will be used as a tool to test the system dynamic response and assess the performance of a particular control system under specific conditions.

With this methodology, the improvement of the dynamic response is pursued. It is understood by this, finding conditions for a faster response with fewer time delays and also reducing the operating conditions that lead to undesirables scenarios like starvation.

6.1.1 Steps to implement the DFC methodology

According to Huang [1996], DFX tools help the decision making the process. They are considered ones of the most effective approaches to implementing concurrent engineering (CE).

As any DFX methodology, a logic flowchart for decisions is included as well as tools to complete them. The DFC methodology will consist of the following steps (see figure 6.1), following the approach proposed by Mak [1997].

6.2 Step 1: Requirement analysis

A test bench is required to assess the dynamic response of the system. Specifications of a test bench are included in the section 4.3.1 as an example of a PEMFC test bench.

Initially, the size of the fuel cell and its intended use has to be defined. The first one is function of the load that will be connected to the fuel cell system including its expected behavior. If there is historical data, it could be used as a better guess.

It should be analyzed the average load and the dynamic variations during the day. For loads with fast changes, it is necessary to include electrical storage systems (i.e batteries banks) to ease the control system response.

The selection of materials will also depend on the particular requirements of the load and the availability of reagents, for example, higher amounts of catalyst can be used if there is pure oxygen available, for open cathode fuel cells the cooling system can be simplified, etc.

Hybridization can be also considered in this stage, so, for locations with other power sources installed, the installation of the fuel cell will produce a hybrid system.

Performance indexes or measurements have to be defined. For a fuel cell system, dynamic response and steady-state parameters have to be considered. These performance measurements will give the user enough information to the user to know if there is an improvement in the fuel cell design.

Once the methodology is applied several times a benchmark could be defined in order to easily define what is considered *"good"* or *"bad"*.

The methodology can also make predictions about the fuel cell system performance, based on preliminary data and the developed model's dynamic response, this will let the user test materials combinations before they actually are installed.

Finally, in this methodology, an iterative process is expected and recommended in order to improve the design process of the fuel cell systems as can be seen in figure 6.1.

6.3 Step 2: Modeling

For *modeling* two things are understood within this methodology.

1. PEM fuel cell dynamic simulation
2. Bill of materials (BOM) and key characteristics.

To have a better understanding of the system response, modeling and simulation are required. In chapter 3 and appendix A a parametric model for a PEM fuel cell was presented. This model let the methodology used to perform a preliminary test before using the test bench, i.e., fewer materials have to be bought and therefore a saving in the budget is expected. In chapter 5 a simulated design of experiments

TABLE 6.1: PEMFC BOM example

Part number	Description	Quantity
1	Collector plates	2
2	Machined graphite blocks	2
3	Membrane	1
4	GDL	2
5	Catalyst	1 mg/cm^2
6	Gaskets	2
7	Bolts	8
8	Connection ports	4

is formulated to assess the material properties impact on the fuel cell system performance. The user can test the effect of different materials combinations before expending significant amounts of money in experimentation, especially for the GDL, which is the most expensive component of the system due to the catalyst layer based on precious materials like platinum, applied on the porous media.

In a BOM should be included the number part, a brief description, and the quantity. For example for a PEM single cell

6.4 Step 3: Performance Measurements

According to chapter 5 there are material properties that have an impact on the dynamic response of the fuel cell system.

To assess the fuel cell system dynamic performance in the first place the dynamic response has to be characterized and dynamic parameters estimated. In the analysis it could be included parameters like time constants (τ), time delays (t_0), the relationship between time delays and time constant (t_0/τ) for the open loop system.

In chapter 5 the assessment of the dynamic performance parameters is completed for the studied fuel cell system. In this procedure, the simulation can be used to get relationships between the main dynamic variables with a strong effect on the system dynamic performance. The results in that chapter can be extrapolated with care to other systems in a qualitative approach, that is, it is expected for the trends to be the same, but the magnitudes will be different for particular systems.

The user has to repeat this procedure in any other PEM fuel cell system under study.

6.4.1 Open loop measurements

For τ and t_0 changes in the MFC set points can be used to estimate the impact of the control inputs on the fuel cell system dynamic. It is suggested to characterize the system under several load conditions in order to identify sever non-linear regions that should be avoided, like the concentration high loss region in the higher current density range of the polarization curve. This process should be done for the simulation and experimental stages. In chapter 4 the procedure is explained in detail for one load level.

6.5 Step 4: Testing

Once the system has been designed simulations and a prototype are required to test its performance. The test bench is used in this stage to analyze the system dynamics of the designed fuel cell configuration. In chapter 4 typical results are presented. This data can be used for two main purposes: 1) validate the simulations results based on the PEM fuel cell dynamic model, and supply data for the parameter adjustment and 2) to assess phenomena hard to model, like the surface defects on the electrodes.

If the cell fulfills the requirements defined in the first step of this methodology, the design process is concluded, otherwise, an iterative process like the one shown in figure 6.1 is repeated.

6.6 Guidelines and support material

For the data collection process, it is recommended to rely on peer-reviewed material and self-made experiments. For fundamental equations during the modeling textbooks are a suitable option as well as handbooks. In the appendixes A - C several material properties and additional parameters are included as well as some additional comments on the modeling of the fuel cell.

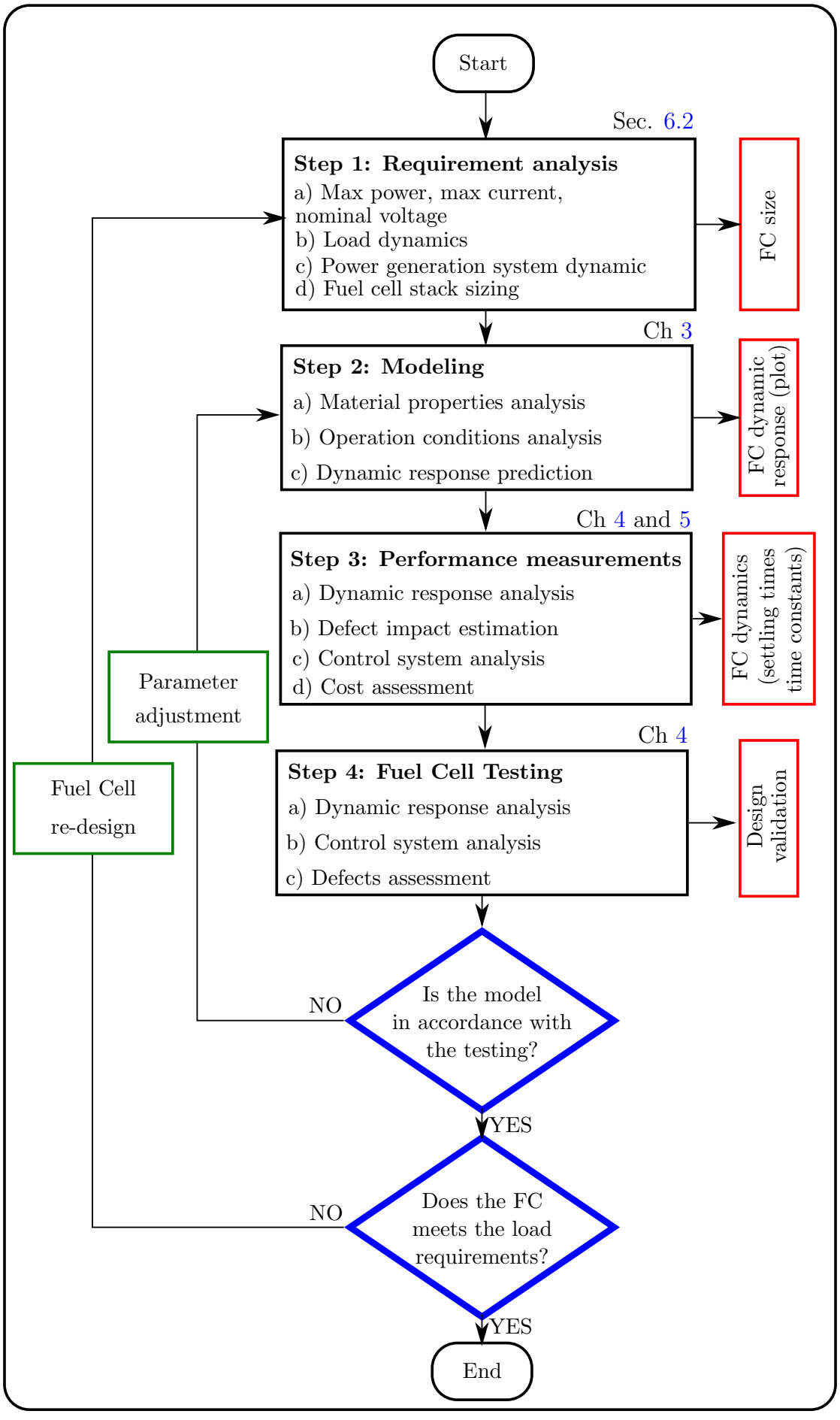

FIGURE 6.1: DFC methodology flowchart

Chapter 7

Conclusions

7.1 Conclusions

Fuel cells are complex devices which involve different phenomena, each one of them with their own dynamic. These phenomena define cell dynamic response and performance. The design of PEMFC is then a complex process due to the interaction between material properties and operating parameters that have a significant impact on the fuel cell dynamic response, and therefore on the control system performance.

An enhanced dynamic model for electrochemical modeling was developed during this research. This model is presented as a support element in the developed methodology working as a test bed for the impact of different materials properties on the dynamic response, and also its interaction with operating conditions.

Using the dynamic model, **relationships between material properties, and operation variables linked to fuel cells dynamic response** were developed as a tool for material selection taking into consideration the cell controllability. It was found for example a strong relationship between the air supply pressure and the GDL porosity. From the model relationships between the aforementioned variables surface responses were presented to ease the analysis. These results can be used as a graphic guideline to predict the expected performance of the fuel cells when new materials are tested.

The effect of a typical surface defect was also linked with the fuel cell dynamic response. The dynamic response was analyzed under changes in the air

MFC set point. The impact of air mass flow variations was then studied, mainly its settling time and time delay. It was found that after a crack is fabricated on the "as received" GDLs vs the "damaged" one, a significant increase in the settling time was found, making the cell slower to changes in the mass flow rate in the supply line.

The set up for a PEMFC dynamic testing was designed and tested during this research. This test bench can be used as a resource for future researches in the fuel cell field at the Universidad del Norte.

Finally, **a methodology which integrates the effect of defects on the PEM performance** based on the previously acquired knowledge is proposed as a logical series of steps and recommendations which can be used to improve the performance of a PEMFC regarding its dynamic response. Although this methodology is intended for PEMFC, it can be adapted to work on different electrochemical devices as long as its dynamic response is characterized and its operating principles are modeled.

Chapter 8

Future Work

From this work, possible futures approaches could expand the capabilities of the methodology proposed:

- The materials used during this research were limited due to their cost. Since the interaction of different material properties is also significant for the system dynamic response, it is recommended to increase the experimental stage with more commercial and non-commercial materials.
- There are many characterizations techniques that can be used to have a better data set for the model simulations. In this research, the characterization was limited to the porosity of the GDL, but additional characterization could be completed in order to have a better understanding of the geometry of the defects on the porous media.
- During the research, the working load was limited due to available equipment restrictions, and the purge was limited to a fixed valve position. The cells should be tested under severe operating conditions to have a better description of their performance.

Appendix A

Fuel Cell Model and Parameters

A.1 1D model

The mass and heat transfer model auxiliary equations are presented in this section.

A.1.1 Mass transfer model

For the oxidant supply: When performing a mass balance on the cathode side cell (here the oxidant is supplied), you have to consider the scenario when the cell uses air. The water content in the air depends on the temperature at which it is present. By definition, absolute humidity is defined as the ratio of the mass of water vapor to the mass of the dry air contained therein.

A.1.1.1 Cathode

$$w = \frac{m_v}{m_a} = 0.622 \frac{\phi_i p_{sat}(T_i)}{p_i - \phi_i p_{sat}(T_i)} \tag{A.1}$$

The water vapor saturation pressure (p_{sat}) can be calculated using the equation proposed by Musio et al. [2011].

$$\log_{10}\left(p_{sat}(T)\right) = -2.1794 + 0.02953T - 9.1873 \times 10^{-5}T^2 + 1.4454 \times 10^{-7}T^3 \tag{A.2}$$

The dry air and water vapor mass flow ratio entering the cell as a stream of moist air are given by the equations A.3 and A.4 respectively.

$$\underbrace{\frac{\dot{m}_{a,i}^{c,ch}}{\dot{m}_{ma,i}}}_{\text{input}} = \frac{1}{1 + \underbrace{w_i}_{\text{Eq. A.1}}} \tag{A.3}$$

$$\frac{\dot{m}_{v,i}^{c,ch}}{\dot{m}_{ma,i}} = \frac{w_i}{1 + w_i} \tag{A.4}$$

Dry air is assumed to consist of oxygen (21%) and nitrogen (79%), and only oxygen is a reactive gas involved in the electrochemical reaction. For a stream of dry air it is assumed that the mass flow of oxygen is given by the equation A.5.

$$\dot{m}_{O_2,i}^{c,ch} = \underbrace{0.21\frac{M_{O_2}}{M_a}}_{mf_{O_2}} \dot{m}_{a,i}^{c,ch} \tag{A.5}$$

where M_{O_2} y M_a are the molar masses of oxygen and air, and $\dot{m}_{a,i}$ is calculated using equation A.3. And the mass flow of nitrogen is given by the equation A.6.

$$\dot{m}_{N_2,i}^{c,ch} = \underbrace{0.79\frac{M_{N_2}}{M_a}}_{mf_{N_2}} \dot{m}_{a,i}^{c,ch} \tag{A.6}$$

where M_{N_2} is the molar mass of nitrogen.

The moisture content inside the cell varies constantly and will depend on the humidity of the gases supplied but also on the electrochemical reaction in the cell, whose by-product is precisely water vapor.

$$\dot{m}_{l,o}^{a,ch} = \frac{m_l^{a,ch}}{t_{pur}} \qquad \text{under the restiction } \dot{m}_{j,o}^{c,ch} > 0 \tag{A.7}$$

The mass of moist air inside the fuel cell cathode channels is:

$$m_{ma}^{c,ch} = \underbrace{m_{O_2}^{c,ch}}_{\text{Eq. 3.1}} + \underbrace{m_{N_2}^{c,ch}}_{\text{Eq. 3.2}} + \underbrace{m_v^{c,ch}}_{\text{Eq. 3.3}} \tag{A.8}$$

The vapor transfer occurs at the cathode due to mass transfer by diffusion which is mainly a function of the difference in concentrations between the cathode and

the GDL.

$$\dot{m}_v^{c,GDL\to c,ch} = A_{fc} n_{fc} M_v \underbrace{\overbrace{\langle D_v^c \rangle}^{\text{Eq. A.10}} \left(\frac{\overbrace{c_v^{c,GDL} - c_v^{c,ch}}^{\text{Eq. A.14}}}{\delta^{GDL}} \right)}_{N_v^{c,GDL\to c,ch}} \tag{A.9}$$

$$\langle D_v^c \rangle = \left[D_v \varepsilon \left(\frac{\varepsilon - 0.11}{1 - 0.11} \right)^{0.785} \left(1 - \underbrace{s^c}_{\text{Eq. A.13}} \right)^2 \right] \tag{A.10}$$

Where, $N_v^{c,GDL\to c,ch}$ is the molar flow of vapor per unit area ($kmols^{-1}m^{-2}$) and $\langle D_v^c \rangle$ is the diffusion coefficient in a porous medium contemplating the effects of the porosity

$$\varepsilon = \frac{V_p}{V^{GDL}} \tag{A.11}$$

and the saturation of the medium (s) Nam and Kaviany [2003], and

$$\langle D_v^c \rangle = D_v f(\varepsilon) g(s) \tag{A.12}$$

$$s^j = \frac{V_l^j}{V_p} \text{ for } j = \underbrace{c, GDL}_{Eq.\ A.16} \text{ and } \underbrace{a, GDL}_{Eq.\ 3.9} \tag{A.13}$$

From the definition of molar concentration $\frac{n}{V}$,where n is the number of moles and V the volume occupied, along with the equation of state of the ideal gases it can be said that the concentration of water vapor is given by:

$$c_v^j = \frac{\overbrace{p_v^j}^{\text{Eq. A.23}}}{R \underbrace{T_{fc}}_{Eq.\ 3.12}} \text{ for } j = c, ch \text{ and } c, GDL \tag{A.14}$$

And the rate at which evaporates or condenses water vapor is given by the equation proposed by Zemansky and Dittman [1979].

$$\dot{m}_{evap}^{c,ch} = \min \left[A_{fc} \left(p_{sat}(T_{fc}) - \underbrace{p_v^{c,ch}}_{\text{Eq. A.23}} \right) \sqrt{\frac{M_v}{2\pi R T_{fc}}}, \underbrace{\dot{m}_l^{c,GDL\to c,ch}}_{\text{Eq. A.17}} \right] \tag{A.15}$$

Where the term $\dot{m}_l^{c,GDL}$ represents the flow of water in the liquid phase in the GDL and is obtained by proposing an additional mass balance.

$$\rho_l^{H_2O}\frac{dV_l^{c,GDL}}{dt} = -\underbrace{\dot{m}_{evap}^{c,GDL}}_{\text{Eq. A.19}} - \underbrace{\dot{m}_l^{c,GDL\to c,ch}}_{\text{Eq. A.17}} \tag{A.16}$$

The last term of the equation A.16 represents the mass flow of liquid water from the GDL to the channels of the cathode associated with the capillary effect that occurs in the GDL since this is a porous medium; the calculation of this flow is explained in detail by Nam and Kaviany [2003] and simplified by del Real et al. [2007].

$$\dot{m}_l^{c,GDL\to c,ch} = \frac{\rho_l A_{fc} n_{fc} K S^3}{\mu_l}\left|\frac{d\rho_c}{dS}\right|\frac{S^c}{\delta^{GDL}} \tag{A.17}$$

The term ρ_c refers to the function of Leverette, which describes the relationship between capillary pressure and saturation of the liquid phase of water. The term $\left|\frac{d\rho_c}{dS}\right|$ can be approximated to a constant value of 30 312 Pa and the liquid saturation can be calculated using the following equation proposed by Nam and Kaviany [2003] and adapted by del Real et al. [2007].

$$S^c = \begin{cases} \frac{s^c - s_{im}}{1 - s_{im}} & \text{for } s_{im} < s^c \leq 1 \\ 0 & \text{for } 0 < s^c \leq s_{im} \end{cases} \tag{A.18}$$

The other term associated with the mass balance of the liquid phase (equation A.16) is that related to the rate of condensation or evaporation $\left(\dot{m}_{evap}^{c,GDL}\right)$. Similar to the phenomenon that occurs in a sponge when submerged in liquid water, in the GDL of the fuel cell there is the transport of condensed fluids due to the capillary effect. The rate at which the water condenses in the porous medium is a function of the partial pressure of the water vapor, the operating temperature of the cell and the coefficient of volumetric condensation.

$$\dot{m}_{evap}^{c,GDL} = -M_{H_2O}\gamma\left[\frac{p^{c,GDL} - p_{sat}(T_{fc})}{R_u T_{fc}}\right]\varepsilon V^{GDL} \tag{A.19}$$

The equation A.19 is subject to the logical constraint: if $V_l^{c,GDL} = 0$ and $\dot{m}_{evap}^{c,GDL} > 0 \rightarrow \dot{m}_{evap}^{c,GDL} = 0$, in this way it is ensured that there is no indication that there is a mass flow of water due to evaporation under conditions in which there is no water in the liquid phase.

The flows to the discharge of the fuel cell are a function of the operating pressures. If we assume a behavior similar to that of a valve, we have that the discharge flow of humid air is given by:

$$\dot{m}_{ma,o}^{c,ch} = K_o^{c,ch} \upsilon_o \left(p^{c,ch} - p_o^{c,ch} \right) \tag{A.20}$$

where, $p^{c,ch}$ is the pressure in the cathode channels and $p_o^{c,ch}$ the discharge pressure of the cell.

The mass flows of each component in the humid air will be proportional to the mass of these contained in the cathode volume.

$$\dot{m}_{j,o}^{c,ch} = \frac{m_j^{c,ch}}{\underbrace{m_{ma}^{c,ch}}_{\text{Eq. A.8}}} \dot{m}_{ma,o}^{c,ch} \text{ for } j = O_2, N_2, v \tag{A.21}$$

For the pressures:

According to Dalton's Law, "*The pressure of a gas mixture is equal to the sum of the pressures each gas would exert if it existed alone at the mixture temperature and volume*"

$$p^{c,ch} = \sum_{j=1}^{3} p_j^{c,ch} \text{ for } j = O_2, N_2, v \tag{A.22}$$

where

$$p_j^{c,ch} = \frac{m_j R_u T_{fc}}{M_j V^{c,ch}} \text{ for } j = \underbrace{O_2, N_2, v}_{\text{Eqs. 3.1, 3.2 and 3.3}} \tag{A.23}$$

$$V^{c,ch} = \delta^{c,ch} A_{fc} n_{fc} \tag{A.24}$$

A.1.1.2 Membrane

$$n_d = 0.0029(\lambda^a)^2 + 0.05\lambda^a - 3.4 \times 10^{-19} \tag{A.25}$$

and the water content, λ_j is fitted using the following experimental relationship Springer et al. [1991]

$$\lambda^j = 0.043 + 17.81a^j - 39.52(a^j)^2 + 36(a^j)^3 \text{ for } j = a, c \tag{A.26}$$

$$a^j = \phi^{j,GDL} = \frac{y_{H_2O} p_v^{j,GDL}}{p_{sat}(T_{fc})} \text{ for } j = a, c \tag{A.27}$$

the concentrations are calculated using Eq. A.28

$$c_{v,j} = \frac{\rho_{memb,dry}}{M_{memb,dry}} \lambda^j \tag{A.28}$$

and the diffusion coefficient D_{H_2O}

$$D_{H_2O} = D_{\lambda^a} \exp\left(2416\left(\frac{1}{303} - \frac{1}{T_{fc}}\right)\right) \tag{A.29}$$

where,

$$D_{\lambda^a} = \begin{cases} 10^{-10} & \lambda^a < 2 \\ 10^{-10}\left(1 + 2\left(\lambda^a - 2\right)\right) & 2 \leq \lambda^a \leq 3 \\ 10^{-10}\left(3 - 1.67\left(\lambda^a - 3\right)\right) & 3 < \lambda^a < 4.5 \\ 1.25 \times 10^{-10} & \lambda^a \geq 4.5 \end{cases} \tag{A.30}$$

$$\log\left(p_{sat}\right) = -2.1794 + 0.02953T - 9.1837 \times 10^{-5}T^2 + 1.4452 \times 10^{-7}T^3 \tag{A.31}$$

A.1.1.3 Anode

$$m_{mh}^{a,ch} = \underbrace{m_{H_2}^{a,ch}}_{\text{Eq. 3.6}} + \underbrace{m_v^{a,ch}}_{\text{Eq. 3.7}} \tag{A.32}$$

$$\dot{m}_v^{a,GDL\to a,ch} = A_{fc} n_{fc} M_v \langle D_v^c \rangle \underbrace{\left(\frac{\overbrace{c_v^{a,GDL} - c_v^{a,ch}}^{\text{Eq. A.34}}}{\delta^{GDL}} \right)}_{N_v^{a,GDL\to a,ch}} \tag{A.33}$$

where

$$c_v^j = \frac{\overbrace{p_v^j}^{\text{Eq. A.43}}}{RT_{fc}} \text{ for } j = a, ch \text{ and } a, GDL \tag{A.34}$$

$$\langle D_v^c \rangle = \left[D_v \varepsilon \left(\frac{\varepsilon - 0.11}{1 - 0.11} \right)^{0.785} \left(1 - \underbrace{s^c}_{\text{Eq. A.13}} \right)^2 \right] \tag{A.35}$$

$$\dot{m}_l^{a,GDL\to a,ch} = \frac{\rho_l A_{fc} n_{fc} K S^3}{\mu_l} \left| \frac{d\rho_c}{dS} \right| \frac{S^a}{\delta^{GDL}} \tag{A.36}$$

$$\dot{m}_{evap}^{a,ch} = \min \left[A_{fc} \left(p_{sat}(T_{fc}) - \underbrace{p_v^{a,ch}}_{\text{Eq. A.43}} \right) \sqrt{\frac{M_v}{2\pi R T_{fc}}}, \underbrace{\dot{m}_l^{a,GDL\to c,ch}}_{\text{Eq. A.36}} \right] \tag{A.37}$$

$$\dot{m}_{evap}^{a,GDL} = -M_{H_2O} \gamma \left[\frac{p^{a,GDL} - p_{sat}(T_{fc})}{R_u T_{fc}} \right] \varepsilon V^{GDL} \tag{A.38}$$

$$\dot{m}_{mh,o}^{a,ch} = K_o^{a,ch} \upsilon_o \left(\underbrace{p^{a,ch}}_{\text{Eq. A.43}} - p_o^{a,ch} \right) \tag{A.39}$$

$$\dot{m}_{j,o}^{a,ch} = \frac{m_j^{a,ch}}{\underbrace{m_{mh}^{a,ch}}_{\text{Eq. A.32}}} \dot{m}_{mh,o}^{a,ch} \text{ for } j = H_2, v \tag{A.40}$$

If $\dot{m}_{j,o}^{a,ch} > 0$ then

$$\dot{m}_{l,o}^{a,ch} = \frac{m_l^{a,ch}}{t_{pur}} \tag{A.41}$$

For the pressures. Analogous to the cathode:

$$p^{a,ch} = \sum_{j=1}^{3} p_j^{a,ch} \text{ for } j = H_2, v \tag{A.42}$$

where

$$p_j^{a,ch} = \frac{m_j R_u T_{fc}}{M_j V^{a,ch}} \text{ for } j = H_2, v \tag{A.43}$$

$$V^{a,ch} = \delta^{a,ch} A_{fc} n_{fc} \tag{A.44}$$

A.1.2 Heat transfer model

The variation of the enthalpy of the different gases that react during the operation of the system is shown by the following equation, it depends on the change of enthalpies due to the temperature change (Δh) as well as the enthalpy of formation (h_f^0) for both the reactants and the products of the reaction.

$$\dot{H}^{reac} = \dot{m}_{H_2}^{reac}\left(h_f^0 + \Delta h\right)_{H_2} + \dot{m}_{O_2}^{reac}\left(h_f^0 + \Delta h\right)_{O_2} - \dot{m}_{H_2O}^{reac}\left(h_f^0 + \Delta h\right)_{H_2O(g)} \tag{A.45}$$

The term $\Delta\dot{H}_{H_2}^{pur}$ refers to the energy that leaves the system with the hydrogen that was purged and therefore was not part of the electrochemical reaction but suffered a change of temperature and therefore takes part of the energy of the system with it. It is assumed that hydrogen enters the stack at room temperature and leaves at the temperature at which the cell is operating.

$$\Delta\dot{H}_{H_2}^{pur} = \dot{m}_{H_2,o}^{a}\Delta h_{H_2}\big|_{@T_{fc}-T_{surr}} \tag{A.46}$$

The term $\Delta\dot{H}_{ma}^{cool}$ is used to contemplate the cooling effect associated with the transfer of heat to the excess air; the supplied air flow is used to supply the oxygen required in the reaction, but the excess will exchange heat with the cell.

$$\begin{aligned}\Delta\dot{H}_{ma}^{cool} = \dot{m}_{N_2,o}^{c}\Delta h_{N_2}\big|_{@T_{fc}-Tsurr} + \dot{m}_{O_2,o}^{c}\Delta h_{O_2}\big|_{@T_{fc}-Tsurr} + \cdots \\ \cdots + \dot{m}_{v,o}^{c}\Delta h_{v}\big|_{@T_{fc}-Tsurr} + \dot{m}_{l,s}^{c}c_p(T_{fc} - T_{surr})\end{aligned} \tag{A.47}$$

During the purge of the anode, it is possible that there is water, both in the liquid phase and in the gas phase, in the current that is carried away by the purged hydrogen. The energy associated with this water stream.

$$\Delta \dot{H}^{purg}_{H_2O} = \dot{m}^{a}_{v,s} \Delta h_{H_2O_{(g)}} \Big|_{@T_{fc} - Tsurr} + \dot{m}^{a}_{l,s} c_p (T_{fc} - T_{surr}) \tag{A.48}$$

A.2 1D model parameters

TABLE A.1: Mass transfer model parameters

Parameter	Value	Reference
$A\ (cm^2)$	5	
$\delta^{a,ch},\ \delta^{c,ch}\ (mm)$	1.25	Ziogou et al. [2011]
$K_o^{c,ch}, K_o^{a,ch}\ \left[kg\ (bar\ s)^{-1}\right]$	0.001	Ziogou et al. [2011]
$\delta_{GDL}\,(mm)$	0.5	
$K\ (m^2)$	2.55×10^{-13}	Nam and Kaviany [2003]
$\mu_l\ \left[kg\ (m\ s)^{-1}\right]$	4.05×10^{-4}	Nam and Kaviany [2003]
s_{im}	0.1	Nam and Kaviany [2003]
γ	0.9×10^3	Nam and Kaviany [2003]
$\rho_l\,(kg\ m^{-3})$	978	
$M_v\,(kg\ kmol^r-1)$	18.02	

TABLE A.2: Mass flow controllers model parameters

Parameter	Value	Reference
$K_v^a\ (m^3\ s^{-1})$	4.7063×10^{-5}	
$M_{H_2}\ (kg\ kmol^{-1})$	2.016	
$M_{air}\ (kg\ kmol^{-1})$	28.97	
N_9	26	ISA [2007]
F_{y,H_2}	1.0036	
$F_{y,air}$	1	
x_T	0.84	ISA [2007]

TABLE A.3: Heat transfer model parameters

Parameter	Value	Reference
$A_{cht}\,(m^2)$	355.27×10^{-4}	Ziogou et al. [2011]
$c_{fc}\ \left(J\ (kg\ K)^{-1}\right)$	727.57	Ziogou et al. [2011]
$h_{amb}\ (W\ m^{-2}\ K^{-1})$	1.73×10^{-3}	Ziogou et al. [2011]
$m_{fc}\ (kg)$	1.378	Ziogou et al. [2011]
$T_{ref}\ (^\circ C)$	25	

TABLE A.4: Electrochemical model parameters

Parameter	Value	Reference
$\Delta G_c^a \ (kJ\ mol^{-1})$	29	Barbir [2013]
$\Delta G_c^c \ (kJ\ mol^{-1})$	66	Barbir [2013]
$i_0^{c,ref} \ (A\ cm^{-2})$	1×10^{-9}	Barbir [2013]
$i_0^{a,ref} \ (A\ cm^{-2})$	1×10^{-4}	Barbir [2013]
α_a	0.2	
α_c	1.8	
$d(\mu m)$	0.5	Liu et al. [2013]
ξ	4	
ε	0.3	Ni et al. [2006]
f_r	10	

TABLE A.5: Parameters for Ω_D Cussler [2009]

	H_2O	H_2	O_2
$\sigma_j \ (\text{Å})$	2.641	2.827	3.467
ϵ_j/k	809.1	59.7	106.7

Appendix B

Chapman-Enskog theory

$$D_{j-H_2O} = \frac{1.86 \cdot 10^{-3} T^{3/2} \left(\frac{1}{M_j} + \frac{1}{M_{H_2O}}\right)^{1/2}}{P \sigma_{j-H_2O}^2 \Omega_D} \tag{B.1}$$

for $j = H_2, O_2$

$$\Omega_D = \frac{1.06036}{\left(T^*_{j-H_2O}\right)^{0.156}} + \frac{0.193}{\exp\left(0.47635 T^*_{j-H_2O}\right)} + \frac{1.03587}{\exp\left(1.52996 T^*_{j-H_2O}\right)} + \frac{1.76474}{\exp\left(3.89411 T^*_{j-H_2O}\right)} \tag{B.2}$$

$T^*_{j-H_2O}$ are the dimensionless temperatures:

$$T^*_{j-H_2O} = \frac{kT}{\epsilon_{j-H_2O}} \tag{B.3}$$

and ε_{j-H_2O} are the Lennard-Jones energies, and σ_{j-H_2O} are the collision diameter, given in angstroms. For hydrogen, oxygen and water the values of σ and ϵ_j/k can be found in the work of Cussler Cussler [2009].

$$\epsilon_{j-H_2O} = \sqrt{\epsilon_j \epsilon_{H_2O}} \tag{B.4}$$

$$\sigma_{j-H_2O} = \frac{\sigma_j + \sigma_{H_2O}}{2} \tag{B.5}$$

where σ_j are the mean molecular radius.

Appendix C

Fuel Cell Material Properties

FuelCellsEtc
Commercial Fuel Cell Components

(979) 635-4706
askus@fuelcellsetc.com

Gas Diffusion Layer Comparison Table

Gas Diffusion Layer (GDL)	Type	Thickness (um)	Density (g/cm³)	Basic Weight (g/m²)	Air Permeability (s)	Through Plane Resistance (mΩcm²)	Tensile Strength (N/cm)	Flexural Modulus (MPa)	Porosity	PTFE Treated	MPL
Plain Carbon Cloth	Cloth	356	1.5	132	-	-	19.25	7.5	-	No	No
GDL-CT	Cloth	410	-	180	< 8	< 13	>10 MD & >5 XMD	-	-	Yes	Yes
ELAT Hydrophilic	Cloth	406	0.346	130	2.156	34 @ 400 lb load	-	-	80%	No	No
ELAT LT 1400 W	Cloth	454	0.8	170	0.104 L/(m²s*Pa)	17 @ 400lb load	-	-	63%	Yes	Yes
ELAT 2400W	Cloth	490	0.8	250	10	-	-	-	31%	Yes	2
Sigracet 10 AA	Paper	390	-	85	85 cm³/(cm²*s)	< 6	-	-	-	No	No
Sigracet 10 BA	Paper	400	-	85	85 cm³/(cm²*s)	< 12	-	-	88%	Yes	No
Sigracet 10 BB	Paper	420	-	125	3 cm³/(cm²*s)	< 15	-	-	84%	Yes	Yes
Sigracet 10 BC	Paper	420	-	135	1.45 cm³/(cm²*s)	< 16	-	-	82%	Yes	Yes
Sigracet 24 AA	Paper	190	-	51	-	-	-	-	-	No	No
Sigracet 24 BA	Paper	190	-	54	60 cm³/(cm²*s)	< 10	-	-	84%	Yes	No
Sigracet 24 BC	Paper	235	-	100	0.6 cm³/(cm²*s)	< 12	-	-	76%	Yes	Yes
Sigracet 25 AA	Paper	190	-	38	-	-	-	-	-	No	No
Sigracet 25 BA	Paper	190	-	40	210 cm³/(cm²*s)	< 10	-	-	88%	Yes	No
Sigracet 25 BC	Paper	235	-	86	1 cm³/(cm²*s)	< 12	-	-	80%	Yes	Yes
Sigracet 34 AA	Paper	280	-	82	-	-	-	-	-	No	No
Sigracet 34 BA	Paper	280	-	86	45 cm³/(cm²*s)	< 11	-	-	83%	Yes	No
Sigracet 34 BC	Paper	315	-	140	0.35 cm³/(cm²*s)	< 14	-	-	75%	Yes	Yes
Sigracet 35 AA	Paper	300	-	51	-	-	-	-	-	No	No
Sigracet 35 BA	Paper	325	-	110	1.5 cm³/(cm²*s)	< 15	-	-	80%	Yes	No
Sigracet 35 BC	Paper	325	-	110	1.5 cm³/(cm²*s)	< 15	-	-	80%	Yes	Yes
AvCarb EP40	Paper	200	0.2	36	4.5	8	-	-	-	No	No
AvCarb P50	Paper	170	0.31	50	35	6.7	-	-	-	No	No
AvCarb P75	Paper	245	0.29	75	15	7.8	-	-	-	No	No
AvCarb GDS1120 P50	Paper	184	0.4	79	-	< 14.5	-	-	-	Yes	Yes
AvCarb GDS3215 EP40	Paper	200	0.3	60	-	< 14	-	-	-	Yes	Yes
AvCarb GDS3250 EP40	Paper	225	0.33	75	-	< 14	-	-	-	Yes	Yes
AvCarb GDS3260 EP40	Paper	210	0.38	80	-	< 14	-	-	-	Yes	Yes

We currently sale all of the GDL that is marked in blue. If you need a GDL that is marked in black please contact us at **sales@fuelcellsetc.com** for pricing.
We also offer teflon treatments at specific percentages for all of our GDLs.

FIGURE C.1: GDL properties (part 1)

Gas Diffusion Layer (GDL)	Type	Thickness (um)	Density (g/cm³)	Basic Weight (g/m²)	Air Permeability (s)	Through Plane Resistance (mΩcm²)	Tensile Strength (N/cm)	Flexural Modulus (MPa)	Porosity	PTFE Treated	MPL
AvCarb GDS2120 P75	Paper	248	0.4	101	-	< 14	-	-	-	Yes	Yes
AvCarb GDS2230 P75	Paper	275	0.4	98	-	< 14	-	-	-	Yes	Yes
AvCarb GDS2240 P75	Paper	275	0.4	110	-	< 14	-	-	-	Yes	Yes
AvCarb GDS22100 P75	Paper	330	0.53	185	-	< 17	-	-	-	Yes	Yes
AvCarb MGL 190	Paper	190	0.44	-	2.2	-	65	45	78%	No	No
AvCarb MGL 280	Paper	280	0.44	-	3.3	-	85	45	78%	No	No
AvCarb MGL 370	Paper	370	0.46	-	4.4	-	120	45	78%	No	No
Freudenberg H1410 I4 C9	Paper	180	-	115	40	7	16	-	-	Yes	Yes
Freudenberg H2315 I6	Paper	210	-	115	160 l/m²*s	7	16	-	-	Yes	No
Freudenberg I2 C6	Paper	250	-	135	70	8	14	-	-	Yes	Yes
Freudenberg C2	Paper	255	-	135	70	10	16	-	-	No	Yes
Freudenberg C4	Paper	255	-	135	50	8	12	-	-	No	Yes
Freudenberg H2415 C5	Paper	270	-	130	40	9	14	-	-	No	Yes
Freudenberg I2 C3	Paper	290	-	150	35	9	22	-	-	Yes	Yes
Freudenberg I2 C8	Paper	230	-	135	90	8	14	-	-	Yes	Yes
Spectracarb 2050A - 0550	Paper	127	0.5	88	35	18	4.2 MD & 2.6 XMD	37	-	No	No
Spectracarb 2050A-0850	Paper	203	0.5	88	35 cfm/ft²	18	4.2 MD & 2.6 XMD	37	-	No	No
Spectracarb 2050A - 1050	Paper	254	0.5	88	35	18	4.2 MD & 2.6 XMD	37	-	No	No
Spectracarb 2050A - 1535	Paper	381	0.35	175	35	15	-	40	-	No	No
Spectracarb 2050A-1550	Paper	381	0.5	175	35 cfm/ft²	15	-	40	78%	No	No
Toray 030	Paper	110	0.4	-	-	80 mΩcm	-	40	80%	No	No
Toray 060	Paper	190	0.44	-	-	80 mΩcm	50	40	78%	No	No
Toray 090	Paper	280	0.44	-	-	80 mΩcm	70	40	78%	No	No
Toray 120	Paper	370	0.45	-	-	80 mΩcm	90	40	78%	No	No

We currently sale all of the GDL that is marked in blue. If you need a GDL that is marked in black please contact us at **sales@fuelcellsetc.com** for pricing.
We also offer teflon treatments at specific percentages for all of our GDLs.

FuelCellsEtc
College Station, TX 77842
www.FuelCellsEtc.com

Contact Us
Phone: (979) 635-4706
Sales: sales@fuelcellsetc.com
Questions: askus@fuelcellsetc.com

FuelCellsEtc does not guarentee that the data listed on this table is of 100% accuracy.

FIGURE C.2: GDL properties (part 2)

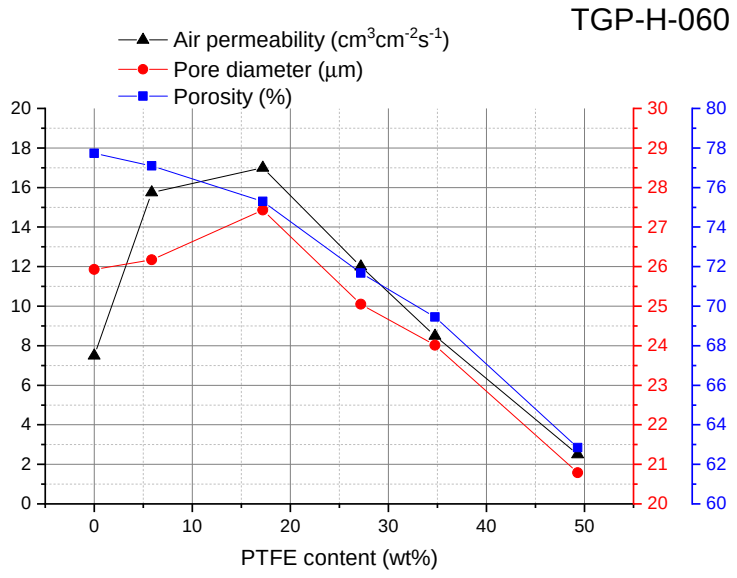

FIGURE C.3: GDL properties (Carbon paper)

Bibliography

Al-dabbagh, A. W., Lu, L., and Mazza, A. (2010). Modelling , simulation and control of a proton exchange membrane fuel cell (PEMFC) power system. *Int. J. Hydrogen Energy*, 35(10):5061–5069.

Barbir, F. (2013). *PEM Fuel Cells*. Elsevier.

Brunauer, S., Emmett, P. H., and Teller, E. (1938). Adsorption of Gases in Multimolecular Layers. *Journal of the American Chemical Society*, 60(2):309–319.

Catlin, G., Advani, S. G., and Prasad, A. K. (2011). Optimization of polymer electrolyte membrane fuel cell flow channels using a genetic algorithm. *J. Power Sources*, 196(22):9407–9418.

Cele, N. P., Sinha-Ray, S., Munda, J., and Jimoh, A. a. (2010). The state of the art proton exchange membrane fuel cells for clean energy. *2010 IEEE Int. Energy Conf.*, pages 865–869.

Cheng, S., Fang, C., Xu, L., Li, J., and Ouyang, M. (2015). Model-based temperature regulation of a PEM fuel cell system on a city bus. *Int. J. Hydrogen Energy*, 40(39):13566–13575.

Cleveland, C. J. and Morris, C. (2014). *Handbook of Energy*, volume II.

Cottrell, C. A., Grasman, S. E., Thomas, M., Martin, K. B., and Sheffield, J. W. (2011). Strategies for stationary and portable fuel cell markets. *Int. J. Hydrogen Energy*, 36(13):7969–7975.

Cussler, E. L. (2009). *Diffusion: Mass Transfer in Fluid Systems*. Cambridge University Press, Cambridge, UK, third edition.

Das, P. K. and Weber, A. Z. (2013). Water Management in PEMFC With Ultra-Thin Catalyst-Layers. In *ASME 2013 11th Int. Conf. Fuel Cell Sci. Eng. Technol.*, page V001T01A002. ASME.

del Real, A. J., Arce, A., and Bordons, C. (2007). Development and experimental validation of a PEM fuel cell dynamic model. *J. Power Sources*, 173(1):310–324.

Dutta, S. and Shimpalee, S. (2001). Numerical prediction of mass-exchange between cathode and anode channels in a PEM fuel cell. *J. Heat Mass Transf.*, 44(11):2029–2042.

EERE (2016). Types of Fuel Cell. Avaliable at `http://energy.gov/eere/fuelcells/types-fuel-cells`.

Fărcaş, A. C. and Dobra, P. (2014). Adaptive Control of Membrane Conductivity of PEM Fuel Cell. *Procedia Technol.*, 12:42–49.

Grove, W. (1839). On Voltaic Series and the Combiantion of Gases by Platinum. *London Edinburgh Philosphical Mag. J. Sci.*, XIV:127–131.

Hatti, M., Meharrar, a., and Tioursi, M. (2011). Power management strategy in the alternative energy photovoltaic/PEM Fuel Cell hybrid system. *Renew. Sustain. Energy Rev.*, 15(9):5104–5110.

Holmes, R. (2008). *The Age of Wonder*, volume 1.

Hoogers, G. (2003). Introduction. *Fuel Cells*.

Huang, G. Q. (1996). Devoloping DFX Tools. In Huang, G. Q., editor, *Design for X*, pages 107–129. Springer Netherlands, Dordrecht.

International Energy Agency (2016). Key World Energy STATISTICS.

ISA (2007). *Flow Equations for Sizing Control Valves*, volume ISA-75.01. Durham, NC. USA.

Kalman, R. E. (1959). On the general theory of control systems. *IRE Transactions on Automatic Control*.

Kalman, R. E. (1970). Contributions to the Theory of Optimal Control.

Kunusch, C., Puleston, P. F., Mayosky, M. A., and Fridman, L. (2013). Experimental results applying second order sliding mode control to a PEM fuel cell based system. *Control Eng. Pract.*, 21(5):719–726.

Liu, H., Li, P., and Wang, K. (2013). Optimization of PEM fuel cell flow channel dimensions—Mathematic modeling analysis and experimental verification. *Int. J. Hydrogen Energy*, 38(23):9835–9846.

Liu, Z., Ling, X. Y., Su, X., and Lee, J. Y. (2004). Carbon-supported Pt and PtRu nanoparticles as catalysts for a direct methanol fuel cell. *Journal of Physical Chemistry B*, 108(24):8234–8240.

Mak, K. L. (1997). THE DFX SHELL: A GENERIC FRAMEWORK FOR DEVELOPING DESIGN FOR X TOOLS. *Robotics*, 13(3):271–280.

Manso, a. P., Marzo, F. F., Barranco, J., Garikano, X., and Garmendia Mujika, M. (2012). Influence of geometric parameters of the flow fields on the performance of a PEM fuel cell. A review. *Int. J. Hydrogen Energy*, 37(20):15256–15287.

Martin, K. and Kopasz, J. (2010). Status of fuel cells and the challenges facing fuel cell technology today. *Fuel Cell Chem. Oper.*, pages 1–13.

Matraji, I., Laghrouche, S., and Wack, M. (2012). Pressure control in a PEM fuel cell via second order sliding mode. *Int. J. Hydrogen Energy*, 37(21):16104–16116.

Meidanshahi, V. and Karimi, G. (2012). Dynamic modeling, optimization and control of power density in a PEM fuel cell. *Appl. Energy*, 93:98–105.

Mench, M. M. (2008). *Fuel Cell Engines*, volume 1. John Wiley & Sons, Inc.

Müller, E. A. and Stefanopoulou, A. G. (2006). Analysis, modeling, and validation for the thermal dynamics of a polymer electrolyte membrane fuel cell system. *fuel cell Sci. Technol.*

Müller, P. C. and Schiehlen, W. O. (1985). Controllability and observability. In *Linear vibrations: A theoretical treatment of multi-degree-of-freedom vibrating systems*, number 1, pages 293–295. Springer Netherlands, Dordrecht.

Musio, F., Tacchi, F., Omati, L., Gallo Stampino, P., Dotelli, G., Limonta, S., Brivio, D., and Grassini, P. (2011). PEMFC system simulation in MATLAB-Simulink® environment. *Int. J. Hydrogen Energy*, 36(13):8045–8052.

Nafion Store (2016). What is Nafion? Avaliable at `http://www.nafionstore.com/store/pg/19-Nafion-_US.aspx`.

Nam, J. H. and Kaviany, M. (2003). Effective diffusivity and water-saturation distribution in single- and two-layer PEMFC diffusion medium. *Int. J. Heat Mass Transf.*, 46(24):4595–4611.

NASA (2016). Global Climate Change. Vital Signs of the Planet.

Ni, M., Leung, M. K. H., and Leung, D. Y. C. (2006). A modeling study on concentration overpotentials of a reversible solid oxide fuel cell. *Journal of Power Sources*, 163(1 SPEC. ISS.):460–466.

Oh, H., Park, J., Min, K., Lee, E., and Jyoung, J.-Y. (2015). Effects of pore size gradient in the substrate of a gas diffusion layer on the performance of a proton exchange membrane fuel cell. *Applied Energy*, 149:186–193.

Ou, K., Wang, Y.-X., Li, Z.-Z., Shen, Y.-D., and Xuan, D.-J. (2015). Feedforward fuzzy-PID control for air flow regulation of PEM fuel cell system. *Int. J. Hydrogen Energy*, 40(35):1–10.

Özbek, M., Wang, S., Marx, M., and Söffker, D. (2013). Modeling and control of a PEM fuel cell system: A practical study based on experimental defined component behavior. *J. Process Control*, 23(3):282–293.

Panos, C., Kouramas, K., Georgiadis, M., and Pistikopoulos, E. (2012). Modelling and explicit model predictive control for PEM fuel cell systems. *Chem. Eng. Sci.*, 67(1):15–25.

Park, S., Lee, J.-W., and Popov, B. N. (2012). A review of gas diffusion layer in PEM fuel cells: Materials and designs. *Int. J. Hydrogen Energy*, 37(7):5850–5865.

Pickl, S. and Krabs, W. (2010). *Dynamical Systems, Stability, Controllability and chaotic behavior*.

Robin, C., Gerard, M., D'Arbigny, J., Schott, P., Jabbour, L., and Bultel, Y. (2015). Development and experimental validation of a PEM fuel cell 2D-model to study heterogeneities effects along large-area cell surface. *International Journal of Hydrogen Energy*, 40(32):10211–10230.

SAE (2016). History of Fuel Cells.

Sanchez, V. M., Barbosa, R., Arriaga, L., and Ramirez, J. M. (2014). Real time control of air feed system in a PEM fuel cell by means of an adaptive neural-network. *Int. J. Hydrogen Energy*, pages 1–13.

Schultze, M. and Horn, J. (2016). Modeling, state estimation and nonlinear model predictive control of cathode exhaust gas mass flow for PEM fuel cells. *Control Eng. Pract.*, 49:76–86.

Segura, F., Andújar, J. M., and Durán, E. (2011). Analog Current Control Techniques for Power Control in PEM Fuel-Cell Hybrid Systems : A Critical Review and a Practical Application. *IEEE Trans. Ind. Electron.*, 58(4):1171–1184.

Sing, K. S. W. (1982). IUPAC report: Reporting physisorpiton data for gas/solid systems. *Pure and Applied Chemistry*, 54(11):2218–2218.

Singhal, S. C., Kendall, K., Anderson, H. U., van Gerwen, R. J. F., and Hendriksen, P. V. (2003). High Temperature Solid Oxide Fuel Cells: Fundamentals, Design and Applications. In Singhal, S. C. and Kendall, K., editors, *Elsevier*, page 393. Elsevier, Oxford, first edit edition.

Smith, C. and Corripio, A. (2005). *Principles and Practice of Automatic Process Control*.

Springer, T. E., Zawodzinski, T. A., and Gottesfeld, S. (1991). Polymer Electrolyte Fuel Cell Model. *J. Electrochem. Soc*, 138(8):2334–2342.

Wang, J. (2015). Barriers of scaling-up fuel cells: Cost, durability and reliability. *Energy*, 80:509–521.

Wang, L. (2003). A parametric study of PEM fuel cell performances. *Int. J. Hydrogen Energy*, 28(11):1263–1272.

Wang, Y., Chen, K. S., Mishler, J., Cho, S. C., and Adroher, X. C. (2011). A review of polymer electrolyte membrane fuel cells: Technology, applications, and needs on fundamental research. *Appl. Energy*, 88(4):981–1007.

Zemansky, M. W. and Dittman, R. H. (1979). Calor y Termodinámica.

Zhan, Y., Wang, H., and Zhu, J. (2012). Modelling and control of hybrid UPS system with backup PEM fuel cell/battery. *Int. J. Electr. Power Energy Syst.*, 43(1):1322–1331.

Zhang, J., Wu, J., Zhang, H., and Zhang, J. (2013). *PEM Fuel Cell Testing and Diagnosis*. Elsevier Science.

Zhou, J., Gao, D., and Zhang, D. (2007). Traffic Monitoring. 56(1):51–59.

Ziogou, C., Papadopoulou, S., Georgiadis, M. C., and Voutetakis, S. (2013). On-line nonlinear model predictive control of a PEM fuel cell system. *J. Process Control*, 23(4):483–492.

Ziogou, C., Voutetakis, S., Papadopoulou, S., and Georgiadis, M. C. (2011). Modeling, simulation and experimental validation of a PEM fuel cell system. *Comput. Chem. Eng.*, 35(9):1886–1900.